

THE UNIVERSITY OF MANITOBA

SCATTERING BY CYLINDRICAL  
REFLECTORS AND THE EFFECTS  
OF DIELECTRIC LOADING

by

BAHMAN AZARBAR

A THESIS

SUBMITTED TO THE FACULTY OF GRADUATE STUDIES  
IN PARTIAL FULFILMENT OF THE REQUIREMENTS FOR THE DEGREE  
OF MASTER OF SCIENCE IN ELECTRICAL ENGINEERING

DEPARTMENT OF ELECTRICAL ENGINEERING

WINNIPEG, MANITOBA

MAY 1975

SCATTERING BY CYLINDRICAL  
REFLECTORS AND THE EFFECTS  
OF DIELECTRIC LOADING

by

BAHMAN AZARBAR

A dissertation submitted to the Faculty of Graduate Studies of  
the University of Manitoba in partial fulfillment of the requirements  
of the degree of

MASTER OF SCIENCE

© 1975

Permission has been granted to the LIBRARY OF THE UNIVERSITY OF MANITOBA to lend or sell copies of this dissertation, to the NATIONAL LIBRARY OF CANADA to microfilm this dissertation and to lend or sell copies of the film, and UNIVERSITY MICROFILMS to publish an abstract of this dissertation.

The author reserves other publication rights, and neither the dissertation nor extensive extracts from it may be printed or otherwise reproduced without the author's written permission.



To my parents  
with deep gratitude

## ABSTRACT

The physical optics approximation is utilized to improve the convergence of the numerical solution using the moment method. As a result, the range of the application of the moment method is extended to objects of large to very large electrical dimensions. The advantage of this method over the conventional moment method is verified by its application to large conducting circular cylindrical reflectors and accurate solutions in relatively less computer time are obtained. The effects of variously shaped dielectric loadings on the radiation characteristics of cylindrical reflectors are also investigated and parameters most important for the overall behavior of such reflectors are determined. Finally, the effects of surface deformations on the radiation patterns of some commonly used reflectors are studied and it is shown that by a proper choice of the parameters involved, directive beams of desired shape can be obtained.

## ACKNOWLEDGEMENTS

The author wishes to express his appreciation to Dr. L. Shafai who proposed and supervised the research throughout.

The financial assistance by the National Research Council of Canada (Grant A-7702) and the Department of Electrical Engineering of the University of Manitoba are gratefully acknowledged.

CHAPTER	TABLE OF CONTENTS	PAGE
	ABSTRACT . . . . .	i
	ACKNOWLEDGEMENTS . . . . .	ii
	TABLE OF CONTENTS . . . . .	iii
	LIST OF FIGURES . . . . .	v
1	INTRODUCTION . . . . .	1
2	INTEGRAL EQUATION FORMULATION OF SCATTERING PROBLEMS . . . . .	12
2.1	INTRODUCTION . . . . .	12
2.2	INTEGRAL REPRESENTATION OF THE EM FIELDS . . . . .	14
2.3	TWO-DIMENSIONAL SCATTERING PROBLEMS . . . . .	23
2.4	TM WAVE SCATTERING . . . . .	26
3	ON THE NUMERICAL SOLUTION OF THE INTEGRAL EQUATION . . . . .	30
3.1	INTRODUCTION . . . . .	30
3.2	MODIFIED MOMENT METHOD FORMULATION . . . . .	35
3.3	RADIATION FIELD . . . . .	47
3.4	NUMERICAL RESULTS . . . . .	51
4	SCATTERING BY DIELECTRIC LOADED CYLINDRICAL REFLECTORS . . . . .	72
4.1	INTRODUCTION . . . . .	72
4.2	FORMULATION OF THE PROBLEM . . . . .	75
4.3	NUMERICAL RESULTS . . . . .	82
5	EFFECTS OF SURFACE DEFORMATION OF CONVENTIONAL REFLECTORS . . . . .	104
5.1	INTRODUCTION . . . . .	104

CHAPTER		PAGE
5.2	NUMERICAL RESULTS . . . . .	106
6	CONCLUSIONS . . . . .	117
	APPENDIX A . . . . .	119

LIST OF FIGURES

FIGURE		PAGE
Fig. 2.1	The general representation . . . . .	14
Fig. 2.2	Notation for Green's theorem . . . . .	18
Fig. 2.3	Geometry of two-dimensional scattering . .	23
Fig. 2.4	The cross sectional geometry of scattering by a metallic cylinder . . . . .	26
Fig. 3.1	Cross sectional view of the problem . . .	35
Fig. 3.2	Selection of the imaginary arc . . . . .	45
Fig. 3.3	Radiation pattern of a circular cylinder .	52
Fig. 3.4	Radiation patterns by the moment method .	54
Fig. 3.5	Radiation patterns by the modified moment method . . . . .	55
Fig. 3.6	Behavior of the surface current by the moment method . . . . .	56
Fig. 3.7	Behavior of the surface current by the modified moment method . . . . .	57
Fig. 3.8	Radiation patterns for different step sizes by the moment method . . . . .	59
Fig. 3.9	Radiation patterns for different step sizes by the modified moment method . . .	60
Fig. 3.10	Radiation patterns for different source separations . . . . .	61
Fig. 3.11	Behavior of the difference current for different step sizes . . . . .	64
Fig. 3.12	Behavior of the difference current for different step sizes . . . . .	65

FIGURE	PAGE
Fig. 3.13 Behavior of the difference current for different sampling lengths . . . . .	66
Fig. 3.14 Behavior of the difference current for different sampling lengths . . . . .	67
Fig. 3.15 Radiation patterns for different step sizes . . . . .	68
Fig. 3.16 Radiation patterns for different step sizes . . . . .	69
Fig. 3.17 Radiation patterns for different sampling lengths . . . . .	70
Fig. 3.18 Radiation patterns for different sampling lengths . . . . .	71
Fig. 4.1 Cross sectional view of the scatterers .	75
Fig. 4.2 Scattering pattern of dielectric cylindrical shell with a plane wave incident . . . . .	83
Fig. 4.3 Result obtained by Richmond . . . . .	84
Fig. 4.4 Scattering pattern of a dielectric semicircular cylindrical shell with a plane wave incident . . . . .	85
Fig. 4.5 Result obtained by Richmond . . . . .	86
Fig. 4.6 Notations for the parameters affecting the radiation pattern . . . . .	87
Fig. 4.7 Radiation patterns for different $b$ . . .	89
Fig. 4.8 Radiation patterns for different $b$ . . .	90

FIGURE	PAGE
Fig. 4.9 Radiation patterns for different a . . . .	91
Fig. 4.10 Radiation patterns for different a . . . .	92
Fig. 4.11 Radiation patterns for different a . . . .	93
Fig. 4.12 Radiation patterns for different electrical thickness . . . . .	94
Fig. 4.13 Radiation patterns for different electrical thickness . . . . .	95
Fig. 4.14 Radiation patterns for different electrical thickness . . . . .	96
Fig. 4.15 Radiation patterns for variously shaped dielectric loading . . . . .	99
Fig. 4.16 Effects of air gap on the radiation pattern for different dielectric constants . . . .	100
Fig. 4.17 Effects of air gap on the radiation pattern for different dielectric constants . . . .	101
Fig. 4.18 Radiation patterns for different dielectric constants . . . . .	102
Fig. 4.19 Effects of air gap on the radiation pattern for different dielectric constants . . . .	103
Fig. 5.1 Radiation patterns of a circular cylindrical reflector for different source separations	108
Fig. 5.2 Radiation patterns of a parabolic reflector for different focal distances . . . . .	109
Fig. 5.3 Radiation patterns of a corner reflector for different source separations . . . .	110

FIGURE	PAGE
Fig. 5.4	Comparison of the radiation patterns of the three types of the reflectors . . . . . 113
Fig. 5.5	Effects of conducting plane sheets on the radiation pattern of a semicircular cylindrical reflector . . . . . 114
Fig. 5.6	Effects of conducting plane sheets on the radiation pattern of a parabolic reflector . . . . . 115
Fig. 5.7	Comparison of the radiation patterns of the modified reflectors . . . . . 116
Fig. A	Pulse function . . . . . 122
Fig. B	Step approximation . . . . . 123
Fig. C	Delta function . . . . . 123

## CHAPTER ONE

## INTRODUCTION

The underlying differential equations, describing the scattering and diffraction phenomena, have long been fully understood. The greatest difficulty in the solution of many problems of electromagnetic theory is usually not the analytical reduction of the original vectorial problem to a set of scalar wave equations, but rather obtaining the solution of such reduced equations. The method of separation of variables serves quite well for the study of some simple electromagnetic wave problems. The wave equation  $\nabla^2\psi + k^2\psi = 0$  is separable only in eleven coordinate systems. But a useful solution, in the presence of an object, can only be found if the object surface coincides with one of the coordinate surfaces. This is a necessity, since the solution is unique if it satisfies the boundary conditions, and it can be applied if the above condition is satisfied. However, even if the boundary surfaces coincide with one of the coordinate surfaces, the solution obtained using the separation of variables, may not be practically useful. This is due to the fact that the eigen functions of some of these coordinate systems cannot readily be computed or the resulting series are slowly convergent. Therefore,

exact analytical solution of electromagnetic boundary value problems are restricted to a small group of objects with simple geometrical shapes. For this reason, attempts have been made to develop approximate solutions, which could provide useful solutions for variety of the problems, under certain conditions. Examples are the low and the high frequency approximations, variational methods as well as the geometrical theory of diffraction. However, one of the drawbacks of these methods is that, their application to each new scattering problem requires a great deal of thought and ingenuity to estimate their accuracy of the solution and to include all necessary rays or effects. In addition all these methods tend to be less accurate in the intermediate frequency range, where the dimensions of the objects are of the same order of the frequency wavelength.

On the other hand, numerical methods may also be used to study the electromagnetic scattering problems by an application of the boundary conditions in a finite set of boundary points. These methods have received increasing attention in recent years due to the availability of the digital computers. They are, however, most useful in the low and intermediate frequency ranges, for which the required computing time is not excessive. In application of these methods to the scattering problems, usually the original differential or the integral equations are transformed into a set of simultaneous equations. A solution for the problem

is then obtained by the solution of these resulting linear equations.

Two distinct approaches have been employed to obtain a set of linear equations for the scattering problems. One is based on the modal expansion of the scattered field in terms of a complete set of certain modal functions with unknown coefficients. These unknown coefficients are then found by a truncation of the modal series and the application of the boundary conditions in a finite number of boundary points and solving the resulting simultaneous equations. Alternatively, the scattered field may also be found in terms of an integral equation of certain unknown quantities, which depending on the object, may be the induced charge and current densities on conductor or the polarization currents in a dielectric region. A solution for such an integral equation is usually obtained by an expansion of the unknown quantities in terms of a series of selected functions with unknown coefficients or a direct numerical evaluation of the integral equations.

The integral equation method was first used by Mei and Van Bladel<sup>1</sup> for determination of the fields scattered by perfectly conducting rectangular cylinders. The unknown quantity of the integrand was the induced current on the cylinder, which was expanded in a set of discontinuous step functions and the boundary conditions were enforced at  $N$  different points on the contour  $C$  of the scatterer. The

integral equation was then approximated by a weighted sum of  $N$  sampled values of the current distribution and the resulting set of  $N$  linear equations were to give the required unknown current. In a later paper by Andreassen<sup>2</sup>, a more refined form of this method was used with better approximations for the current distribution and the numerical integration (parabolic approximation) to determine the scattered field of a set of conducting cylinders of arbitrary cross sections.

Following these papers, the application of this method has been extended to various two and three-dimensional antenna and scattering problems. The publications in this area are numerous, but may be summarized as; scattering from bodies of revolution<sup>3</sup>, scattering from cylinders with arbitrary surface impedance<sup>4</sup>, scattering by a dielectric cylinder of arbitrary cross section using a volume integral formulation<sup>5,6</sup>, straight and circular wires with arbitrary excitation and loading<sup>7,8</sup>, scattering from conducting loops and solution of circular loop antennas<sup>9</sup> and the conical-equiangular spiral antennas<sup>10</sup>.

The results of these and numerous other works in this area are used by Harrington<sup>11,12</sup> to present a unified approach for solving field problems using digital computers. More recently Mittra et al have summarized all these numerical methods in their book<sup>13</sup> and have provided useful discussions on their advantages and limitations. The

method is also considered by Wallenberg<sup>14</sup>, where he has described it in terms of the concept of generalized network parameters.

In application of these methods to scattering bodies with sharp edges, difficulties arise when certain field components become infinite and an accurate evaluation of these components require their careful treatments. One way, which has been used by Shafai<sup>15,16,17</sup> is to relate these singularities at the sharp edges to the geometry of the scatterer using a transformation method. The resulting integral then has a new unknown function, which is regular and readily obtainable. In another approach, utilized by Abdelmessih and Sinclair<sup>18</sup>, the exact behavior of the fields at the edges was described by the Meixner<sup>19</sup> edge conditions and its contribution was included in solving the integral equation. However, the simplest approach is to ignore the contribution of the edge currents by placing the sampling points near but not on the edge itself. This approach has been applied to the problem of scattering by a perfectly conducting rectangle<sup>20</sup> and has shown that for step sizes less than  $\lambda/10$ , the resulting error in the computed induced current, due to a mesh size, will not exceed two per cent.

Of prime importance to the user of the moment method is how to solve the integral equation easily, accurately and rapidly. A limitation of this method, when used to analyze scattering problems, is that the scattering

body cannot be longer than a few wavelengths, since large bodies result in large matrices which require excessive computer storage and running time. In addition, aside from the excessive computation time, the accumulation of error, while inverting large matrices, greatly impairs the accuracy of the solution thus obtained. The best one can do then, is to seek for a way to improve the rate of the convergence of this method. In a paper by Kinzel<sup>21</sup>, a sectioning method is suggested for treating the two-dimensional scattering problems which involve large bodies. In this method, the scatterer is divided into a number of small sections where a section might typically be of the order of one wavelength long. Each section is then divided into more subsections. The next step is to compute the current distribution on three adjacent sections, using the method of moment, and ignoring the contribution of the current distribution over the remaining sections. The calculated approximate current distributions are stored for only the middle section. The procedure is continued for determining the current distribution over the entire contour of the scatterer. This technique essentially assumes that the current on one section is significantly affected only by the currents in the adjoining sections, which is only a good approximation if the sections are not too small.

One of the drawbacks of this method is in completely neglecting the contribution from the edge current

distribution, which is quite significant, on the other sections. Moreover, the computational time saved by this method becomes significant only when the number of sections is much larger than nine. Therefore, to extend the application of the method of moment to objects with large cross sectional dimensions, relative to the wavelength, a further modification of the method is required which does not suffer from the drawbacks given for the sectioning method.

For problems of conducting objects, the physical optics approximation usually provides an approximate value for the induced currents. This would suggest the use of the concept of "a priori knowledge of the solution" for improving the rate of the convergence of the moment method. In a recent paper<sup>22</sup>, this technique has been applied to the case of two-dimensional scattering from a perfectly conducting strip illuminated normally by a plane wave. This method is essentially a combination of the physical optics approximation and the point matching technique. On the illuminated side of the conducting surface, the physical optics current has a value,

$$\tilde{J}_{po} = 2\hat{n} \times H_i$$

Thus, assuming the total current in the form of,

$$\tilde{J} = \tilde{J}_{po} + \tilde{J}_d$$

the  $J_{po}$  is readily known from the incident field of the source and  $J_d$  is the only unknown current to be determined. However, the difference current  $J_d$  is due to the surface discontinuities and the shadow region and is localized to the edges of the scatterer. Thus, as the scatterer size increases, the contribution of the difference current decreases, but due to its localized nature can always be determined by choosing enough matching points near the edges.

In chapter three of this thesis, the above method is applied to the problem of two-dimensional scattering from circular cylindrical reflectors in the presence of an electric line source. The improvement in the rate of the convergence is demonstrated for a medium size reflector and finally the method is applied for treating large reflectors which are not solvable by a direct moment method.

Ordinarily, the ultimate goal in the antenna design and studies is to seek a way of controlling the radiation characteristics of the antenna, in a predetermined manner. This task is usually achieved by introduction of some passive elements in the path of rays, for phase correction. For example, reflectors, dielectric materials or metal plates are quite suitable for this purpose, since they perform the same basic function, that is, a modification of the phase.

So far, a number of theoretical and experimental investigations have been carried out to study the possible control of antenna characteristics by dielectrically loading the conventional antennas and reflectors. Among these works are; the dielectric loaded axial slot antennas on a circular cylinder, which is solved analytically within certain simplifying assumptions, for investigation of the external slot admittance<sup>23</sup>, investigations on the optimum dielectric thickness for maximum power radiation<sup>24</sup>, experimental studies of the variously shaped dielectric inserts on the radiation patterns of loaded horns and corner reflectors<sup>25, 26, 27</sup>, the effects of the symmetrical loading of a horn aperture with E-plane dielectric slabs for obtaining high aperture efficiencies<sup>28</sup>, radiation by dielectric-loaded spherical, circular cylindrical antennas, wedges and corner reflectors<sup>29</sup> and resonance effects due to dielectric loading in cylindrical and spherical slots<sup>30, 31</sup>.

Due to the scarcity of quantitative theoretical data on the effects of various parameters involved in scattering from dielectrically loaded cylindrical reflectors, chapter four of this work is oriented to study numerically the general scattering properties of this class of reflectors. The advantages of the numerical method are based on the fact that the approximate solution tends to converge to the exact solution as the number of matching points increases and has the flexibility of treating

problems of arbitrary cross sections and two-dimensional source distributions.

Another method of controlling the radiation characteristics of the antennas, as stated before, is by changing the geometrical structure of the antenna system. Reflectors and metal plates are quite suitable for this purpose, and if done judiciously, it is possible to shape the radiation pattern of the radiating element in a desired fashion.

So far, most of the information available for conventional reflectors, has been obtained through the use of ray theory, which is only applicable if the characteristic dimension of the reflector is much greater than the wavelength. However, for dimensions of the order of the wavelength, this approach most likely is not able to yield results with acceptable accuracy. The purpose of the fifth chapter is to investigate the radiation characteristics of a few commonly used types of reflectors of moderate cross section sizes, by means of numerical technique. It also studies the possibilities of beam shaping by surface deformations, and improving the radiation characteristics of these types of reflectors in a desired manner.

In summary, this thesis considers the numerical investigation of the scattering properties of circular cylindrical reflectors. The integral equation approach has been adopted and the problem is solved by the method of

moment. In chapter two, the problem is rigorously formulated in the form of a set of integral equations. The general form of the equations are then reduced to the forms describing the two-dimensional case. Particular attention is paid to the case of transverse magnetic(TM)scattering which is the general topic of this study. Chapter three deals with the numerical processing of the integral equations. The advantages and limitations of the method of moment are described and the concept of using "a priori knowledge of the solution" is applied for extending the range of applicability of the numerical technique to large reflectors without excessive storage and computer running time. Chapter four is intended to investigate the general scattering properties of dielectrically loaded cylindrical reflectors. Since all the effects cannot be observed in one geometry, a number of selected geometries are investigated. One of the aims of this chapter is the determination of the most effective parameters for investigation of overall radiation characteristics of such loaded reflectors. A knowledge of the effects of the parameters, would in fact, be of great help to the designer to obtain a predetermined radiation pattern. Chapter five is intended to show the possibilities of beam shaping by deforming the reflecting surfaces of the conventional reflectors. Certain geometries are selected and the radiation patterns are compared against each other. The computed results are discussed in chapter six.

## CHAPTER TWO

## INTEGRAL EQUATION FORMULATION OF SCATTERING PROBLEMS

## 2.1 Introduction

From the point of view of classical theory, any precise treatment of electromagnetic scattering and diffraction phenomena, generally involves the complete solution of a boundary value problem. However, there are few cases in which this rigorous approach is productive. The best one can do then, is to find an approximate solution to the original problem.

In recent years, due to the high speed and large storage capacity of digital computers, considerable interest has been shown in the use of numerical solution techniques to the evaluation of scattering and radiation problems. The scattering properties of complex bodies can be computed with very high accuracy through the application of numerical techniques. However, the differential equation formulation is not efficient for this purpose. Of the many approaches available, considering the adaptability of the formulation for computer use, the integral equation representation has proven to be the most efficient form for the computer solution.

It is the purpose of this chapter to reduce the

original vectorial boundary value problems associated with the electromagnetic scattering phenomena, to a set of integral equations, most suitable for numerical solution using a digital computer.

## 2.2- Integral representation of the EM fields.

Consider the region  $V$ , illustrated in figure 2.1, bounded by the surfaces  $S_1$  and  $S_2$ .

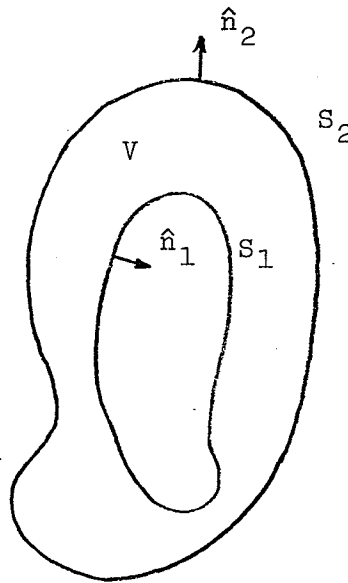


Fig. ( 2.1 ) The general representation.

It is assumed that constitutive parameters of region  $V$  differ from those of the medium in the surrounding space. Vectors  $\hat{n}_1$  and  $\hat{n}_2$  are the unit vectors normal to the bounding surfaces, directed out of the region  $V$ .

Considering the time harmonic case, in a linear, isotropic and homogeneous region, the field quantities must obey Maxwell's equations,

$$\nabla \times \vec{H} = j\omega\epsilon \vec{E} + \vec{J} \quad (2.1)$$

$$\nabla \times \vec{E} = -j\omega\mu \vec{H} - \vec{K} \quad (2.2)$$

$$\nabla \cdot \vec{E} = \rho/\epsilon \quad (2.3)$$

$$\nabla \cdot \vec{H} = m/\mu \quad (2.4)$$

where,

E electric field intensity.

H magnetic field intensity.

J electric current density.

K magnetic current density.

$\rho$  electric charge density.

m magnetic charge density.

$\epsilon$  permittivity of the medium.

$\mu$  permeability of the medium.

complemented by the relationships defining the conservation of charge, given by,

$$\nabla \cdot \vec{J} = -j\omega\rho \quad (2.5)$$

$$\nabla \cdot \vec{K} = -j\omega m \quad (2.6)$$

where an  $\exp(j\omega t)$  time dependence is assumed and suppressed throughout for convenience. A simple vector manipulation of the equations 2.1 and 2.2 leads to,

$$\nabla \times \nabla \times \tilde{\mathbf{E}} - k^2 \tilde{\mathbf{E}} = -j\omega\mu \tilde{\mathbf{J}} - \nabla \times \tilde{\mathbf{K}} \quad (2.7)$$

$$\nabla \times \nabla \times \tilde{\mathbf{H}} - k^2 \tilde{\mathbf{H}} = -j\omega\epsilon \tilde{\mathbf{K}} + \nabla \times \tilde{\mathbf{J}} \quad (2.8)$$

where,

$$k = \omega\sqrt{\epsilon\mu} \quad (2.9)$$

using the vector Green's theorem,

$$\int_V \left( \tilde{\mathbf{A}} \cdot \nabla \times \nabla \times \tilde{\mathbf{B}} - \tilde{\mathbf{B}} \cdot \nabla \times \nabla \times \tilde{\mathbf{A}} \right) dv = \int_S \left( \tilde{\mathbf{B}} \times \nabla \times \tilde{\mathbf{A}} - \tilde{\mathbf{A}} \times \nabla \times \tilde{\mathbf{B}} \right) \cdot \hat{\mathbf{n}} ds \quad (2.10)$$

which is the result of the vector identity,

$$\nabla \cdot (\tilde{\mathbf{A}} \times \nabla \times \tilde{\mathbf{B}}) = \nabla \times \tilde{\mathbf{A}} \cdot \nabla \times \tilde{\mathbf{B}} - \tilde{\mathbf{A}} \cdot \nabla \times \nabla \times \tilde{\mathbf{B}} \quad (2.11)$$

and application of the divergence theorem, it is possible to transform the vector wave equations 2.7 and 2.8 into a set

32 13

of integral equations. The equation 2.10 is valid for any two arbitrary continuous vector functions of position with continuous first and second derivatives within the region  $V$  and on the bounding surface  $S$ . The approach adopted is to assume  $\tilde{E}$  and  $\psi \hat{a}$  for  $\tilde{A}$  and  $\tilde{B}$  respectively. Here  $\hat{a}$  is a unit vector of arbitrary orientation and  $\psi \hat{a}$  is the Green's function representing the magnetic vector potential of a point current source in a homogenous space and is given by,

$$\Psi = \exp(-jk|\tilde{r}-\tilde{r}'|)/|\tilde{r}-\tilde{r}'| \quad (2.12)$$

with  $\tilde{r}$  and  $\tilde{r}'$  representing the positional vectors of the observation and source points respectively. The discontinuity of the field on the boundary surfaces marking the abrupt change of the constitutive parameters of two different media and the singularity of  $(\Psi)$  at  $\tilde{r}=\tilde{r}'$  restrict the usefulness of the equation 2.10. However the latter difficulty can be avoided by making explicit use of the vector differential equation for the Green's function given by,

$$\nabla \times \nabla \times (\Psi \hat{a}) - k^2 (\Psi \hat{a}) - \nabla \nabla \cdot (\Psi \hat{a}) = 4\pi \delta(\tilde{r}-\tilde{r}') \hat{a} \quad (2.13)$$

where  $(\delta)$  represents the Dirac's Delta function.

In order to overcome the problem of the discontinuous nature of the field on the boundary surfaces, we surround the observation point  $P$ , by a small sphere  $S_4$  of radius  $r$  and consider the portion  $V_r$  of  $V$  which is bounded by the surfaces  $S_1, S_2, S_3$  and  $S_4$ , figure 2.2.

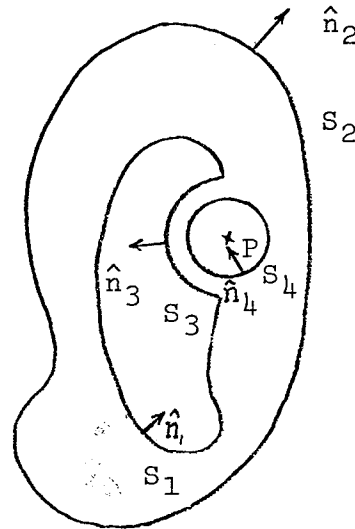


Fig. 2.2 Notation for Green's theorem

Substituting  $\tilde{E}$  and  $\Psi \hat{a}$  for  $\tilde{A}$  and  $\tilde{B}$  respectively in 2.11 leads to,

$$\int_{V_r} \{ (\Psi \cdot \hat{a}) \cdot \nabla' \times \nabla' \times \tilde{E} - \tilde{E} \cdot \nabla' \times \nabla' \times (\Psi \cdot \hat{a}) \} dv' =$$

$$\sum_i \int_{S_i} \{ \tilde{E} \times \nabla' \times (\Psi \cdot \hat{a}) - (\Psi \cdot \hat{a}) \times \nabla' \times \tilde{E} \} \cdot \hat{n}' ds'$$

(2.14)

where primes are used to indicate vector operations in source coordinates and  $\hat{n}'_i$ 's are the normal unit vectors to the bounding surfaces of like subscript, directed out of the region  $V_r$  and can take on the representations  $\hat{n}_1, \hat{n}_2, \hat{n}_3$ , and  $\hat{n}_4$ . After extensive vector manipulations and making use of the equations 2.1, 2.3 and 2.7, the equation 2.14 reduces to,

$$\int_{V_r} \{ j\omega\mu \vec{J} \Psi + \vec{K} \times \nabla' \Psi - (\rho/\epsilon) \nabla' \Psi \} dv' = \sum_i \int_{S_i} \{ j\omega\mu (\hat{n}' \times \vec{H}) \Psi - (\hat{n}' \cdot \vec{E}) \nabla' \Psi \} ds' \quad (2.15)$$

In the limit, when  $(r = |\vec{r} - \vec{r}'|)$  approaches zero, the contribution of the first term of the surface integral over the surface  $S_4$  goes to zero, since  $S_4$  decreases as  $r^2$  and  $(\Psi)$  varies as  $1/r$ . The contribution of the second term over surfaces  $S_4$  and  $S_3$  is shown to be,

$$I = - \vec{E}(\vec{r}) \{ 4\pi - \Omega \} \quad (2.16)$$

where  $(\Omega)$  represents the absolute value of the solid angle subtended by a surface like  $S$  at  $\vec{r}$ , in the limit as  $r$  vanishes. The value of  $(\Omega)$  depends on the location of the observation point  $P$  and is given by,

$$\Omega = \begin{cases} 2\pi & \text{on the bounding surface} \\ 0 & \text{anywhere within } V \end{cases} \quad (2.17)$$

Application of the foregoing argument to 2.15 results in an integral equation representing the electric field at any point within region  $V$  in terms of the sources existing in  $V$  and the fields on the bounding surfaces, namely,

$$\begin{aligned} \tilde{\mathbf{E}}(\tilde{\mathbf{r}}) = & -(\mathbb{T}/4\pi) \int_V (j\omega\mu \tilde{\mathbf{J}}\Psi + \tilde{\mathbf{K}} \times \nabla'\Psi - \rho/\epsilon \nabla'\Psi) dv' \\ & -(\mathbb{T}/4\pi) \int_{S_1+S_2} \{ j\omega\mu(\hat{\mathbf{n}}' \times \tilde{\mathbf{H}})\Psi - (\hat{\mathbf{n}}' \times \tilde{\mathbf{E}}) \times \nabla'\Psi \\ & - (\hat{\mathbf{n}}' \cdot \tilde{\mathbf{E}}) \nabla'\Psi \} ds' \end{aligned} \quad (2.18)$$

where,

$$\mathbb{T} = 1/\{1 - \Omega/4\pi\}$$

and keeping in mind that an infinitesimal region surrounding point  $P$  is to be excluded.

By a similar argument or using the duality of Maxwell's equations, one arrives at an expression for magnetic field at any point within  $V$  given by,

$$\begin{aligned} \tilde{\mathbf{H}}(\tilde{\mathbf{r}}) = & -(\mathbb{T}/4\pi) \int_V (-j\omega\epsilon \tilde{\mathbf{K}}\Psi + \tilde{\mathbf{J}} \times \nabla'\Psi + m/\mu \nabla'\Psi) dv' \\ & +(\mathbb{T}/4\pi) \int_{S_1+S_2} \{ j\omega\epsilon(\hat{\mathbf{n}}' \times \tilde{\mathbf{E}})\Psi + (\hat{\mathbf{n}}' \times \tilde{\mathbf{H}}) \times \nabla' \\ & + (\hat{\mathbf{n}}' \cdot \tilde{\mathbf{H}}) \nabla'\Psi \} ds' \end{aligned} \quad (2.19)$$

For a source free region, the equations 2.18 and 2.19 reduce to,

$$\begin{aligned} \tilde{\mathbf{E}}(\tilde{\mathbf{r}}) = & -(\mathbb{T}/4\pi) \int_{S+S_1+S_2} \{ j\omega\mu(\hat{\mathbf{n}}' \times \tilde{\mathbf{H}})\Psi - (\hat{\mathbf{n}}' \times \tilde{\mathbf{E}}) \times \nabla' \Psi \\ & - (\hat{\mathbf{n}}' \cdot \tilde{\mathbf{E}}) \nabla' \Psi \} ds' \end{aligned} \quad (2.20)$$

$$\begin{aligned} \tilde{\mathbf{H}}(\tilde{\mathbf{r}}) = & (\mathbb{T}/4\pi) \int_{S+S_1+S_2} \{ j\omega\epsilon(\hat{\mathbf{n}}' \times \tilde{\mathbf{E}})\Psi + (\hat{\mathbf{n}}' \times \tilde{\mathbf{H}}) \times \nabla' \Psi \\ & + (\hat{\mathbf{n}}' \cdot \tilde{\mathbf{H}}) \nabla' \Psi \} ds \end{aligned} \quad (2.21)$$

which represent the effect of sources located outside the region  $V$ . Considering the analogy of the integrands of the volume and surface integrals in 2.18 and 2.19, one can represent the effect of sources existing outside volume  $V$  by surface distribution of charges and currents on the bounding surface  $S$ , namely,

$$\hat{\mathbf{n}}' \times \tilde{\mathbf{H}} = \tilde{\mathbf{J}}_s \quad (2.22)$$

$$-\hat{\mathbf{n}}' \times \tilde{\mathbf{E}} = \tilde{\mathbf{K}}_s \quad (2.23)$$

$$\epsilon(\hat{\mathbf{n}}' \cdot \tilde{\mathbf{E}}) = \rho_s \quad (2.24)$$

$$\mu(\hat{\mathbf{n}}' \cdot \tilde{\mathbf{H}}) = m_s \quad (2.25)$$

where subscript  $s$  denotes surface distribution.

For an unbounded region ( when  $S_2$  in figure 2.1 recedes to infinity ) and assuming the sources in  $V$  being confined to a region of finite extent, the radiation condition requires that the contribution of the surface integral over  $S_2$  be independent of the bounded sources, that is,

$$\begin{aligned} \tilde{E}(\tilde{r}) = T \tilde{E}_i(\tilde{r}) - (T/4\pi) \int_V \{j\omega\mu \tilde{J} \Psi + \tilde{K} \times \nabla' \Psi \\ - (\rho/\epsilon) \nabla' \Psi\} dv' - (T/4\pi) \int_{S_1} \{j\omega\mu \tilde{J}_s \Psi + \tilde{K}_s \times \nabla' \Psi \\ - (\rho_s/\epsilon) \nabla' \Psi\} ds' \end{aligned} \quad (2.26)$$

$$\begin{aligned} \tilde{H}(\tilde{r}) = T \tilde{H}_i(\tilde{r}) + (T/4\pi) \int_V \{-j\omega\epsilon \tilde{K} \Psi + \tilde{J} \times \nabla' \Psi \\ + (m/\mu) \nabla' \Psi\} dv' + (T/4\pi) \int_{S_1} \{-j\omega\epsilon \tilde{K}_s \Psi + \tilde{J}_s \times \nabla' \Psi \\ + (m_s/\mu) \nabla' \Psi\} ds' \end{aligned} \quad (2.27)$$

where use has been made of the equations 2.22 to 2.25 and  $\tilde{E}_i, \tilde{H}_i$  are the fields due to the sources ( if any ) lying out of the surface  $S_1$ .

### 2.3 - Two dimensional scattering problems.

In this section we shall consider two-dimensional sources and scatterers, that is, sources and scatterers which are invariant along a particular axis. For convenience, we take this axis as the  $z$ -coordinate and assume the incident field to be propagating in a direction normal to the  $z$  axis. In this case, all the field quantities are also invariant along the axis. Considering figure 2.3,  $(\Psi)$  may be represented as,

$$\Psi = \exp\{-jk \cdot |\tilde{\rho} - \tilde{\rho}' + (z - z')\hat{k}|\} / |\tilde{\rho} - \tilde{\rho}' + (z - z')\hat{k}| \quad (2.28)$$

where  $(\tilde{\rho})$  and  $(\tilde{\rho}')$  represent the transverse positional vectors of the observation and source points respectively.

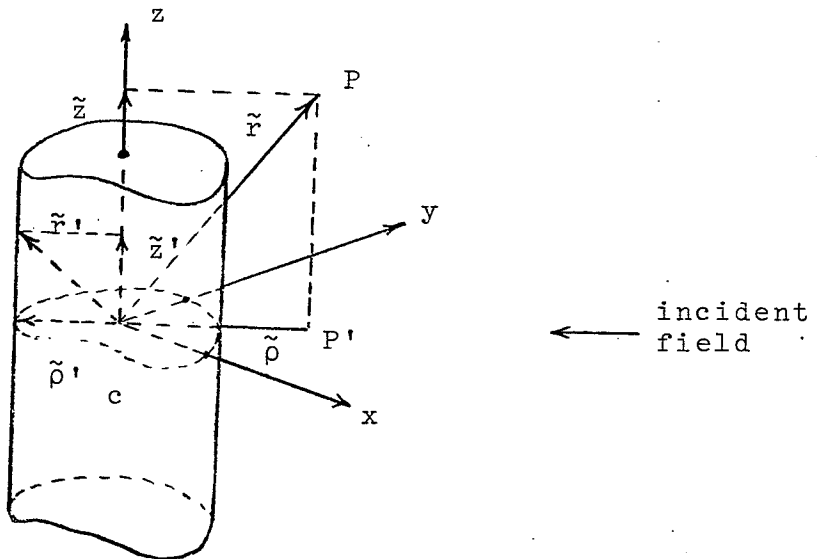


Figure 2.3 Geometry of two-dimensional scattering.

substituting 2.28 in 2.26 and 2.27 leads to,

$$\begin{aligned} \tilde{E}(z, \tilde{\rho}) &= T \tilde{E}_i(z, \tilde{\rho}) - (T/4\pi) \int_S \{ j\omega\mu \tilde{J} + \tilde{K} \times \nabla' \\ &- (\rho/\epsilon)\nabla' \} \int_{-\infty}^{\infty} \Psi dz' ds' - (T/4\pi) \int_c \{ j\omega\mu \tilde{J} + \tilde{K} \times \nabla' \\ &- (\rho/\epsilon)\nabla' \} \int_{-\infty}^{\infty} \Psi dz' ds' \end{aligned} \quad (2.29)$$

$$\begin{aligned} \tilde{H}(z, \tilde{\rho}) &= T \tilde{H}_i(z, \tilde{\rho}) + (T/4\pi) \int_S \{ -j\omega\epsilon \tilde{K} + \tilde{J} \times \nabla' \\ &+ (m/\mu)\nabla' \} \int_{-\infty}^{\infty} \Psi dz' ds' + (T/4\pi) \int_c \{ -j\omega\mu \tilde{K} + \tilde{J} \times \nabla' \\ &+ (m/\mu)\nabla' \} \int_{-\infty}^{\infty} \Psi dz' ds' \end{aligned} \quad (2.30)$$

where  $s$  is the transverse plane,  $c$  is the cross sectional contour of  $S$  and  $(\nabla'_t)$  is the transverse del operator in source coordinates. Since only the variation of fields in the  $(x-y)$  plane needs to be considered, we set  $z$  in the equations 2.28 to 2.30 equal to zero. To simplify the above equations, we take advantage of the known integral<sup>34</sup>,

$$G = \int_{-\infty}^{\infty} \Psi dz' = (\pi/j) H_0^2(k|\tilde{\rho}-\tilde{\rho}'|) \quad (2.31)$$

where  $H_0^2$  is the zero-order Hankel function of the second kind. Substituting 2.31 in 2.29 and 2.30 results in,

$$\begin{aligned} \tilde{E}(\tilde{\rho}) &= T \tilde{E}_i - (T/4\pi) \int_S (j\omega\mu \tilde{J} + \tilde{K} \times \nabla'_t - \frac{\rho}{\epsilon} \nabla'_t) G ds' - (T/4\pi) \int_c (j\omega\mu \tilde{J}_s + \tilde{K}_s \times \nabla'_t \\ &- \frac{\rho_s}{\epsilon} \nabla'_t) G dc' \end{aligned} \quad (2.32)$$

$$\begin{aligned} \tilde{H}(\tilde{\rho}) &= T \tilde{H}_i + (T/4\pi) \int_S (-j\omega\epsilon \tilde{K} + \tilde{J} \times \nabla'_t + \frac{m}{\mu} \nabla'_t) G ds' + (T/4\pi) \int_c (-j\omega\epsilon \tilde{K}_s + \tilde{J}_s \times \nabla'_t \\ &+ \frac{m_s}{\mu} \nabla'_t) G dc' \end{aligned} \quad (2.33)$$

It should be noted that the above set of integral equations do not represent the only solution for the two-dimensional scattering problems. They are however, the most useful forms commonly used for the numerical solution of the scattering problems involving arbitrarily shaped cylinders.

## 2.4- TM wave scattering.

In the case of two dimensional scattering problems, the transverse electric (TE) and the transverse magnetic (TM) fields, may be decoupled and treated separately. However in this section attention will be devoted to (TM) scattering from perfectly conducting cylinders.

Consider a time harmonic plane wave (source at infinity) normally incident on a metallic infinite cylinder of cross sectional contour  $c$  (figure 2.4).

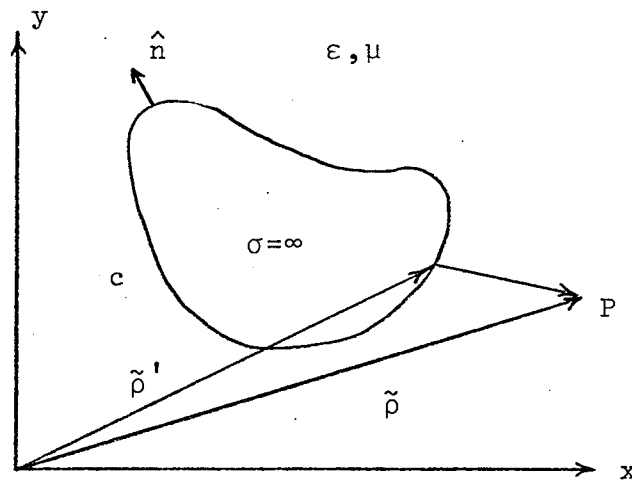


Figure 2.4 The cross sectional geometry of scattering by a metallic cylinder.

For (TM) fields, assume the incident field is z-polarized, and has the electric field along the z direction only. For

an unbounded, linear, homogeneous, isotropic and source free region, the equations 2.32 and 2.33 reduce to,

$$\begin{aligned} \tilde{E}(\tilde{\rho}) = \tilde{E}_z(\tilde{\rho}) = T \tilde{E}_{iz}(\tilde{\rho}) - (Tk\eta/4) \int_c \tilde{J}_{sz}(\tilde{\rho}') \\ \cdot H_0^2(k|\tilde{\rho}-\tilde{\rho}'|) dc' \end{aligned} \quad (2.34)$$

$$\begin{aligned} \tilde{H}(\tilde{\rho}) = \tilde{H}_t(\tilde{\rho}) = T \tilde{H}_{it}(\tilde{\rho}) + (Tk/4j) \int_c \tilde{J}_{sz}(\tilde{\rho}') \\ \cdot H_1^2(k|\tilde{\rho}-\tilde{\rho}'|) \{ \sin\{\tilde{\rho}', (\tilde{\rho}-\tilde{\rho}')\} \hat{\rho}' \\ + \cos\{\tilde{\rho}', (\tilde{\rho}-\tilde{\rho}')\} \hat{\phi}' \} dc' \end{aligned} \quad (2.35)$$

where use has been made of,

$$\begin{aligned} \nabla_t' G = \frac{\partial G}{\partial \rho} \hat{\rho}' + \frac{1}{\rho} \frac{\partial G}{\partial \phi} \hat{\phi}' = \frac{-\pi}{j} k H_0^2(k|\tilde{\rho}-\tilde{\rho}'|) \\ \cdot \{ \sin(\tilde{\rho}', \tilde{\rho}-\tilde{\rho}') \hat{\phi}' - \cos(\tilde{\rho}', \tilde{\rho}-\tilde{\rho}') \hat{\rho}' \} \end{aligned} \quad (2.36)$$

$$\eta = \sqrt{\mu/\epsilon} \quad (2.37)$$

The boundary conditions on the surface of the scatterer requires that,

$$\begin{aligned} \hat{n} \times \tilde{E} = 0 \\ \hat{n} \cdot \tilde{H} = m = 0 \end{aligned} \quad \text{on } c \quad (2.38)$$

hence,

$$E_{iz}(\tilde{\rho}_c) = (k\eta/4) \int_c J_{sz}(\tilde{\rho}') H_0^2(k|\tilde{\rho}_c - \tilde{\rho}'|) dc' \quad (2.39)$$

$$J_{sz}(\tilde{\rho}_c) = 2 |H_{it}(\tilde{\rho}_c)| + (k/2j) \int_c J_{sz}(\tilde{\rho}') H_1^2(k|\tilde{\rho}_c - \tilde{\rho}'|) \cdot \cos(\hat{n}', \tilde{\rho} - \tilde{\rho}') dc' \quad (2.40)$$

where the subscript  $c$  indicates that the field point is on the contour  $c$ .

Either of the above equations can be used to solve for the induced surface current  $J_s$ . However, for scatterers with sharp discontinuities, care must be used in evaluating 2.40, due to the geometrical factor in the integrand.

If the source of impressed field is a  $z$ -directed line source of strength  $I$  and located at  $(\tilde{\rho}_s)$ , the equations 2.32 and 2.33 lead to,

$$E_z(\tilde{\rho}) = -(Tk\eta/4) I(\tilde{\rho}_s) H_0^2(k|\tilde{\rho} - \tilde{\rho}_s|) - (Tk\eta/4) \int J_{sz}(\tilde{\rho}') \cdot H_0^2(k|\tilde{\rho} - \tilde{\rho}'|) dc' \quad (2.41)$$

$$\begin{aligned} H_t(\tilde{\rho}) = & \{Tk I(\tilde{\rho}_s)/4j\} H_1^2(k|\tilde{\rho} - \tilde{\rho}_s|) \{ \sin(\tilde{\rho}', \tilde{\rho} - \tilde{\rho}') \hat{\rho}' \\ & + \cos(\tilde{\rho}', \tilde{\rho} - \tilde{\rho}') \hat{\phi}' \} + (Tk/4j) \int J_{sz}(\tilde{\rho}') H_1^2(k|\tilde{\rho} - \tilde{\rho}'|) \{ \sin(\tilde{\rho}', \\ & \tilde{\rho} - \tilde{\rho}') \hat{\rho}' + \cos(\tilde{\rho}', \tilde{\rho} - \tilde{\rho}') \hat{\phi}' \} dc' \end{aligned} \quad (2.42)$$

On the boundary  $c$ , we have,

$$- I(\tilde{\rho}_s) H_0^2(k|\tilde{\rho}-\tilde{\rho}'|) = \int_c J_{sz}(\tilde{\rho}') H_0^2(k|\tilde{\rho}-\tilde{\rho}'|) dc' \quad (2.43)$$

$$\begin{aligned} J_{sz}(\tilde{\rho}_c) = & - (k/2j) \int_c J_{sz}(\tilde{\rho}') H_1^2(k|\tilde{\rho}-\tilde{\rho}'|) \\ & \cdot \cos(\hat{n}', \tilde{\rho}-\tilde{\rho}') dc' - (k/2j) I(\tilde{\rho}_s) H_1^2(k|\tilde{\rho}-\tilde{\rho}'|) \end{aligned} \quad (2.44)$$

where  $I(\tilde{\rho}_s)$  emphasizes that the current filament is located at  $(\tilde{\rho}_s)$ .

Once the current distribution is determined, other parameters of interest, such as the radiation field and the scattering cross section can be computed by the required integrations.

## CHAPTER THREE

## ON THE NUMERICAL SOLUTION OF INTEGRAL EQUATION.

## 3.1- Introduction.

In the last chapter, the problem of two-dimensional scattering was rigorously formulated in the form of a set of integral equations. These equations however are of little use unless they can be reduced to approximate forms which can either be evaluated analytically or can be computed numerically with the aid of a digital computer. The choice between these two approaches largely depends on the characteristic dimensions of the scatterer.

For scatterers of arbitrary shape, whose dimensions are either very small or very large with respect to the wavelength, the classical Rayleigh scattering theory and the physical optics approximations will yield fairly accurate results. In the intermediate range, the numerical procedure known as the method of moments (appendix A) has proven to be the most efficient approximate method for obtaining results of acceptable accuracy. The result of the application of this approach to scattering problems is essentially a transformation of the original integral equation into a set of  $N$  linear equations in  $N$  unknowns. A linear combination of the  $N$  unknowns forms an approximation to the original unknown quantity appearing in the associated integral

equation.

The above procedure may be cast into a matrix equation of the form,

$$(A)(f) = (g) \quad (3.1)$$

where (A) is the coefficient matrix, (f) is the unknown quantity and (g) is the known quantity of the matrix equation. The matrix equation 3.1 may be solved numerically, however, in methods using factorization or inversion, the required computer time for solving 3.1 is approximately given by,

$$T \propto aN^2 + bN^3 \quad (3.2)$$

where a and b are proportionality factors, N is the number of unknowns (matching points) and  $aN^2$  and  $bN^3$  account for the calculation of the coefficient matrix and the solution of 3.1 respectively.

The accuracy of the solution largely depends on the number of sampling points N and the approximate methods used for evaluation of the elements of the matrix (A). Since the determination of (A) requires approximate evaluation of sub integrals over N intervals or areas (depending on the configuration of the scatterer), a better accuracy would require more accurate approximation techniques. This in turn

results in a higher value for the proportionality factor  $a$  appearing in 3.2. In view of the relation 3.2, it seems advantageous to keep  $N$  as low as possible and use more accurate techniques for evaluating  $(A)$ , which in fact, within certain limits, yields the same accuracy with a less computation time. However, there is a lower limit for  $N$ , beyond which the accuracy of the solution would greatly be impaired. Andreassen<sup>2</sup>, by a reasoning similar to Shannon's communication theorem, has shown that for a smooth portion of the scatterer, the distance between two adjacent sampling points must not exceed  $\lambda/4$ . Furthermore, for regions close to the sharp edges, additional sampling points must be introduced.

From the above argument and in view of the relation 3.2, the limitation of the method of moment for analyzing scattering problems which involve large scatterers can be realized. When the characteristic dimension of the scatterer is more than a few wavelengths, solution via factorization or inversion can no longer be seriously considered. Aside from the excessive computer running time, the accumulation of error, while inverting large matrices, greatly impairs the accuracy of the solution thus obtained. For the case of scatterers of moderate size further difficulties may also arise from the complexity of the geometry and an accurate solution becomes too complicated and costly to obtain. Here the application of the higher order approximate methods for

expanding the unknown quantity and better numerical techniques for evaluating the coefficient matrix becomes too complex and costly to be useful. On the other hand, simple approximation techniques result in slowly converging solutions for large values of  $N$ . As it will be shown later, when dealing with conducting objects for which the standing wave effects are more pronounced than non-metallic ones, a true convergent solution may not be obtained even for segment sizes of the order of  $(0.1\lambda)$ . The situation becomes worse when there exists regions with large curvatures on the structure.

In order to overcome these problems, in a recent paper (Tew<sup>22</sup>) has employed the concept of using a priori knowledge of the solution, to improve the convergence of the moment solution. He has applied this method, for the case of two-dimensional scattering from a perfectly conducting strip, illuminated by a plane wave. This method is essentially a combination of the physical optics approximation and point matching technique.

The idea is that known approximation such as the physical optics current may be subtracted from the unknown total current. The resulting integral equation then must be solved for the difference current distribution  $J_d$  which then becomes the unknown quantity of the integral equation thus obtained. Naturally, one expects that the residual difference current converges more rapidly, since the

physical optics approximation for fairly large objects gives acceptable result for induced current distribution over the smooth portions of the scatterer.

Once the difference current is determined by numerical techniques, the total distribution can be obtained by summing the two currents,

$$\mathbf{J} = \mathbf{J}_{po} + \mathbf{J}_d \quad (3.3)$$

The usefulness of this method becomes more significant when the dimension of the scattering object is too large to be handled by direct moment method. For this kind of scatterers, the difference current may be set to zero in the regions where the physical optics approximation is sufficiently accurate. This will reduce the size of the matrix equation to be solved and it would become feasible to obtain a reasonably accurate solution to the associated integral equation.

It is the purpose of this chapter to extend the application of an "a priori knowledge", to the problem of (TM) scattering from large conducting circular cylindrical reflectors which cannot otherwise be handled by a direct moment method.

### 3.2- Modified moment method formulation.

In the last chapter it was shown that a solution of the electromagnetic fields in the presence of an infinitely long conducting cylinder of arbitrary cross section, illuminated normally by a z-polarized incident field parallel to the axis of the cylinder can be obtained by,

$$\tilde{\mathbf{E}}(\tilde{\rho}) = \mathbf{T} \tilde{\mathbf{E}}_i(\tilde{\rho}) - (\mathbf{T}k\eta/4) \int_c \mathcal{J}(\tilde{\rho}') H_0^2(k|\tilde{\rho}-\tilde{\rho}'|) dc' \quad (3.4)$$

$$\begin{aligned} \tilde{\mathbf{H}}(\tilde{\rho}) = \tilde{\mathbf{H}}_t(\tilde{\rho}) = \mathbf{T} \tilde{\mathbf{H}}_{it}(\tilde{\rho}) + (\mathbf{T}k/4j) \int_c \mathcal{J}(\tilde{\rho}') H_1^2(k|\tilde{\rho}-\tilde{\rho}'|) \\ \{ \sin\{\tilde{\rho}', (\tilde{\rho}-\tilde{\rho}')\} \hat{\rho}' + \cos\{\tilde{\rho}', (\tilde{\rho}-\tilde{\rho}')\} \hat{\phi}' \} dc' \end{aligned} \quad (3.5)$$

For brevity and clarity of the approach, we consider the geometry of figure 3.1.

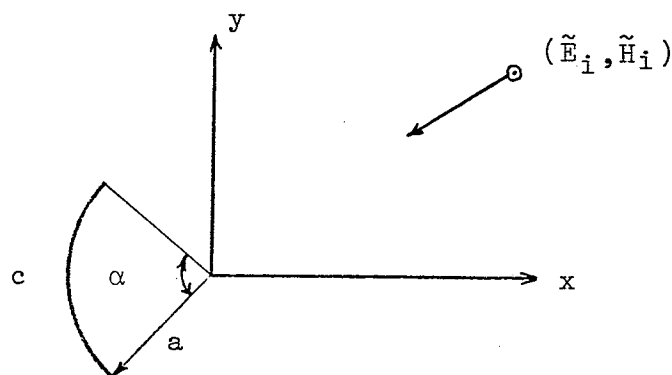


Figure 3.1 Cross sectional view of the problem.

Where the cross section of the cylinder is a circular arc of arbitrary radius  $a$ , measured from the origin of the coordinate system,  $C$  is the contour of the cylinder and  $(\alpha)$  is the angle subtended by  $C$ .

On the boundary of the cylinder, one may write,

$$\begin{aligned} \vec{J}_s(\vec{\rho}) &= \hat{n} \times \vec{H}(\vec{\rho}) = 2\hat{n} \times \vec{H}_i(\vec{\rho}) - (k/2j) \int_C \vec{J}(\vec{\rho}') \\ &\cdot H_1^2(k|\vec{\rho}-\vec{\rho}'|) \cos(\hat{n}', \vec{\rho}-\vec{\rho}') \, dc' \end{aligned} \quad (3.6)$$

Recalling the well known physical optics approximation,

$$\vec{J}_{po}(\vec{\rho}) = \begin{cases} 2 \hat{n} \times \vec{H}_i(\vec{\rho}) & \text{illuminated region} \\ 0 & \text{shaded region} \end{cases} \quad (3.7)$$

and comparing it with the equation 3.6, one comes to the conclusion that physical optics approximation results from completely neglecting mutual interaction effects on the illuminated portion of the object. Furthermore, this approximation assumes that in the shadow region, the mutual interaction term completely cancels the incident field. For a large scatterer of smooth curved contour, the contribution from the integral term over the central portion of  $C$ , where it is free of discontinuities, may be neglected without

incurring a significant error in the solution. Nevertheless, the inability of the physical optics approximation to represent the current distribution over the regions with sharp discontinuities and shadow boundaries can be a source of significant error.

To overcome this difficulty, we may assume the correct distribution over the contour  $C$  to be the sum of the physical optics term and a difference current, which is unknown and accounts for any discrepancies of the physical optics approximation from the true current distribution. This can be formally represented by,

$$\tilde{J}(\rho) = \tilde{J}_{po}(\tilde{\rho}) + \tilde{J}_d(\tilde{\rho}) \quad (3.8)$$

According to the geometry of the problem considered here (figure 3.1) and the direction of the polarization of the incident field, the induced current and the electric field will be z-directed and the total field at any point on the transverse plane is given by,

$$\begin{aligned} E(\tilde{\rho}) &= E_i(\tilde{\rho}) - (k\eta/4) \int \{ \tilde{J}(\tilde{\rho}') + \tilde{J}_d(\tilde{\rho}') \} \\ &\cdot H_0^2(k|\tilde{\rho}-\tilde{\rho}'|) d\tilde{c}' \end{aligned} \quad (3.9)$$

where,

$$\tilde{J}_{po}(\tilde{\rho}) = 2|\hat{n} \times H_i(\tilde{\rho})| \quad (3.10)$$

and it is understood that J's and E's are z-directed and subscript z is dropped for convenience.

Applying the boundary condition on C and rearranging 3.9 leads to,

$$\begin{aligned} E_z(\tilde{\rho}_c) &= (k\eta/4) \int_C J_{p_0}(\tilde{\rho}') H_0^2(k|\tilde{\rho}_c - \tilde{\rho}'|) dc' \\ &= (k\eta/4) \int_C J_d(\tilde{\rho}') H_0^2(k|\tilde{\rho}_c - \tilde{\rho}'|) dc' \end{aligned} \quad (3.11)$$

Now, the unknown quantity of the integral equation is  $J_d$  and the equation 3.11 can be solved by standard moment method procedure given in appendix A. As it is seen from 3.11,  $J_d$  accounts for only a part of the total induced current on the surface of the scatterer. Therefore error resulting from the numerical processing of the associated matrix equation only affects a part of the total induced current.

The integral appearing on the left hand side of 3.11 also needs to be evaluated numerically. Even though the computational error, to some extent, is compensated for by  $J_d$  in the process of determining the difference current (in view of self correcting scheme of the equation 3.11), nevertheless, more accurate evaluation of this integral will result in a faster converging solution.

Considering excitation by a z-directed line source of strength ( $I=1$ ), located at  $(\tilde{\rho}_s)$ , we have,

$$E_1(\tilde{\rho}) = -(k\eta/4) H_0^2(k|\tilde{\rho}-\tilde{\rho}_s|) \quad (3.12)$$

$$\begin{aligned} J_{po}(\tilde{\rho}_c) &= 2|\hat{n} \times H_1(\tilde{\rho}_c)| = (kj/2) H_1^2(k|\tilde{\rho}_c-\tilde{\rho}|) \{a-\rho_s \cos(\phi-\phi_s)\} \\ &/ \{ \sqrt{a^2+\rho_s^2-2a\rho_s \cos(\phi-\phi_s)} \} \end{aligned} \quad (3.13)$$

where  $(\tilde{\rho}_s)$  is the radial distance from the origin to the source point and  $(\phi)$  and  $(\phi_s)$  are the polar angles of  $(\tilde{\rho})$  and  $(\tilde{\rho}_s)$  respectively. Substituting the equations 3.12 and 3.13 into 3.11 leads to,

$$\begin{aligned} &- H_0^2(k|\tilde{\rho}_c-\tilde{\rho}_s|) - (jka/2) \int_{\alpha} H_1^2(k|\tilde{\rho}'-\tilde{\rho}_s|) H_0^2(k|\tilde{\rho}_c-\tilde{\rho}'|) \\ &\{ a - \rho_s \cos(\phi'-\phi_s) \} / \{ \sqrt{a^2+\rho_s^2-2a\rho_s \cos(\phi'-\phi)} \} d\phi' \\ &= a \int_{\alpha} J_d(\tilde{\rho}') H_0^2(k|\tilde{\rho}_c-\tilde{\rho}'|) d\phi' \end{aligned} \quad (3.14)$$

where a use has been made of,

$$dc = a d\phi \quad (3.15)$$

The equation 3.14 can be solved for  $J_d$  with the aid of the method of moment. Application of this method to 3.14 will reduce the integral equation to the approximate matrix equation,

$$(A)(f) = (g) \quad (3.16)$$

where,

$$J_d = f = \sum_{n=1}^N f_n \quad (3.17)$$

Choosing the pulse and Dirac's delta functions as the expansion and the testing functions respectively, we find that,

$$A_{mn} = \begin{cases} \Delta C_n H_0^2(k|\tilde{\rho}_m - \tilde{\rho}_n|) & m \neq n \\ \Delta C_n \{ 1 - (2j/\pi) \text{Ln}(k\Delta C_n \gamma/4e) \} & m = n \end{cases} \quad (3.18)$$

$$g_m = -H_0^2(k|\tilde{\rho}_m - \tilde{\rho}_s|) - (jka/2) \int_{\alpha} H_1^2(k|\tilde{\rho}' - \tilde{\rho}_s|) H_0^2(k|\tilde{\rho}_m - \tilde{\rho}'|) \\ \cdot \{ a - \rho_s \cos(\phi' - \phi_s) \} / \{ \sqrt{a^2 + \rho_s^2 - 2a\rho_s \cos(\phi' - \phi_s)} \} d\phi' \quad (3.19)$$

where  $(\tilde{\rho}_m)$  is the position vector of the mid-point of the interval  $\Delta C$ ,  $(e)$  is the Neper constant given by,

$$e = 2.718282 \quad (3.20)$$

and,

$$\gamma = 1.781072 \quad (3.21)$$

Since the scatterer is symmetric about the  $x$ -axis, a symmetrical choice of matching points about this axis yields a symmetric coefficient matrix  $(A)$ . It is shown<sup>2</sup> that by expanding the unknown induced current into a sum of odd and even functions of  $(\phi)$ , it is always possible to reduce the original matrix equation into two independent sets of linear equations in  $(N/2)$  unknowns, no matter what the exciting field is. This would save a substantial amount of computer time, since the time required to solve  $N$  linear equations is proportional to  $N^3$ . However for the problem considered here, due to the symmetric behavior of current distribution about the  $x$ -axis, further simplification occurs, since it is only necessary to solve one set of linear equations in  $N/2$  unknowns.

To clarify, we consider the equation 3.16. This equation represents  $N$  linear equations in  $N$  unknowns given by,

$$\sum_{n=1}^N A_{mn} f_n = g_m \quad m = 1, 2, 3, \dots, N$$

$$(3.22)$$

Since,

$$f_n = f_{N+1-n}$$

and,

$$A_{mn} = A_{nm}$$

the equation 3.22 can be reduced to,

$$\sum_{n=1}^{N/2} (A_{mn} + A_{nm}) f_n = g_m \quad m = 1, 2, 3, \dots, N/2 \quad (3.25)$$

therefore it is only needed to solve the above set of linear equations and determine the total current distribution over the scatterer by using the equation 3.22.

As it was stated before, for a fast convergent solution the integral term of 3.19 should be evaluated as accurate as possible. Because of the singularity of Hankel function at  $(\tilde{\rho}' = \tilde{\rho}_m)$ , the main contribution to the integral term of 3.19 is expected to be due to the part of the contour  $C$  in the vicinity of the observation point  $\tilde{\rho}_m$

where the integrand varies most rapidly. Therefore the integrand must be adequately sampled in this region. For this reason, in all the computations of this chapter, integration of the physical optics term over the singular region has been performed using fortyth-order Gaussian quadrature to provide a dense sampling in the immediate vicinity of  $(\tilde{\rho}_m)$ . The evaluation of the integral over the

rest of the contour C has been performed using the same integration method but of order ten. This provides tapering to a lighter sampling as one moves away from the singular region and will avoid unnecessary computation time for regions where their contribution to the integral is not significant.

Determination of each element ( $g_m$ ) of 3.19 requires evaluation of an integral over the entire contour C of the scatterer. However, for the special case when the driving element is located at the origin of the coordinate system and ( $\alpha = \pi$ ), substantial saving in computation time can be achieved through the use of a combination of analytical and numerical techniques. This approach differs from those of strictly numerical or analytical techniques. To clarify the problem, recall the equation 3.14,

$$\begin{aligned}
 & - H_0^2(k|\tilde{\rho}-\tilde{\rho}'|) - (jka/2) \int_{\alpha} H_1^2(k|\tilde{\rho}'-\tilde{\rho}'|) H_0^2(k|\tilde{\rho}-\tilde{\rho}'|) \\
 & \cdot |a - \rho_s \cos(\phi' - \phi_s)| / |\sqrt{a^2 + \rho_s^2 - 2a\rho_s \cos(\phi' - \phi_s)}| d\phi' \\
 & = a \int_{\alpha} J_d(\tilde{\rho}') H_0^2(k|\tilde{\rho}-\tilde{\rho}'|) d\phi' \quad (3.26)
 \end{aligned}$$

Setting,

$$\rho_s = 0$$

$$\alpha = \pi$$

leads to,

$$\begin{aligned}
 & - H_0^2(k\tilde{\rho}) - (jka/2) H_1^2(ka) \int_{\pi/2}^{3\pi/2} H_0^2(k|\tilde{\rho}-\tilde{\rho}'|) d\phi' \\
 & = a \int_{\pi/2}^{3\pi/2} J_d(\tilde{\rho}') H_0^2(k|\tilde{\rho}-\tilde{\rho}'|) d\phi' \quad (3.27)
 \end{aligned}$$

The integral on the left hand side may be written as,

$$I = \int_{\pi/2}^{3\pi/2} H_0^2\{2ka|\sin(\phi-\phi')/2|\} d\phi' \quad (3.28)$$

A change of variable in the form of,

$$(\phi-\phi')/2 = \psi \quad (3.29)$$

reduces the equation 3.28 to,

$$\begin{aligned}
 I & = 2 \int_0^{\frac{\phi}{2} - \frac{\pi}{4}} H_0^2(2ka \sin\psi) d\psi + 2 \int_0^{\pi/2} H_0^2(2ka \sin\psi) d\psi \\
 & - 2 \int_{\frac{3\pi}{4} - \frac{\phi}{2}}^{\pi/2} H_0^2(2ka \sin\psi) d\psi \quad (3.30)
 \end{aligned}$$

The second term on the right hand side of the above equation is a known integral given by,

$$\begin{aligned}
 \int_{\pi/2}^{\pi} H_0^2(2ka \sin\psi) d\psi & = \int_0^{\pi/2} H_0^2(2ka \sin\psi) d\psi \\
 & = (\pi/2) J_0(ka) \{1 - j Y_0(ka)\} \quad (3.31)
 \end{aligned}$$

where  $J_0$  and  $Y_0$  are Bessel and Neumann functions of zero order, respectively. Substitution of 3.31 into 3.30 results in,

$$I = 2 \int_{\pi/2}^{\phi/2} H_0^2(2ka \sin\psi) d\psi - 2 \int_{\pi-\phi/2}^{\pi} H_0^2(2ka \sin\psi) d\psi + \pi J_0(ka) \{1 - j Y_0(ka)\} \quad (3.32)$$

For interpreting each term of 3.32, we consider figure 3.2.

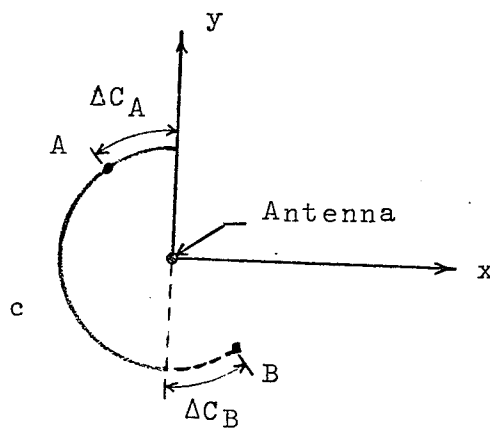


Figure 3.2 Selection of the imaginary arc.

where C is the actual contour of the object, A is the location of the matching point and,

$$\Delta C_B = \Delta C_A$$

is an imaginary circular arc of the same radius as C, added

to the actual contour for utilizing the known integral given earlier. The first term of 3.32 accounts for the contribution from  $(\Delta C_A)$  to the integral (I). The third term represents the contribution from the rest of the contour plus the contribution from the imaginary arc  $(\Delta C_B)$ . Finally the second term is added to cancel the contribution due to  $(\Delta C_B)$ .

From the foregoing argument it is clear that instead of numerical integration over the entire contour  $C$ , it is only sufficient to perform two numerical integrations over  $(\Delta C_A)$  and  $(\Delta C_B)$ . As the matching point  $A$  moves toward the centre of the scatterer,  $(\Delta C_A)$  and  $(\Delta C_B)$  increase and require more computation time. However, since  $(\Delta C_A + \Delta C_B)$  never exceeds  $C$ , the amount of computer running time for determining the elements of  $(g_m)$  would always be less than the case of numerical integration over the entire contour.

## 3.3- Radiation field.

Having obtained the induced surface current, it is next desired to compute the radiation field. This can be done by utilizing the formulas given in the last section. For instance, in the case of excitation by a line source, the total field in the transverse plane is given by,

$$\begin{aligned}
 E(\tilde{\rho}) = & - (k\eta/4) H_0^2(k|\tilde{\rho}-\tilde{\rho}_s|) - (jk^2na/8) \int_{\alpha} H_1^2(k|\tilde{\rho}'-\tilde{\rho}_s|) \\
 & \cdot H_0^2(k|\tilde{\rho}-\tilde{\rho}'|) \{ a - \rho_s \cos(\phi'-\phi) \} \{ a^2 + \rho_s^2 - 2a\rho_s \\
 & \cdot \cos(\phi'-\phi) \}^{-\frac{1}{2}} d\phi' - (k\eta a/4) \int_{\alpha} J_d(\tilde{\rho}') H_0^2(k|\tilde{\rho}-\tilde{\rho}'|) d\phi'
 \end{aligned}
 \tag{3.33}$$

Letting  $(\tilde{\rho})$  approaches infinity, this leads to a relation for the field given by,

$$\begin{aligned}
 E(\tilde{\rho}) = & - (k\eta/4) \sqrt{(2j/\pi k\rho)} \exp(-jk\rho) \{ \exp(jk\rho_s \cos(\phi-\phi_s)) \} \\
 & k\rho \rightarrow \infty \\
 & + (jka/2) \int_{\alpha} H_1^2(k|\tilde{\rho}'-\tilde{\rho}_s|) \{ a - \rho_s \cos(\phi'-\phi) \} \\
 & / \sqrt{ \{ a^2 + \rho_s^2 - 2ka\rho_s \cos(\phi'-\phi) \} } \exp(jka \cos(\phi-\phi')) d\phi' \\
 & + a \int_{\alpha} J_d(\tilde{\rho}') \exp(jka \cos(\phi-\phi')) d\phi'
 \end{aligned}
 \tag{3.34}$$

where a use has been made of the large argument asymptotic expansion formula for the Hankel function,<sup>36</sup>

$$H_n^2(z) \sim \sqrt{(2/\pi z)} \exp(-j(z - n\pi/2 - \pi/4)) \quad (3.35)$$

In view of the approximation used for determining  $J_d$ , the last integral term of 3.34 can be approximated to,

$$\sum_{n=1}^N f_n \Delta C_n \exp(jka \cos(\phi - \phi'_n)) \approx \int_c^d J(\tilde{\rho}') \exp(jka \cos(\phi - \phi')) dc' \quad (3.36)$$

The first integral term of 3.35 must be evaluated by numerical methods. However, for the special case ( $\rho_s = 0$ ), the equation 3.33 can be reduced to a form which requires no integration. This approach utilizes the "addition theorem"<sup>34</sup> of the Bessel functions represented by,

$$H_0^2(k|\tilde{\rho} - \tilde{\rho}'|) = \sum_{n=1}^{\infty} \epsilon_n J_n(k\rho') H_n^2(k\rho) \cos n(\phi - \phi') \quad \rho > \rho' \quad (3.37)$$

$$H_0^2(k|\tilde{\rho} - \tilde{\rho}'|) = \sum_{n=1}^{\infty} \epsilon_n J_n(k\rho) H_n^2(k\rho') \cos n(\phi - \phi') \quad \rho < \rho' \quad (3.38)$$

where ( $\epsilon_n$ ) is Neumann factor given by,

$$\epsilon_n = \begin{cases} 1 & n = 0 \\ 2 & n \neq 0 \end{cases}$$

Hence,

$$\begin{aligned}
 E(\vec{\rho}) \approx & - (k\eta/4) \sqrt{(2j/\pi k\rho)} \exp(-jk\rho) \{ 1 + (jka/2) \\
 & k\rho \rightarrow \infty \\
 & \cdot H_1^2(ka) \sum_{p=1}^{\infty} \frac{J_p(ka)}{p} \exp(jp\pi/2) \int_{\pi/2}^{3\pi/2} \cos p(\phi-\phi') d\phi' \\
 & + \sum_{n=1}^N f_n \Delta C_n \exp(jka \cos(\phi-\phi'_n)) \} \quad (3.39)
 \end{aligned}$$

But,

$$\int_{\pi/2}^{3\pi/2} \cos p(\phi-\phi') d\phi' = \begin{cases} 0 & p \text{ even} \\ \pi & p = 0 \\ (2/p) \sin(\phi-\pi/2) & p \text{ odd} \end{cases}$$

therefore,

$$\begin{aligned}
 E(\vec{\rho}) = & - (k\eta/4) \sqrt{(2j/\pi k\rho)} \exp(-jk\rho) \{ 1 + (jka/2) \\
 & k\rho \rightarrow \infty \\
 & \cdot H_1^2(ka) \{ \pi J_0(ka) + 4j \sum_{p \text{ odd}}^{\infty} \frac{J_p(ka)}{p} \sin(p\pi/2) \sin p(\phi-\pi/2) \\
 & /p \} + \sum_{n=1}^N f_n \Delta C_n \exp(jka \cos(\phi-\phi'_n)) \} \quad (3.41)
 \end{aligned}$$

The infinite series appearing in 3.41 is a fast converging series due to the presence of the factor  $(1/p)$  and the property of the Bessel functions which reduce rapidly for orders larger than the argument. Therefore, it is possible to truncate the infinite series after a few terms without incurring a significant amount of error in the solution. According to the definition of the radiation pattern, the equation 3.41 immediately gives,

$$R(\phi) = \frac{|E|^2}{|E|_{\phi=0}^2} \quad (3.42)$$

### 3.4- Numerical results.

A computer program based on the earlier sections was written to evaluate the physical optics integral, the difference current distribution and the radiation field for the antenna geometry shown in figure 3.1. As an indication of the validity of the computer program, the radiation field of a conducting circular cylinder in the presence of a line source was calculated and compared against the results obtained for the same problem, using the exact solution in terms of the harmonic series<sup>34</sup>. The result is shown in figure 3.3. Excellent agreement between the analytical and the numerical solutions is evident. For  $0.12\lambda$  sampling interval, the accuracy over a wide range ( $0 < \phi < 150$ ) is approximately about 0.2 dB. However, for ( $\phi > 150$ ) the deviation from the analytical value increases and approaches to its maximum value 0.6 dB at ( $\phi = 180$ ), the centre of the shadow region.

The dependence of the numerical solution accuracy on the structure segmentation is shown by varying the sampling interval  $\Delta C$ . As it can be seen in figure 3.3, increasing  $\Delta C$  results in lower accuracy. However, even for  $\Delta C = 0.25\lambda$ , the error does not exceed 1.4 dB.

In order to show the improvement in the convergence of the moment method solution through the use of the physical optics approximation, the radiation pattern of a cylindrical reflector of radius ( $ka = 10$ ) and ( $\alpha = \pi$ ), in the

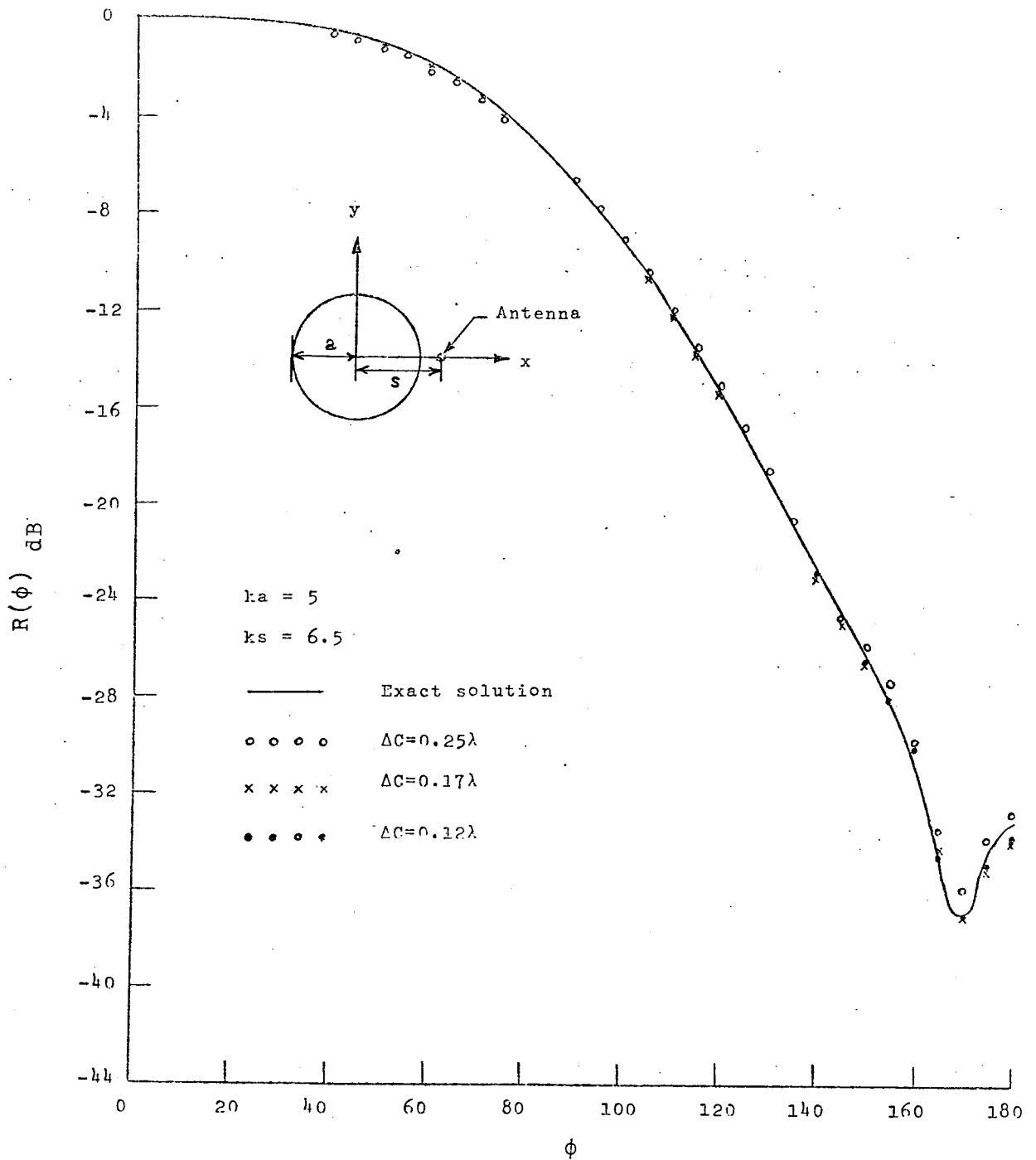


Figure 3.3 Radiation pattern of a circular cylinder

presence of a line source located at the origin of the coordinate system was computed by the "direct" and the "modified" moment methods. Figures 3.4 and 3.5 show the rate of the convergence of the radiation pattern for different values of the sampling interval for the two cases respectively. It is evident from figure 3.4 that, even for  $\Delta C = 0.05\lambda$ , the direct moment method does not yield a convergent solution. However, in the case of the modified moment method, a convergent solution can be achieved for step sizes not less than  $(0.17\lambda)$  which in turn results in less computer running time. Moreover, for both cases, when sampling interval is increased beyond  $0.25\lambda$ , the accuracy of the solution decreases rapidly.

In figures 3.6 and 3.7 the total normalized current distribution for both cases has been studied. As expected, in both figures, the singular behavior of the current distribution is localized to the edges of the reflector. This is due to the surface discontinuity (edges). Even though 3.6 and 3.7 show the same rate of convergence for various number of the segments on the reflector, the nature of the points on the two curves are quite different in these two figures. The points shown in figure 3.6 represents discrete pulses of current (line sources) distributed uniformly on the surface of the reflector. Therefore, between each two adjacent points, there is a sharp discontinuity of the current. However, in figure 3.7 each point represents a

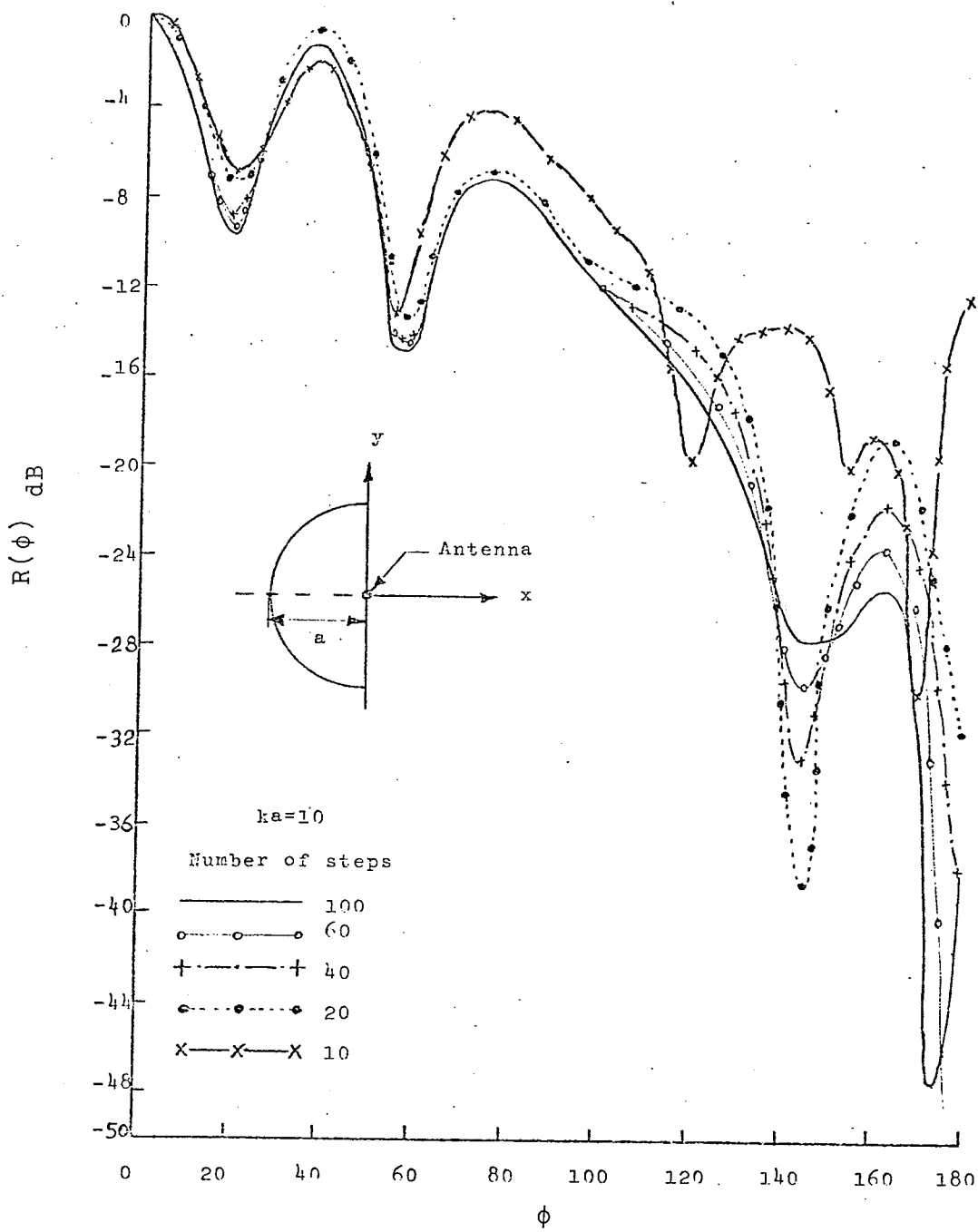


Figure 3.4 Radiation patterns by the moment method

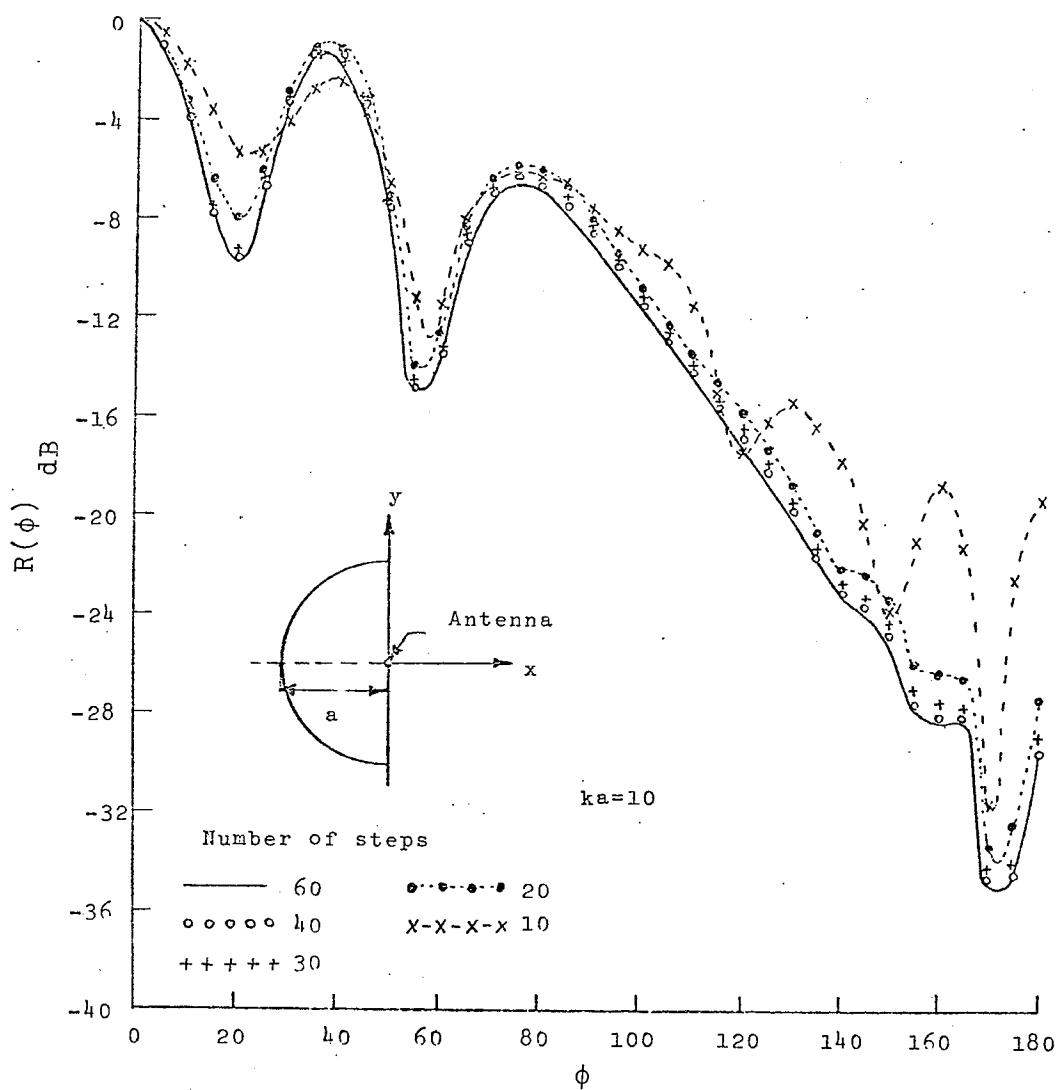


Figure 3.5 Radiation patterns by the modified moment method

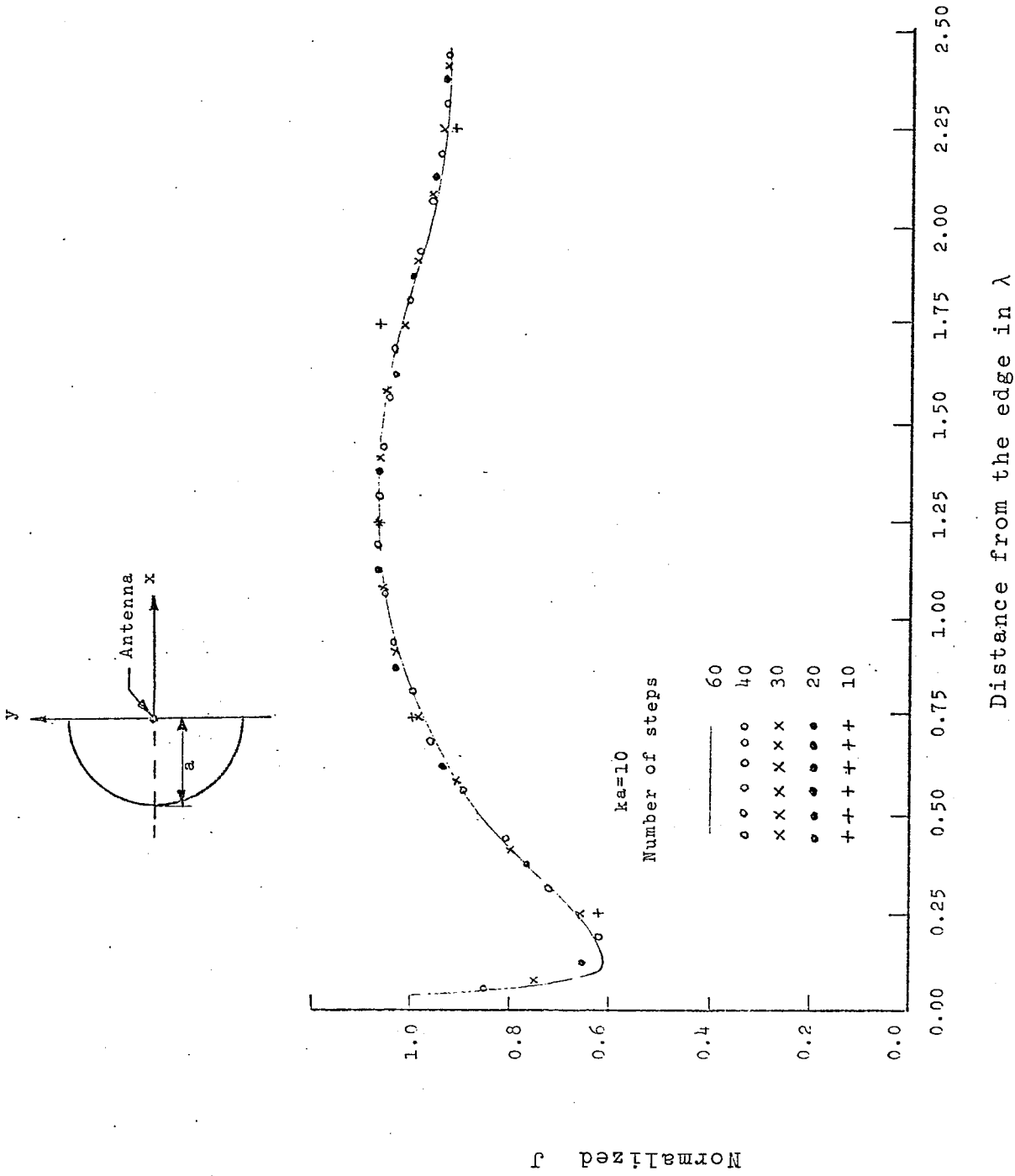


Figure 3.6 Behavior of the surface current by the moment method

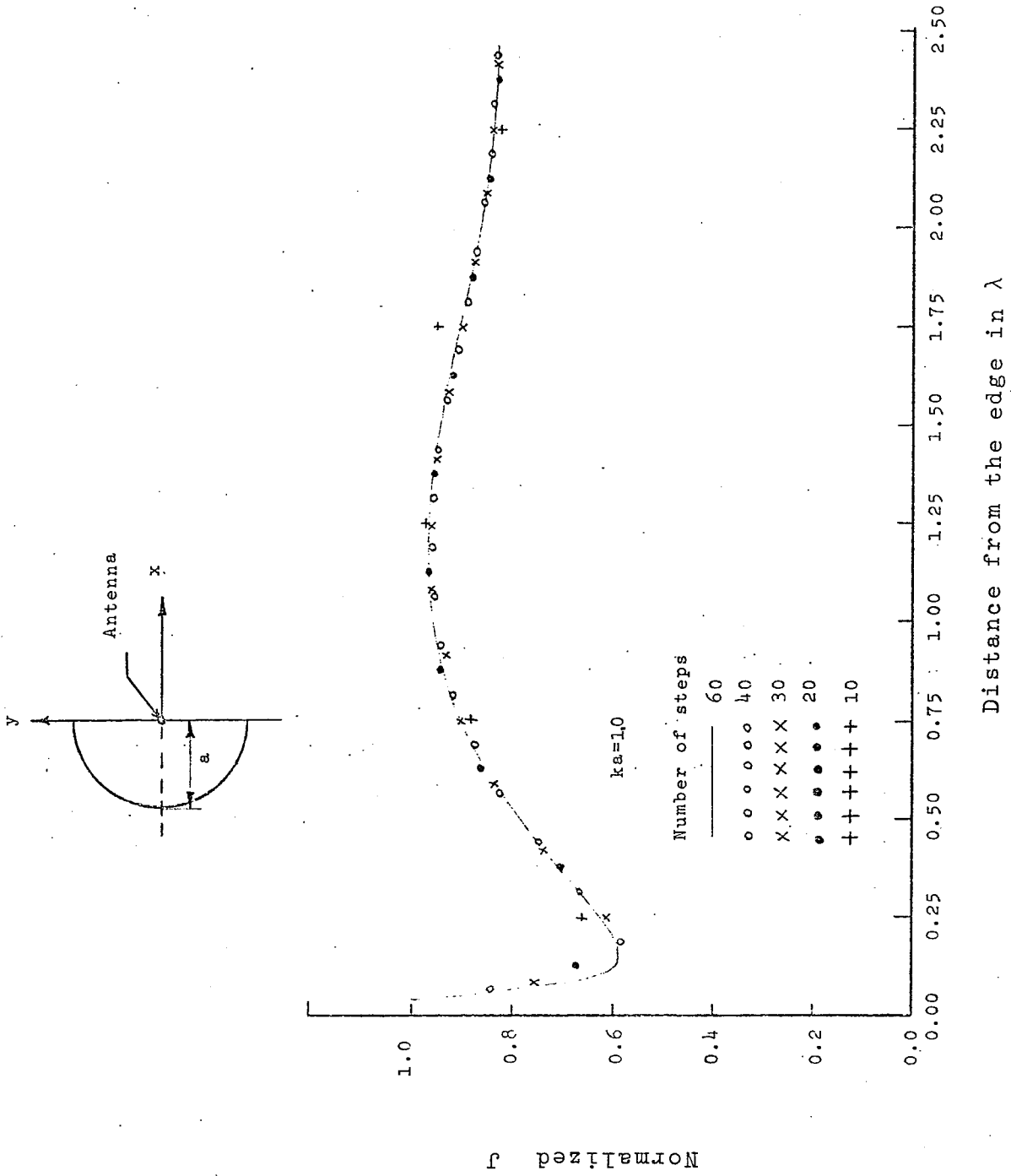


Figure 3.7 Behavior of the surface current by the modified moment method

small fraction of the total current at that point and they are superimposed as ripples on a current distribution (physical optics term) of a continuous nature.

Figures 3.8 and 3.9 depict the radiation patterns for the same geometry but the source is slightly off the centre of the reflector and are computed by the two different methods. Again, the advantage of the modified moment method in obtaining a fast converging solution is evident.

In order to investigate the effects of the source separation from the reflector, the radiation patterns for moderate source separations are computed by the modified moment method and are presented in figure 3.10. As expected, when the source moves away from the object, the variations of the pattern with polar axis ( $\phi$ ) increases with antenna separations. However, as the number of ripples increases, their size decreases, tending gradually to the total pattern of a uniform plane wave normally incident on the scatterer, a result that can be viewed as a check on the validity of the solution thus obtained.

The significant amount of increase in the rate of the convergence of the solution offered by the modified moment method, can be utilized to treat scattering problems involving objects with large cross sectional dimensions relative to the wavelength. Assuming the total current in the form,

$$\tilde{J} = \tilde{J}_{op} + \tilde{J}_d \quad (3.43)$$

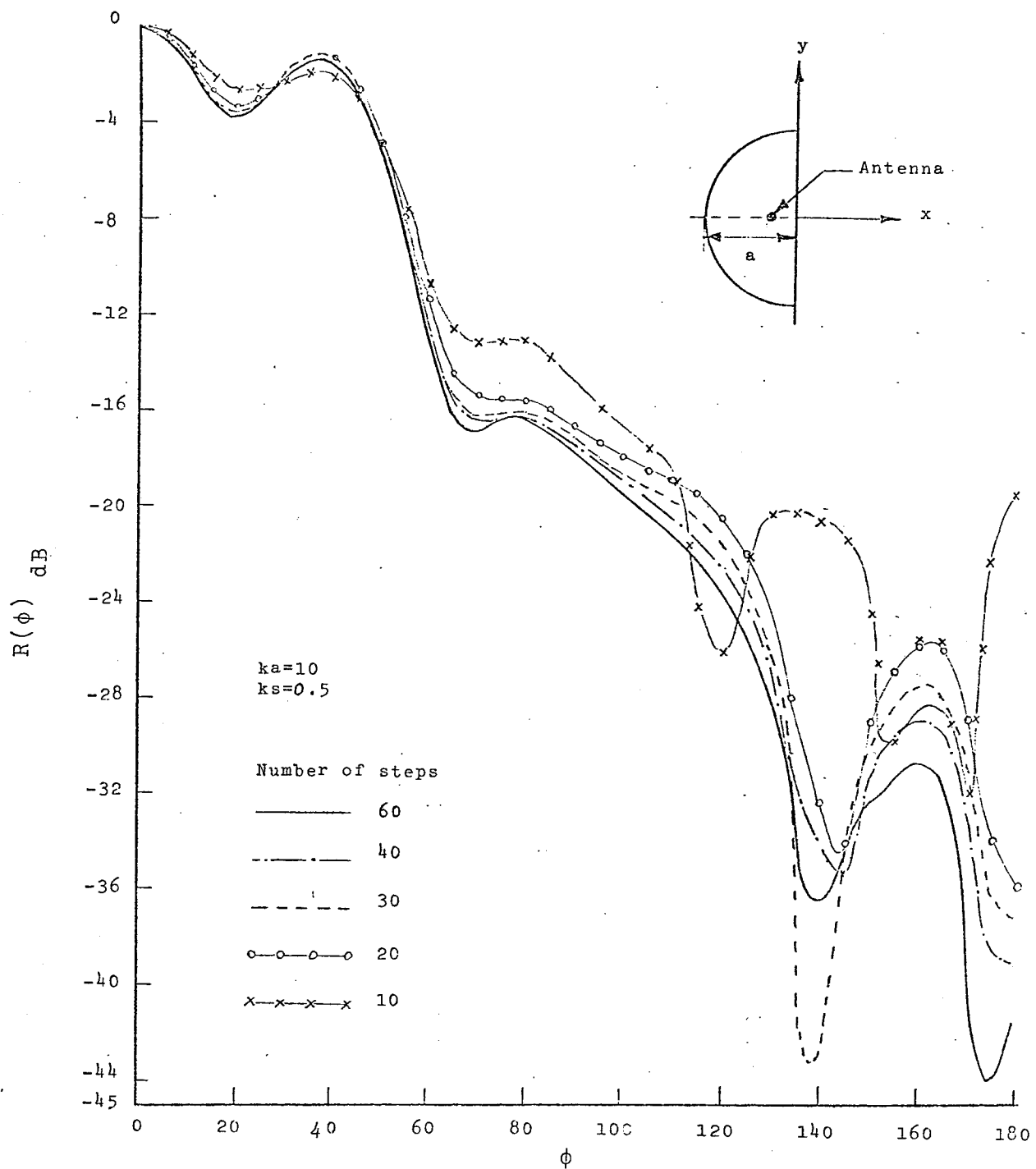


Figure 3.8 Radiation patterns for different step sizes by the moment method

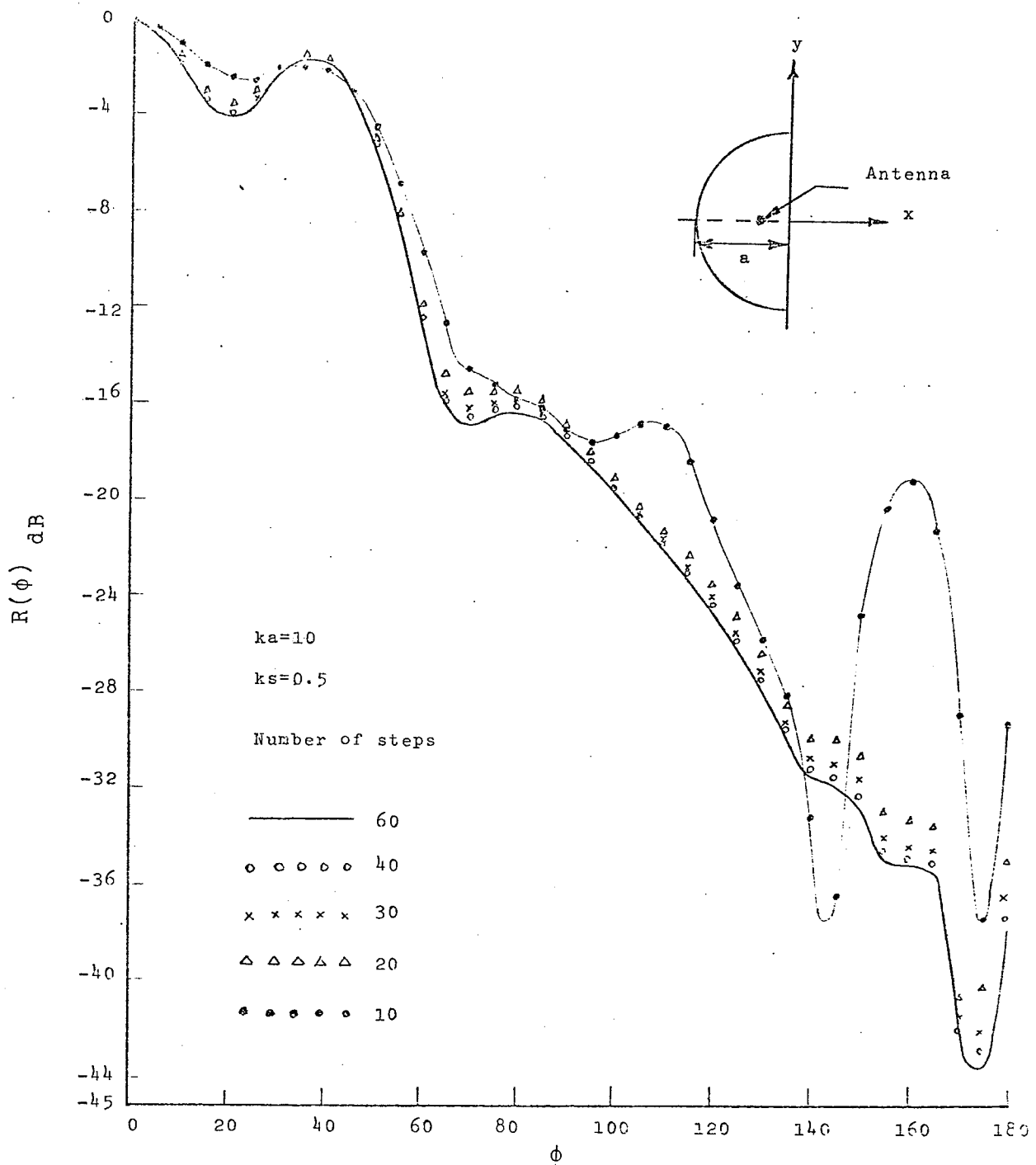


Figure 3.9 Radiation patterns for different step sizes by the modified moment method

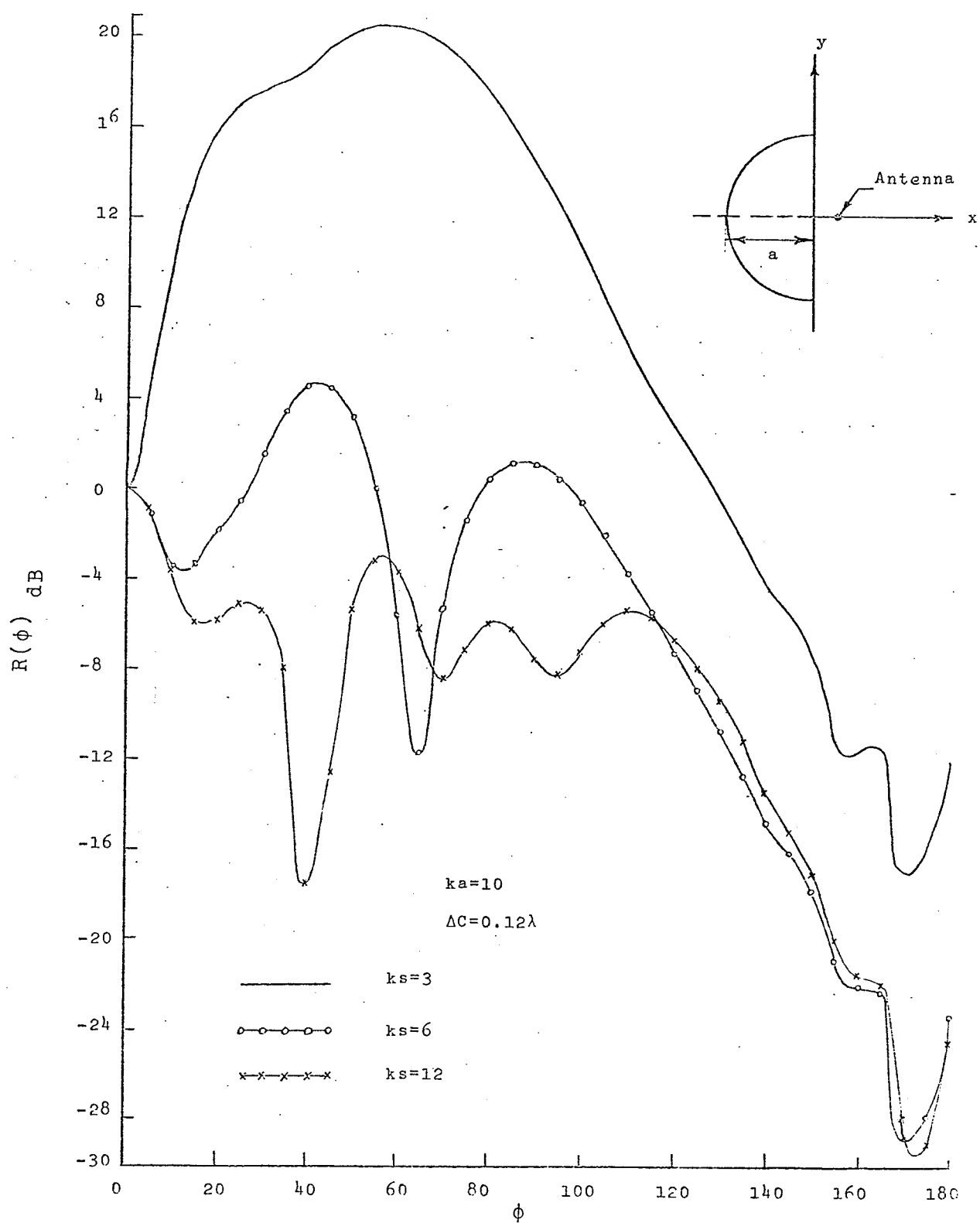


Figure 3.10 Radiation patterns for different source separations

$J_{op}$  is readily known from the incident field of the source and the difference current is the only unknown to be determined. However,  $J_d$  is due to the surface discontinuities and is localized to the edges of the reflector. Thus, as the reflector size increases, the contribution of ( $J_d$ ) decreases, but due to its localized nature,  $J_d$  can always be determined by choosing enough segments near the edges.

To study the case of large reflectors, the above argument has been applied to large reflectors and the results are given in figures 3.11 to 3.18. The difference current is now computed near the edges and its behavior is shown in these figures for two cases of ( $ka=50$ ) and ( $ka=100$ ). The residual current distribution has a significant value only near the reflector edges. The computed values are proved to be in good agreement and are shown for the following cases,

a- fixed sampling length (SL), but different segment size  $\Delta C$  (figures 3.11 and 3.12).

and,

b- fixed  $\Delta C$ , but different values of SL (figures 3.13 and 3.14). The radiation patterns are also computed for these cases and are shown in figures 3.15 to 3.18. Their agreement is excellent except near the centre of the shadow region. This discrepancy could be due to the location and magnitude of the edge currents, which are different for different step

sizes.

The application of the method to reflectors of different shapes and excitations is trivial, but in general numerical integrations are required to find the contribution of the physical optics currents.

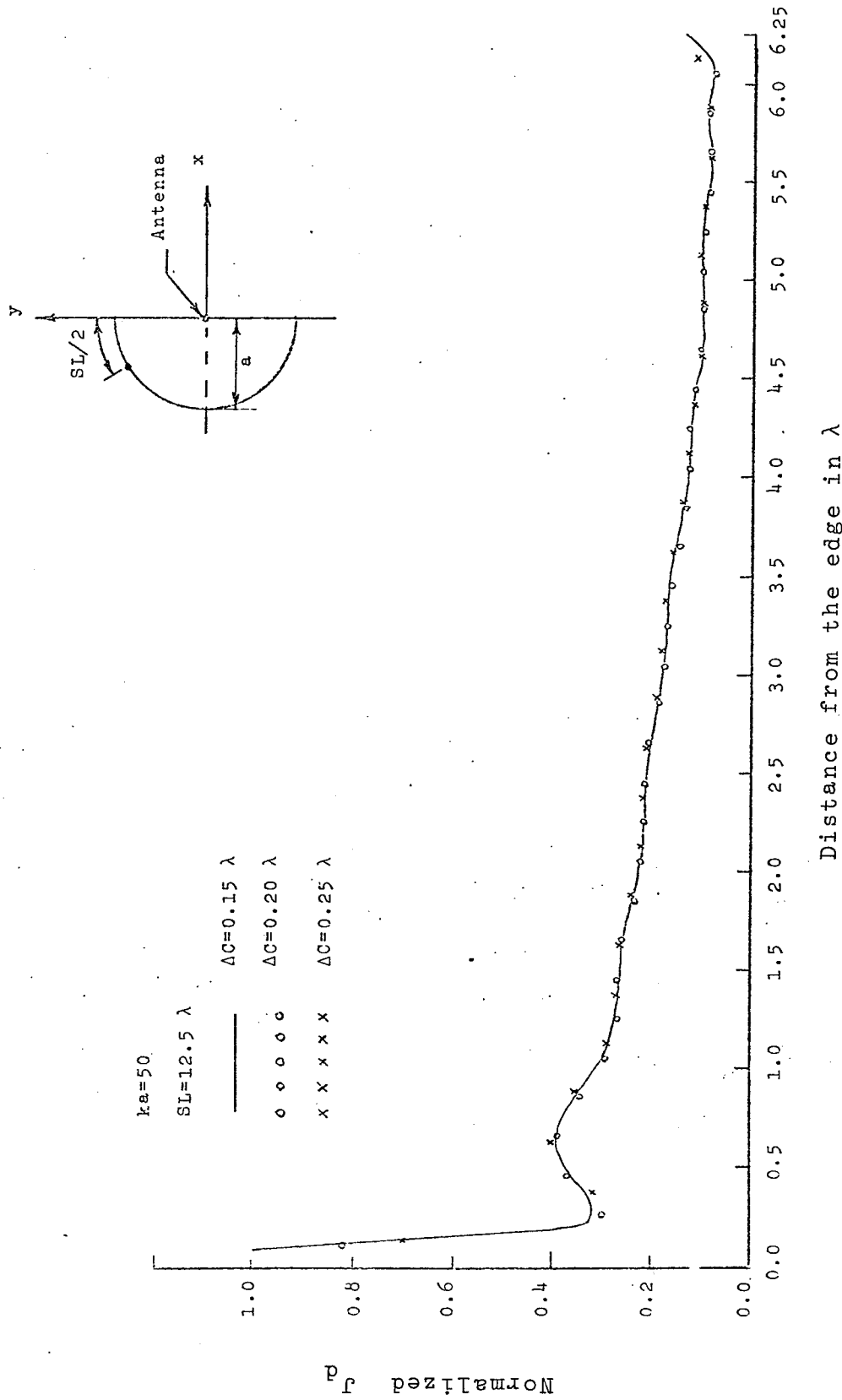


Figure 3.11 Behavior of the difference current for different step sizes

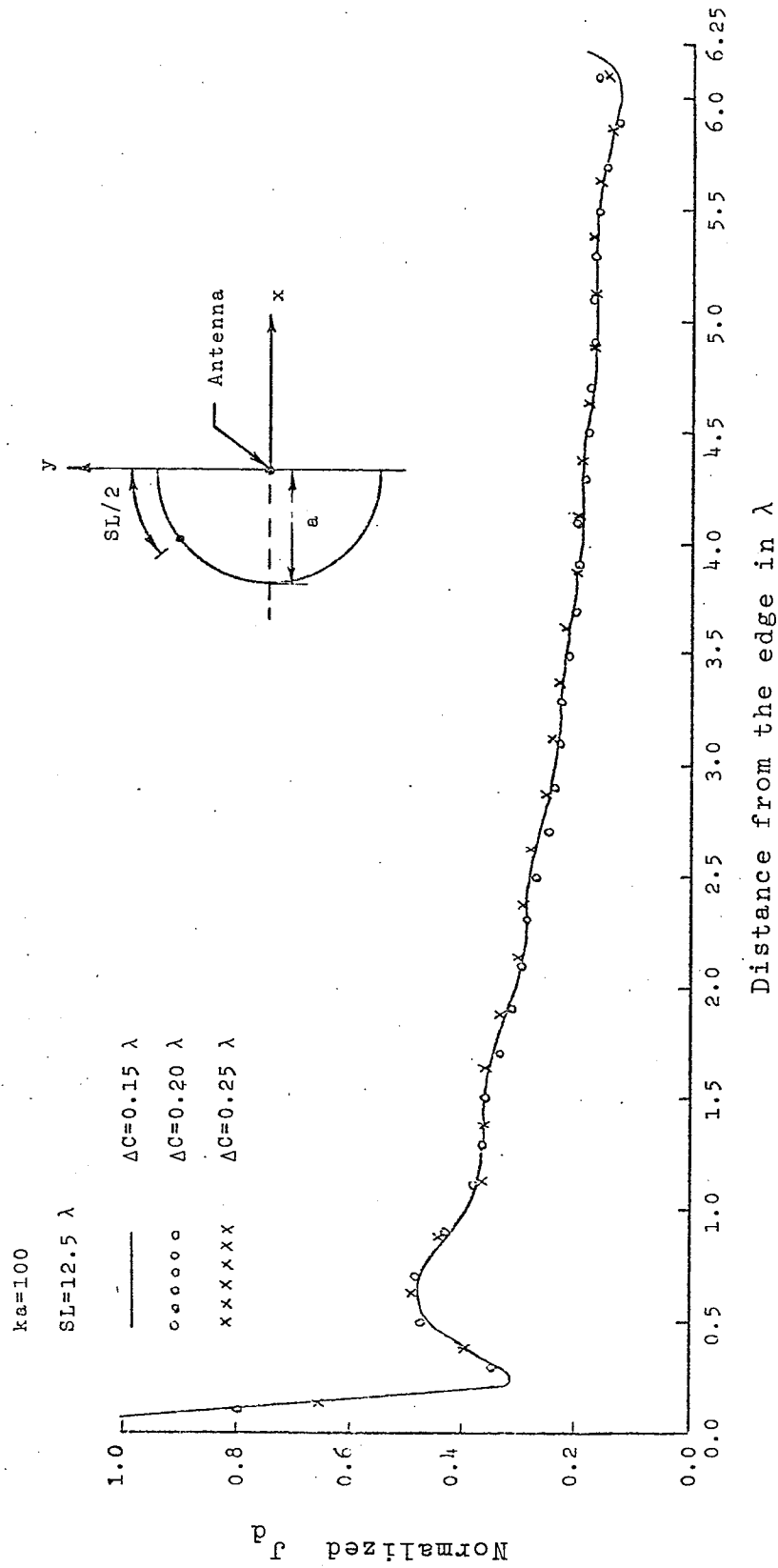


Figure 3.12 Behavior of the difference current for different step sizes

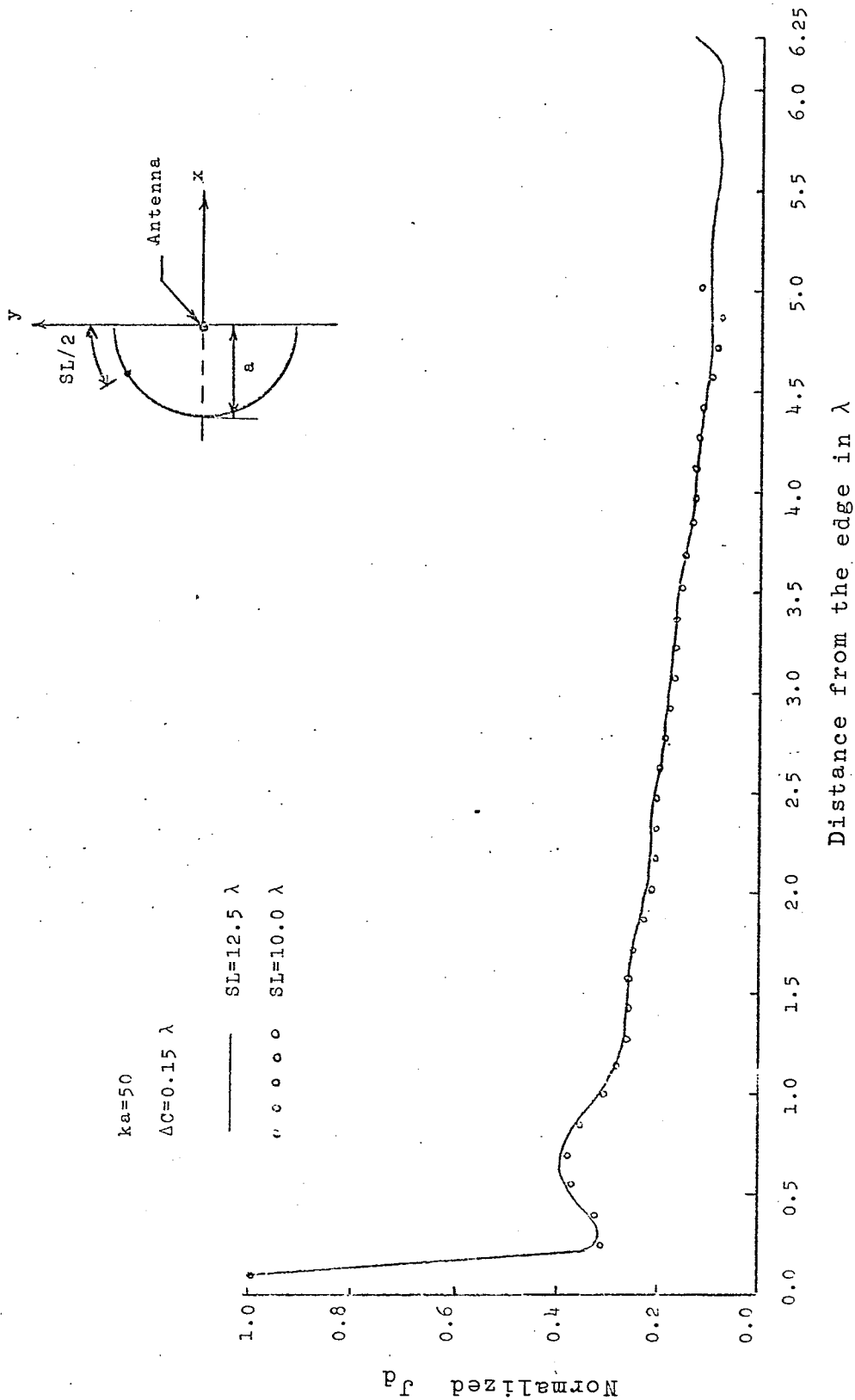


Figure 3.13 Behavior of the difference current for different sampling lengths

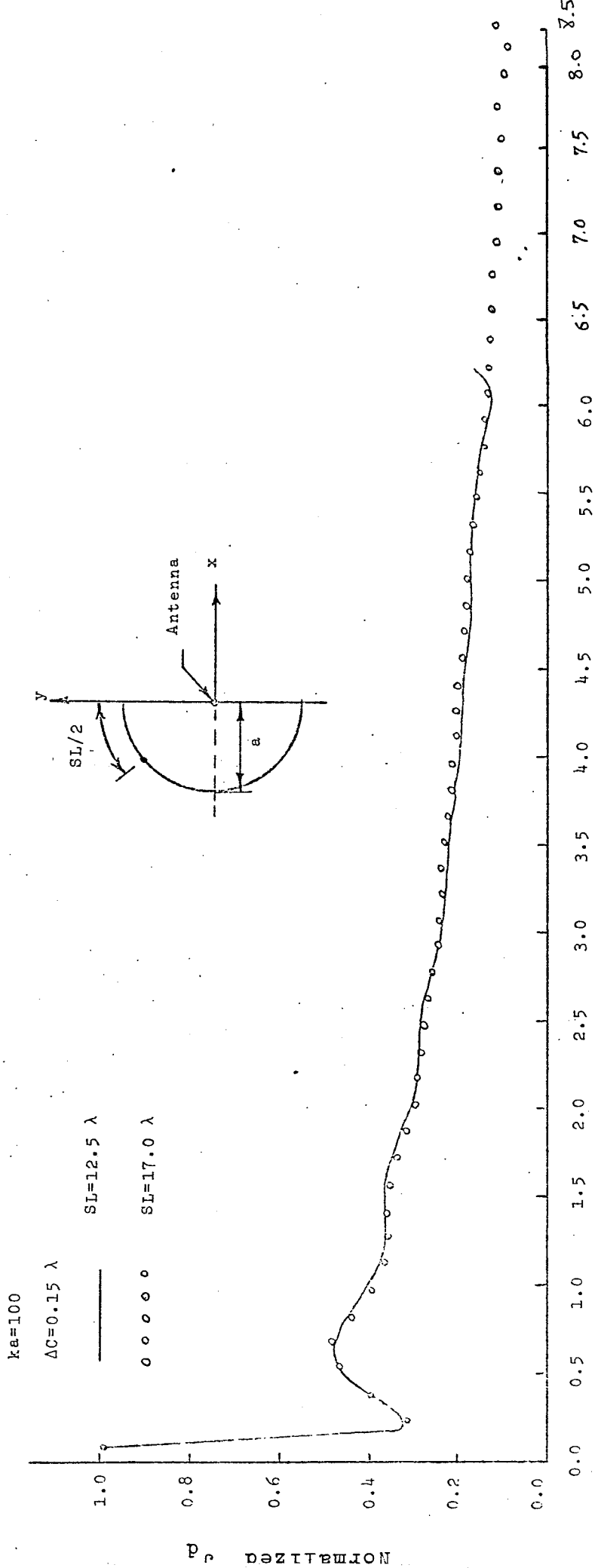


Figure 3.14 Behavior of the difference current for different sampling lengths

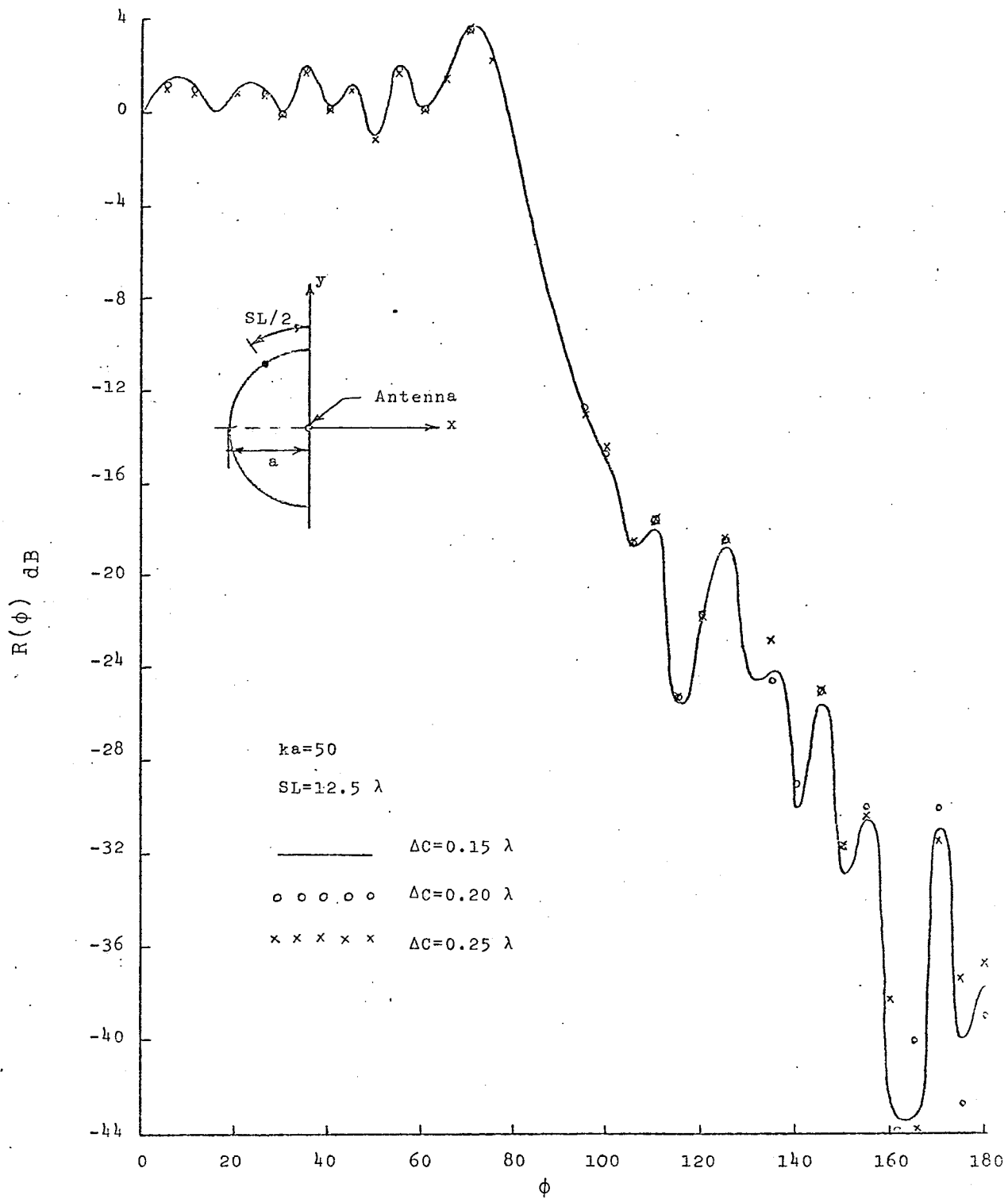


Figure 3.15 Radiation patterns for different step sizes

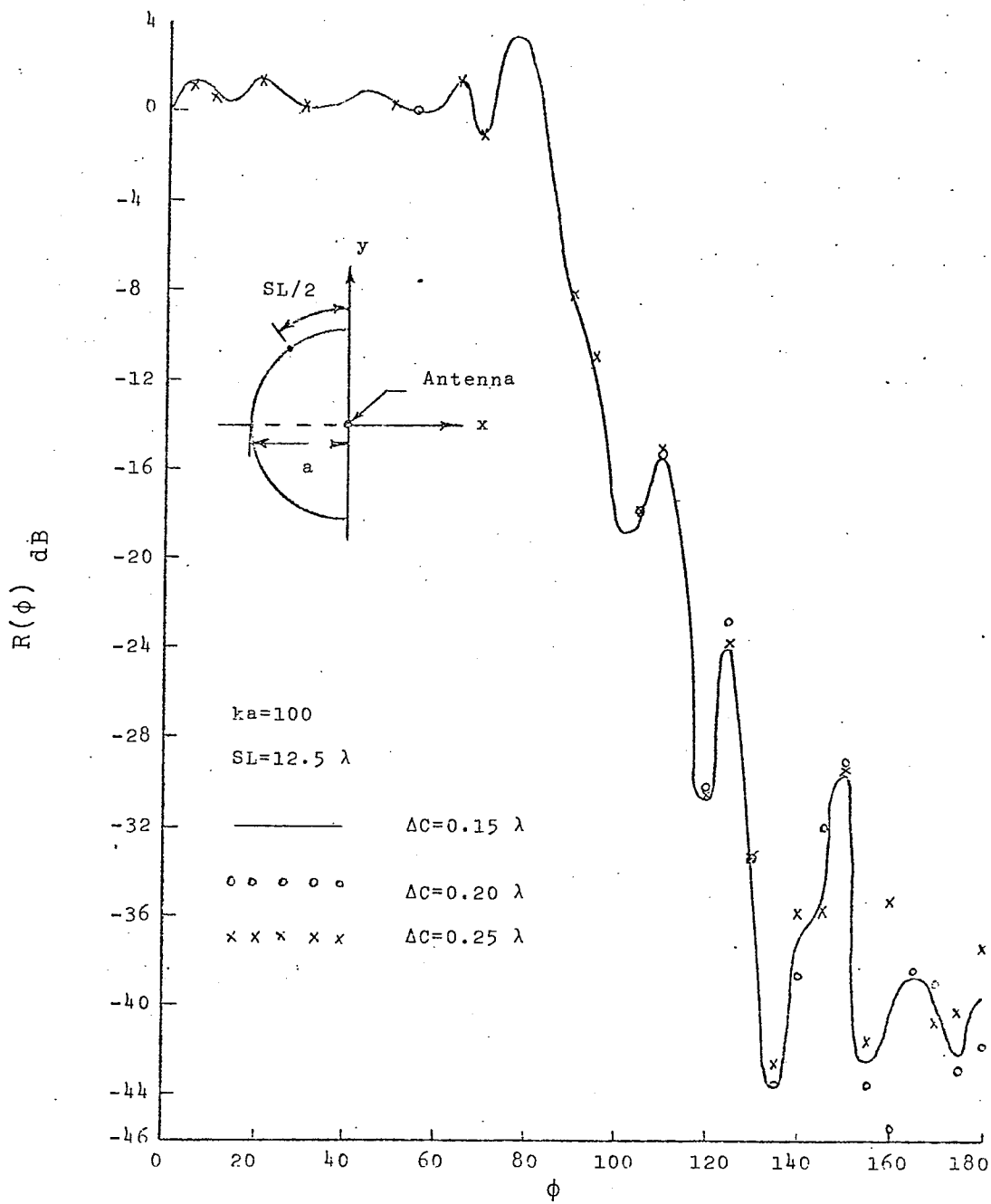


Figure 3.16 Radiation patterns for different step sizes

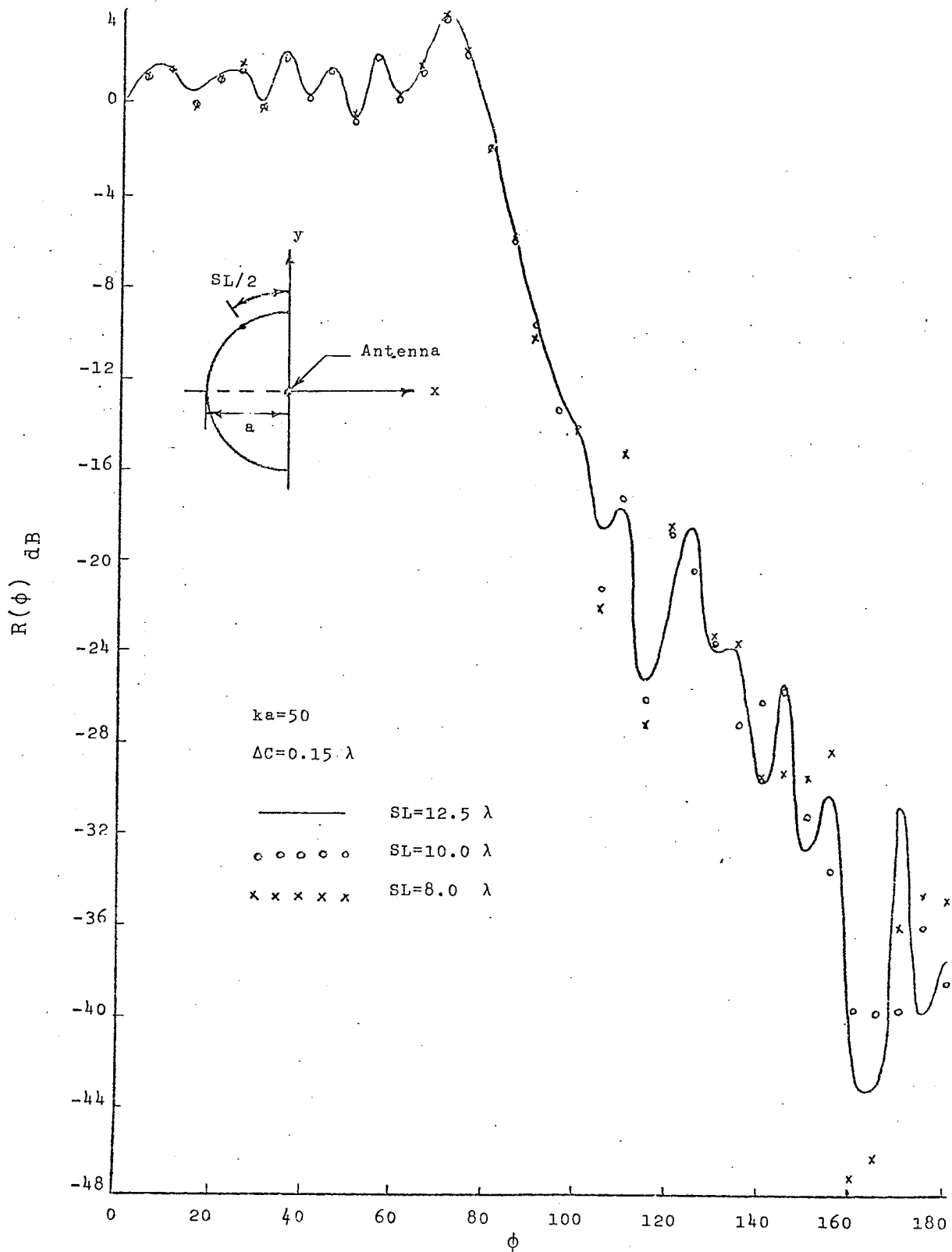


Figure 3.17 Radiation patterns for different sampling lengths

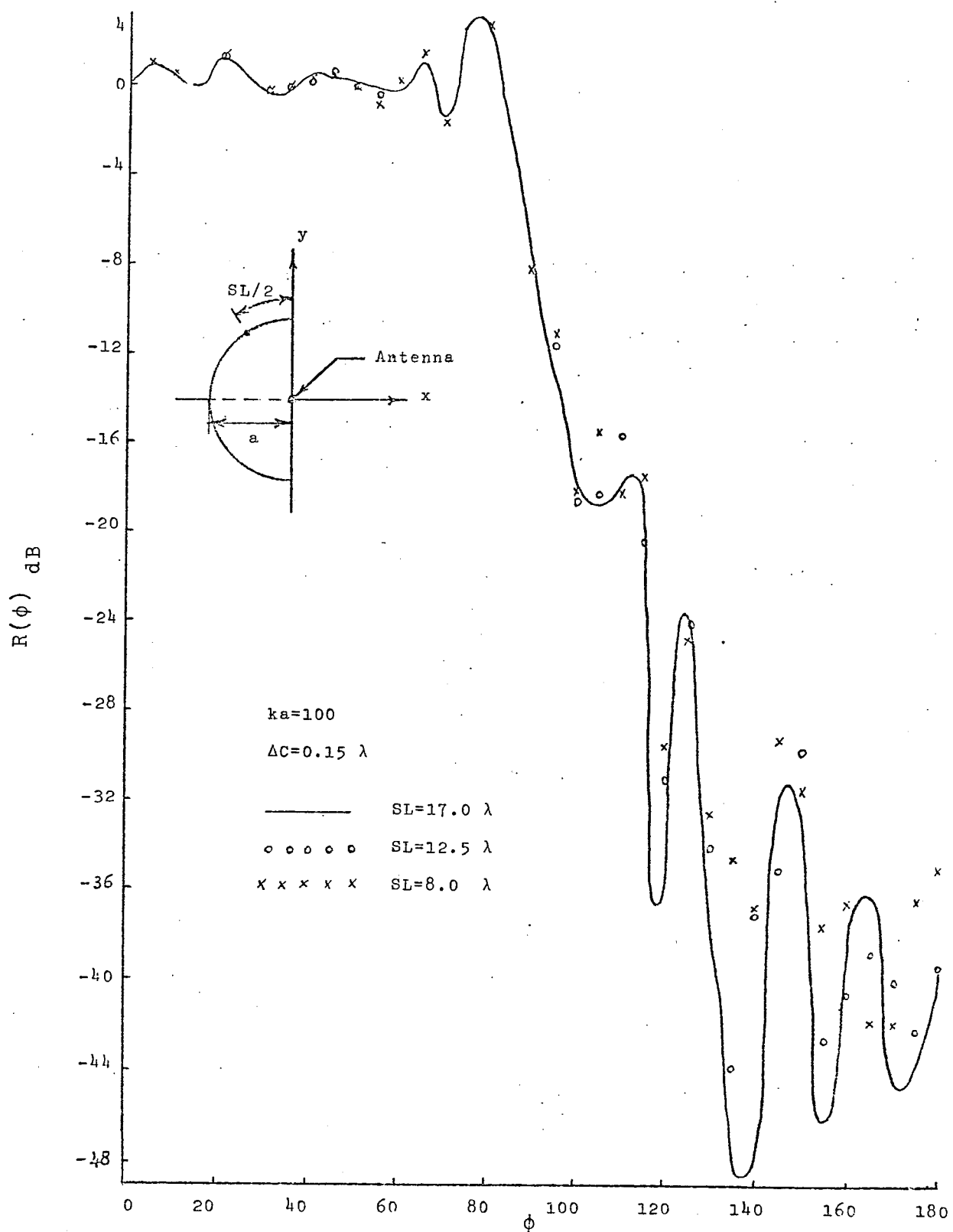


Figure 3.18 Radiation patterns for different sampling lengths

## CHAPTER FOUR

## SCATTERING BY DIELECTRIC LOADED CYLINDRICAL REFLECTORS

## 4.1- Introduction

The problem of scattering and diffraction by dielectric loaded antennas is one, which so far has received insufficient attention. Among few research works reported in this area is that of dielectric loaded circular cylindrical axial slot antennas (Knop et al)<sup>23</sup>. Here the problem is attacked analytically within certain simplifying assumptions and the work is carried out to find an integral relation for the external admittance of the slot and have shown its behavior for various thickness of a dielectric coating. Following this work, (El Moazzen, Shafai)<sup>24</sup> have found an optimum value for the thickness in order to have maximum power transfer through the slot. Using variously shaped dielectric inserts, (Hamid et al)<sup>25, 26, 27</sup> have shown experimentally that beneficial effects on beam width and directivity can occur for horn and corner reflectors. In a recent paper by (Tsandoulas, Fitzgerald)<sup>28</sup>, the effects of the symmetrically loading of a horn aperture with E-plane dielectric slabs is examined and is shown that high aperture efficiencies may be obtained easily, through the use of dielectric coating.

Due to the scarcity of quantitative theoretical data on the effects of various parameters involved in scattering from dielectrically loaded cylindrical

reflectors, the present chapter is oriented to study numerically the general scattering properties of these reflectors. The approach adopted here is based on the integral equation for the field of a harmonic source in the presence of a dielectric cylinder of arbitrary cross section shape, backed by a conducting cylindrical reflector.

Following(5), the dielectric cylinder is divided into cells, which are small enough, so that the electric field intensity is nearly uniform in each cell. The surface of the conducting cylinder is also divided into small segments and then employing the standared moment method technique, the integral equation is enforced at the centre of each cell and segment, with the condition that the total field must equal the sum of the incident and scattered fields within the dielectric, and the tangential component of the electric field must vanish on the surface of the conductor. The result is a system of  $N$  linear equations in  $N$  unknowns where  $N$  stands for the total number of cells and segments. The system of equations can be solved for the unknowns with the aid of a digital computer.

The advantages of this technique is in its flexibility to treat problems of arbitrary cross sections and arbitrary two dimensional sources (line source, any array of line sources or a plane wave source). Moreover the accuracy of the solution can be increased to the desired degree, by increasing the number of divisions on the

scatterer.

In the following section the problem will be formulated in a form suitable for computer use.

#### 4.2- Formulation of the problem.

Consider a harmonic wave in free space incident on a dielectric cylinder backed by a conducting surface of arbitrary cross section as suggested in figure 4.1.

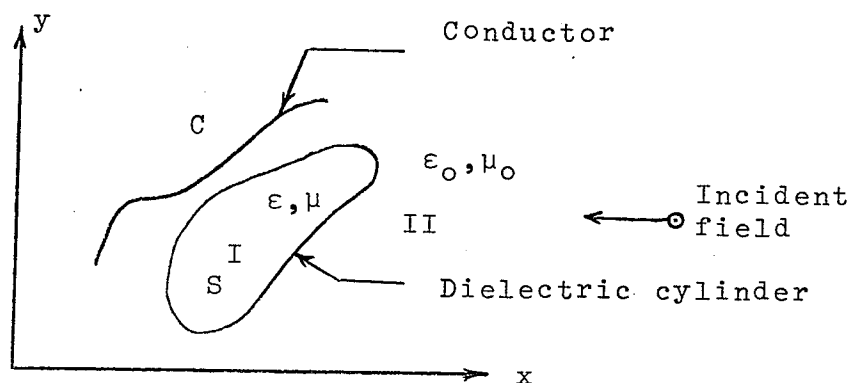


Figure 4.1 Cross sectional view of the scatterers.

where  $S$  and  $C$  are the cross sections of the dielectric cylinder and the reflector. For the present problem it is assumed that the incident electric field  $\tilde{E}$  is  $z$ -directed and the source and the scatterer do not vary along the  $z$ -axis. It is also assumed that the dielectric cylinder has the same permeability as free-space ( $\mu = \mu_0$ ) and its permittivity ( $\epsilon$ ) is a real constant. However, it is to be mentioned that in the general approach suggested by (5), the method can also be applied to inhomogeneous and dissipative dielectrics ( $\epsilon$  complex and a function of  $x, y$ ).

Let  $\tilde{\mathbf{E}}$  represent the total field set up by the source in the presence of the dielectric and the conducting cylinders. If we represent the region occupied by the dielectric by I, and the remaining region by II, we will have,

$$\nabla \times \tilde{\mathbf{E}} = -j\omega\mu_0\tilde{\mathbf{H}}$$

in region II

$$\nabla \times \tilde{\mathbf{H}} = j\omega\epsilon_0\tilde{\mathbf{E}}$$

$$\nabla \times \tilde{\mathbf{E}} = -j\omega\mu_0\tilde{\mathbf{H}}$$

in region I

$$\nabla \times \tilde{\mathbf{H}} = j\omega\epsilon\tilde{\mathbf{E}} = j\omega\epsilon_0\tilde{\mathbf{E}} + j\omega(\epsilon - \epsilon_0)\tilde{\mathbf{E}}$$

(4.1)

Considering the modification made in the last of these equations, we note that all fields can now be assumed as existing in free space with a dependent current (polarization current) confined to the region occupied by the dielectric S, given by,

$$\tilde{\mathbf{J}}_p = -j\omega(\epsilon - \epsilon_0)\tilde{\mathbf{E}} \quad (4.2)$$

and the induced surface current on C given by,

$$\tilde{\mathbf{J}}_s = \hat{\mathbf{n}} \times \tilde{\mathbf{H}} \quad (4.3)$$

In the light of above argument and with the aid of 2.32, we can formulate our problem in the form of,

$$E(\tilde{\rho}) = T E_i(\tilde{\rho}) - (T/4\pi) \int_C j\omega\mu J(\tilde{\rho}') G dc' + (Tk^2/4\pi) \int_S (\epsilon_r - 1) E(\tilde{\rho}') G ds' \quad (4.4)$$

where it is understood that all the field components of the above equation are z-directed and,

$$\epsilon_r = \epsilon/\epsilon_0 \quad (4.5)$$

$$G = (\pi/j) H_0^2(k|\tilde{\rho}-\tilde{\rho}'|) \quad (4.6)$$

and prime denotes to the coordinate of the source point. Substituting 4.5 into 4.3 results in,

$$E(\tilde{\rho}) = T E_i(\tilde{\rho}) - (Tk\eta/4) \int_C J(\tilde{\rho}') H_0^2(k|\tilde{\rho}-\tilde{\rho}'|) dc' - (jTk^2/4) (\epsilon_r - 1) \int_S E(\tilde{\rho}') H_0^2(k|\tilde{\rho}-\tilde{\rho}'|) ds' \quad (4.7)$$

The above equation is valid for both regions I and II. Since the factor T is equal to one for all points of space except the boundary C on which it takes the value two, and because on the boundary C, electric field must vanish, we may drop

out the factor  $T$ , leaving,

$$\begin{aligned}
 E_i(\tilde{\rho}) &= E(\tilde{\rho}) + (k\eta/4) \int_C J(\tilde{\rho}') H_0^2(k|\tilde{\rho}-\tilde{\rho}'|) dc' \\
 &+ (jk^2/4) (\epsilon_r - 1) \int_S E(\tilde{\rho}') H_0^2(k|\tilde{\rho}-\tilde{\rho}'|) dc'
 \end{aligned}
 \tag{4.8}$$

Now, let us divide the cross section  $S$  and  $C$  into cells and segments sufficiently small so that the electric field intensity and the surface current density are essentially constant over the respective divisions. Now suppose that the total number of cells is  $M$  and the total number of segments on  $C$  is equal to  $N$ . The only boundary condition to be satisfied is,

$$E(\tilde{\rho}) = 0 \quad \text{on } C \tag{4.9}$$

Therefore, enforcing the equation 4.7 at the center of each cell and segment on  $S$  and  $C$  respectively results in,

$$E_i(\tilde{\rho}_j) = \sum_{n=M+1}^{N+M} A_{jn} f_n + \sum_{m=1}^M B_{jm} E_m \quad (\text{matching points in } S)$$

(4.10)

where, from 3.18 we have,

$$A_{jn} = \begin{cases} (k\eta/4) \Delta C_n H_0^2(k|\tilde{\rho}_j - \tilde{\rho}_n|) & j \neq n \\ (k\eta/4) \Delta C_n \{1 - (2j/\pi) L_n(k\Delta C_n \gamma / 4e)\} & j = n \end{cases}$$

(4.11)

and  $B_{jm}$  is given by,

$$B_{jm} = \epsilon_{jm} + (jk^2/4) (\epsilon_r - 1) \sum_{m=1}^M \int_{\text{cell } m} H_o^2(k|\tilde{\rho}_j - \tilde{\rho}_m|) ds'$$

$$\epsilon_{jm} = \begin{cases} 0 & j \neq m \\ 1 & j = m \end{cases} \quad (4.12)$$

and  $j$  takes the values from one to  $M+N$ .

A closed form solution for the integral appearing in equation 4.11, except for a circular region, is not available. However, if the cells are sufficiently small, little error is incurred in approximating the cells with circular cells of the same cross section area. Therefore,

$$(jk^2/4) \int_{\text{cell } m} H_o^2(k|\tilde{\rho}_j - \tilde{\rho}_m|) ds' \approx (j/2) \{ \pi k a_m H_1^2(ka_m) - 2j \} \quad \text{if } j=m$$

$$\approx (j\pi k a_m / 2) J_1(ka_m) H_o^2(k|\tilde{\rho}_j - \tilde{\rho}_m|) \quad \text{if } j \neq m$$

$$(4.13)$$

where  $a_m$  is the radius of the equivalent circular cell which has the same cross section area as the cell  $m$ . Substituting 4.12 into 4.11 leads to,

$$B_{jm} = \begin{cases} 1 + (\frac{\epsilon_r - 1}{r}) (j/2) (\pi k a_m H_1^2(k a_m) - 2j) & j = m \\ (j k a_m \pi / 2) (\epsilon_r - 1) J_1(k a_m) H_0^2(k |\tilde{\rho}_j - \tilde{\rho}_m|) & j \neq m \end{cases} \quad (4.14A)$$

$$(4.14B)$$

By the above formulation, the boundary condition is implemented in the coefficient  $B_{jm}$ . When the matching point is on C, the index  $j$  is greater than  $M$  and  $B_{jm}$  is given by 4.14B. Once the system of linear equations in  $M+N$  unknowns is set up and solved for the unknowns, the scattered field and the total radiation field and other parameters of interest can be computed easily from the information about the field and current distribution in the dielectric region and on the conducting cylinder respectively. For instance, the radiation field is given by,

$$E(\rho, \phi) = E_i(\rho, \phi) - (k\eta/4) \sqrt{(2j/\pi k\rho)} \exp(-jk\rho) R(\phi) \quad (4.15)$$

$$= E_i + E_s$$

where,

$$R(\phi) = \sum_{n=M+1}^{M+N} f_n \Delta C_n \exp\{jk\rho_n \cos(\phi - \phi_n)\} + (2\pi/\eta) (\frac{\epsilon_r - 1}{r})$$

$$\cdot \sum_{m=1}^M E_m a_m J_1(k a_m) \exp\{jk\rho_m \cos(\phi - \phi_m)\} \quad (4.16)$$

and the echo width <sup>34</sup>, in the case of an incident plane wave, is given by,

$$W(\phi) = \lim_{k\rho \rightarrow \infty} 2\pi\rho \frac{|E(\rho, \phi)|^2}{s} / \frac{|E(\rho, \phi)|^2}{i} = (k\eta^2/4) \frac{|R(\phi)|^2}{|E|_i^2}$$

In this section, the problem of scattering by dielectric loaded conducting cylindrical reflectors was analyzed and formulated in a manner suitable for the computer use. The purpose of the following section will be the application of this method to certain geometries in order to study their general scattering properties.

#### 4.3- Numerical results.

A computer program, based on the section 4.2 was developed to solve the integral equation 4.7. The resulting computer program has the flexibility to solve the general scattering problem for virtually any cross section of a dielectric cylinder in the presence or absence of a conducting cylinder of any cross section. The validity of the generalized program was verified in various ways. First, numerical solution was obtained for the specific case of a circular dielectric cylindrical shell, for which an exact result is available and is shown in figure 4.2. Figure 4.3 shows the exact solution and the result obtained by (5) for the same problem. Excellent agreement between numerical and the exact solution is evident. Figure 4.4 illustrates the plane-wave scattering pattern of a semicircular cylindrical shell. No exact solution is available for comparison with the result shown in figure 4.4. However as a base for comparison, the result obtained for the same problem by (5) is illustrated in figure 4.5. For the case when a conducting cylinder is placed in the vicinity of the dielectric cylinder, since no exact or numerical solution was available, validity of the program was verified by interchanging the direction of incidence and the observation for several test cases. According to the reciprocity theorem, the observed scattered field must be the same in both cases. Several cases were examined and

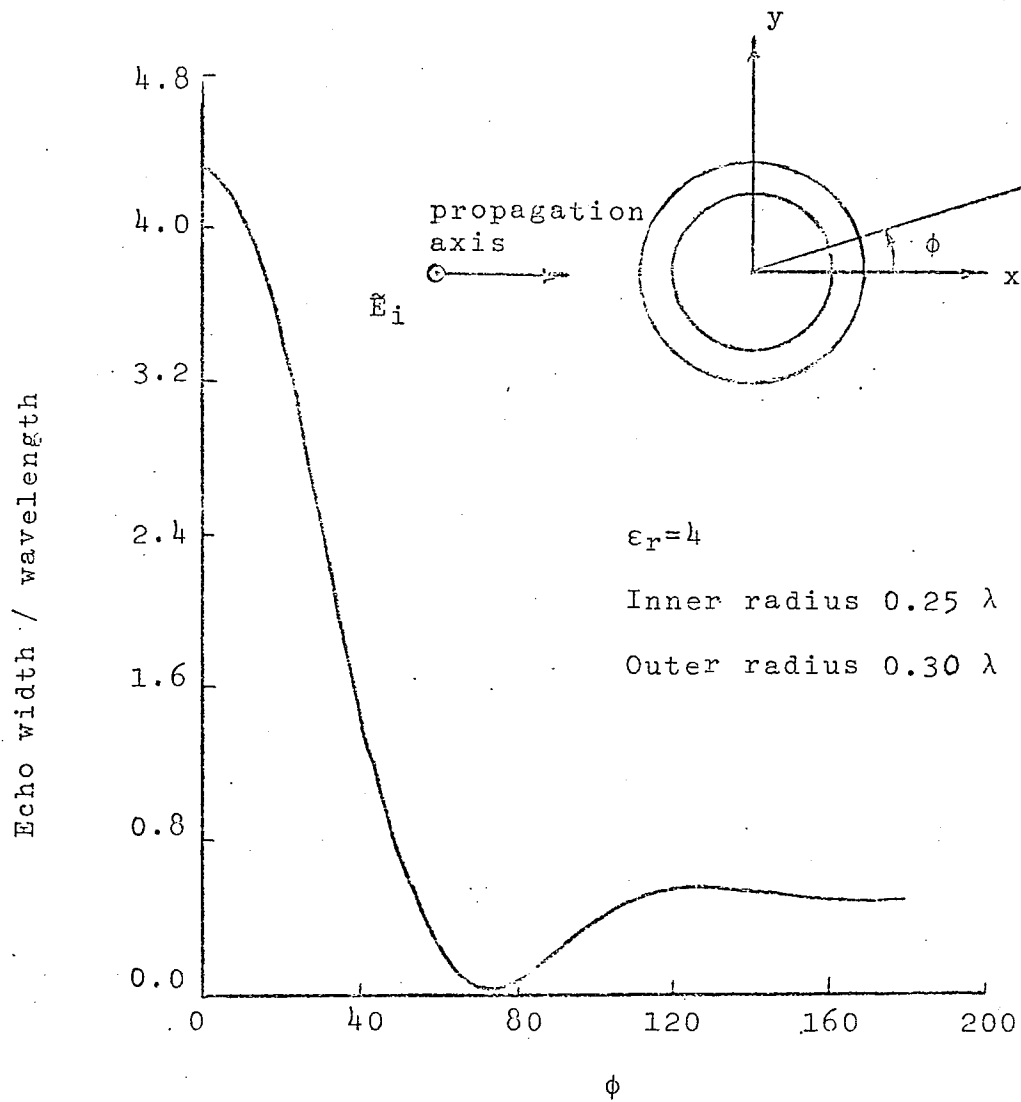


Figure 4.2 Scattering pattern of dielectric cylindrical shell with a plane wave incident

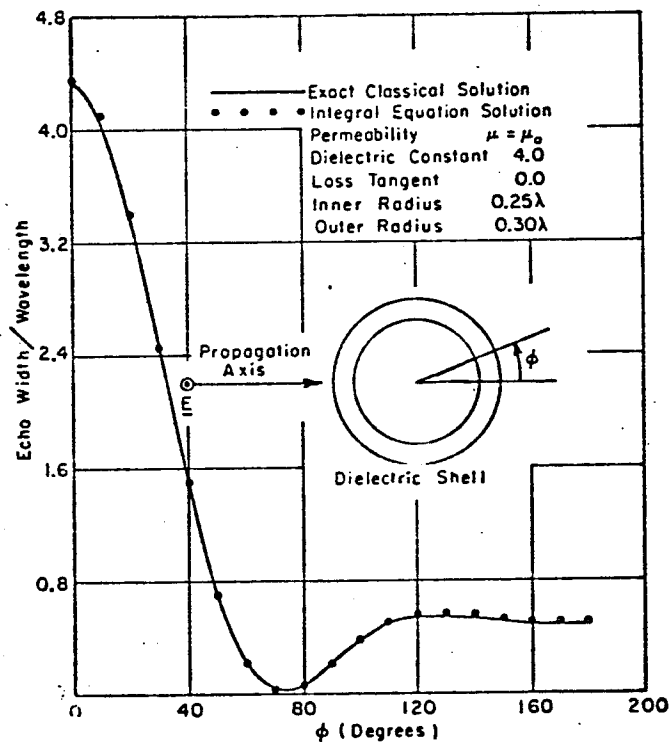


Fig. 4. Distant scattering pattern of circular dielectric cylindrical shell with plane-wave incident.

Figure 4.3 Result obtained by  
Richmond

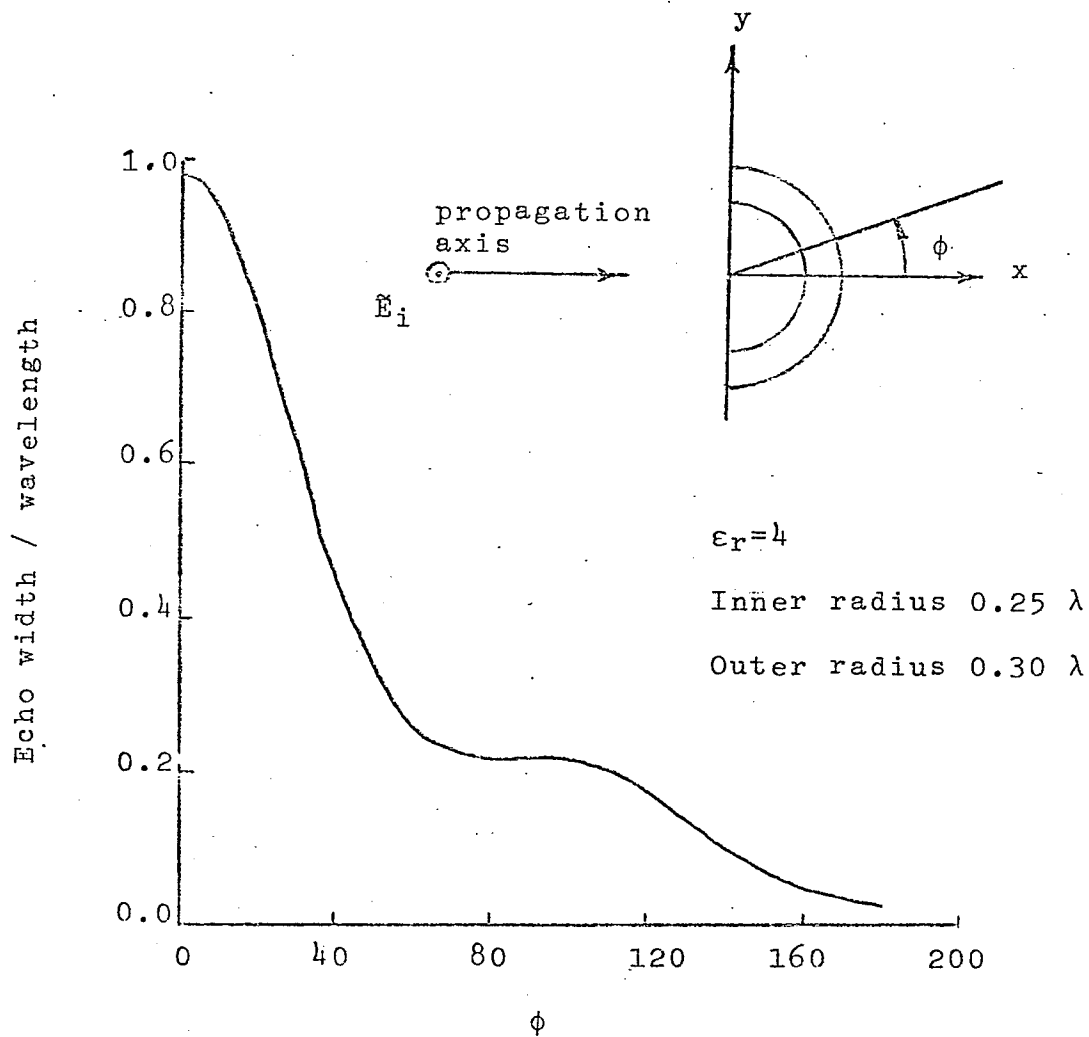


Figure 4.4 Scattering pattern of a dielectric semicircular cylindrical shell with a plane wave incident

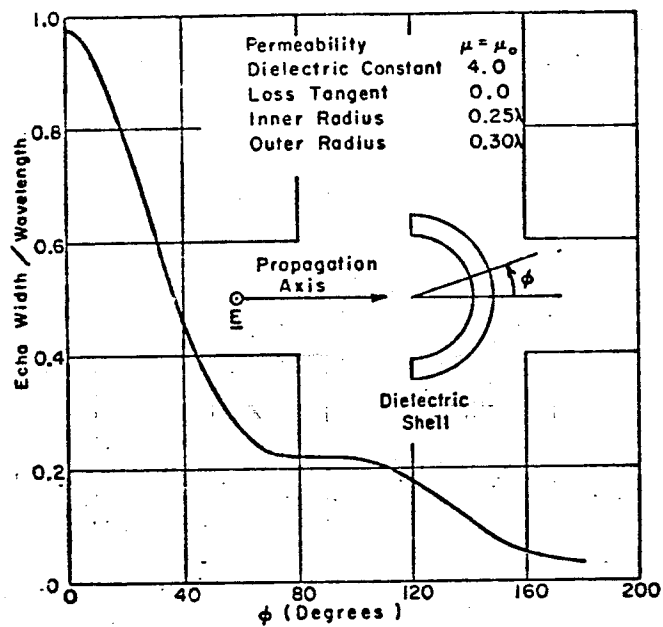


Fig. 6. Scattering pattern of a semicircular dielectric cylindrical shell with plane-wave incident, calculated with the integral-equation technique.

Figure 4.5 Result obtained by  
Richmond

were found to be so within the range of the computational errors.

Considering the geometry shown in figure 4.6, the parameters involved in the overall radiation characteristics of a dielectric loaded cylindrical reflector are as follows.

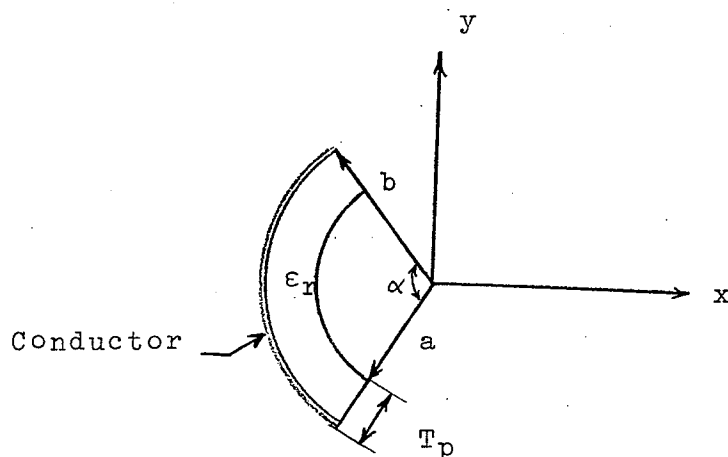


Figure 4.6. Notations for the parameters affecting the radiation pattern.

$b$  radius of curvature of the conducting surface.

$a$  radius of curvature of the inner surface of the dielectric cylinder.

$\alpha$  the angle of the reflector.

$T_p$  physical thickness of the dielectric layer.

$T_{\epsilon_r}$  electrical thickness of the dielectric layer.

where  $\epsilon_r$  is the relative permittivity of the dielectric material.

In order to study the effects of the above parameters on the performance of the loaded reflector, the radiation pattern for such a reflector in the presence of a

line source was computed for several test cases and the results are shown in figures 4.7 to 4.14. For purposes of presentation, it has been found convenient to arrange the results of this series of computations in a particular order. Figures 4.7 and 4.8 are intended to show the effects of variation of the curvature of the conducting cylinder and the physical thickness on the radiation pattern. The other parameters are held constant at a reasonable value. From these figures it is believed that the variation of  $b$  has no significant effect on the general shape of the radiation pattern. The physical aspects of the problem would lead one to expect that as the physical thickness of the dielectric layer increases, the variations in the curvature of the metallic cylinder would be less noticeable in the radiation patterns, since most of the energy will be reflected before touching the surface of the conductor, and is found to be so by comparing figures 4.7 and 4.8. Moreover, as the physical thickness decreases, the curvature of the conducting cylinder increases and confines the energy to smaller region. This is believed to be the reason why the energy level in front direction increases continuously as  $b$  decreases in figure 4.7. However in figure 4.8, the front direction energy level is fairly constant, a result that can be attributed to the discussion given earlier that the dielectric layer is thick enough for blocking the energy from seeing the variations in  $b$ . Figures 4.9 to 4.11 show

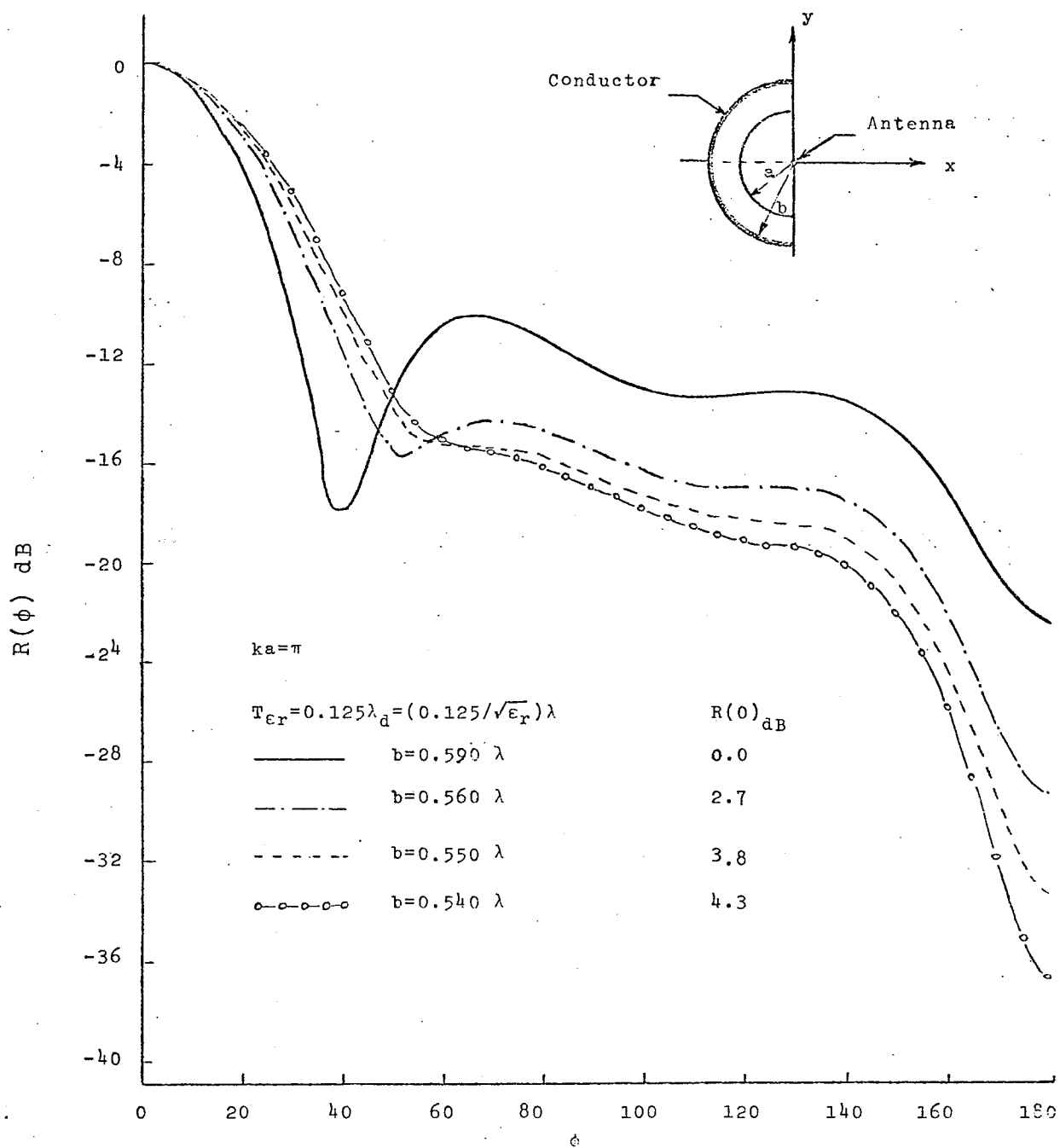
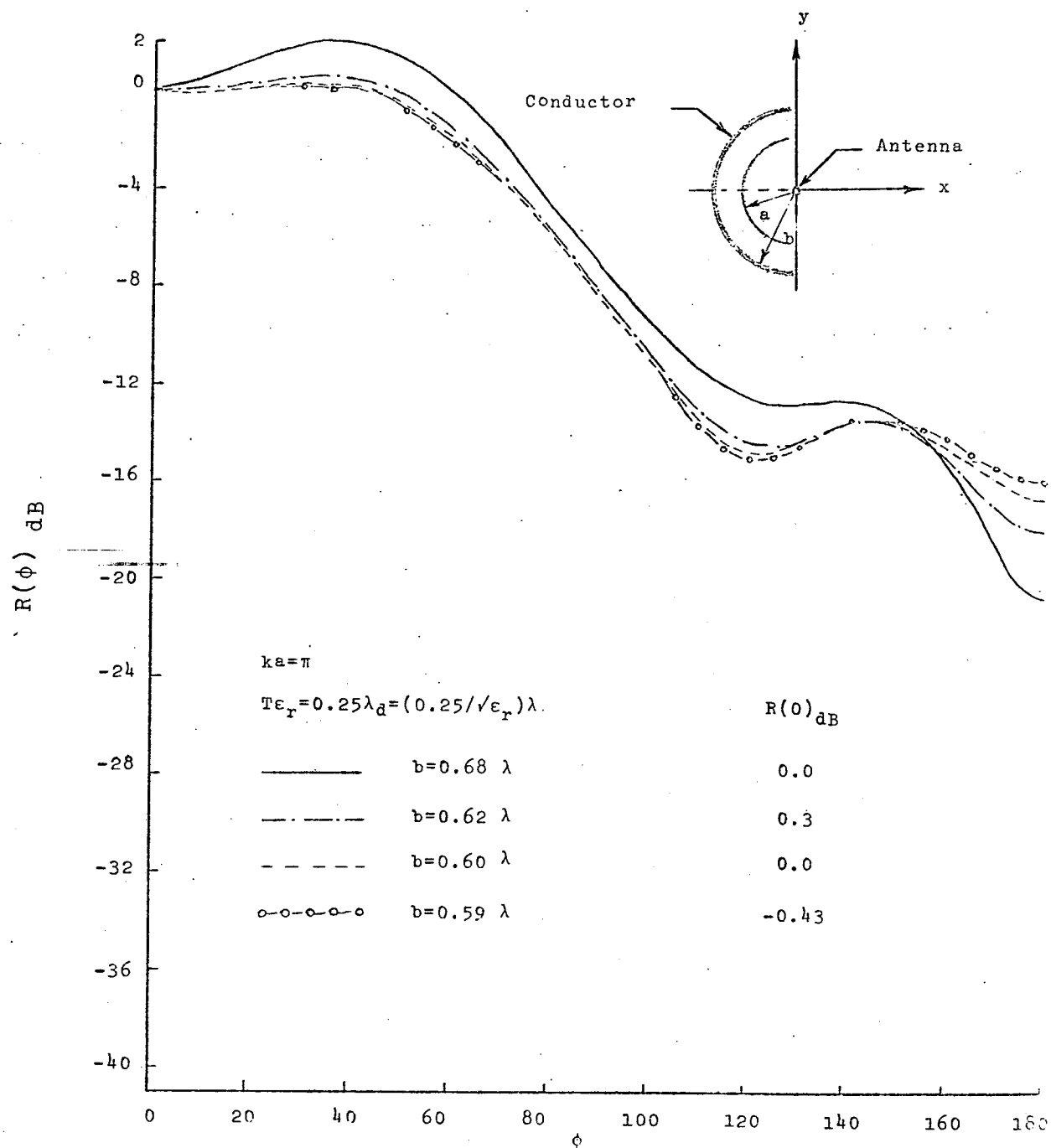
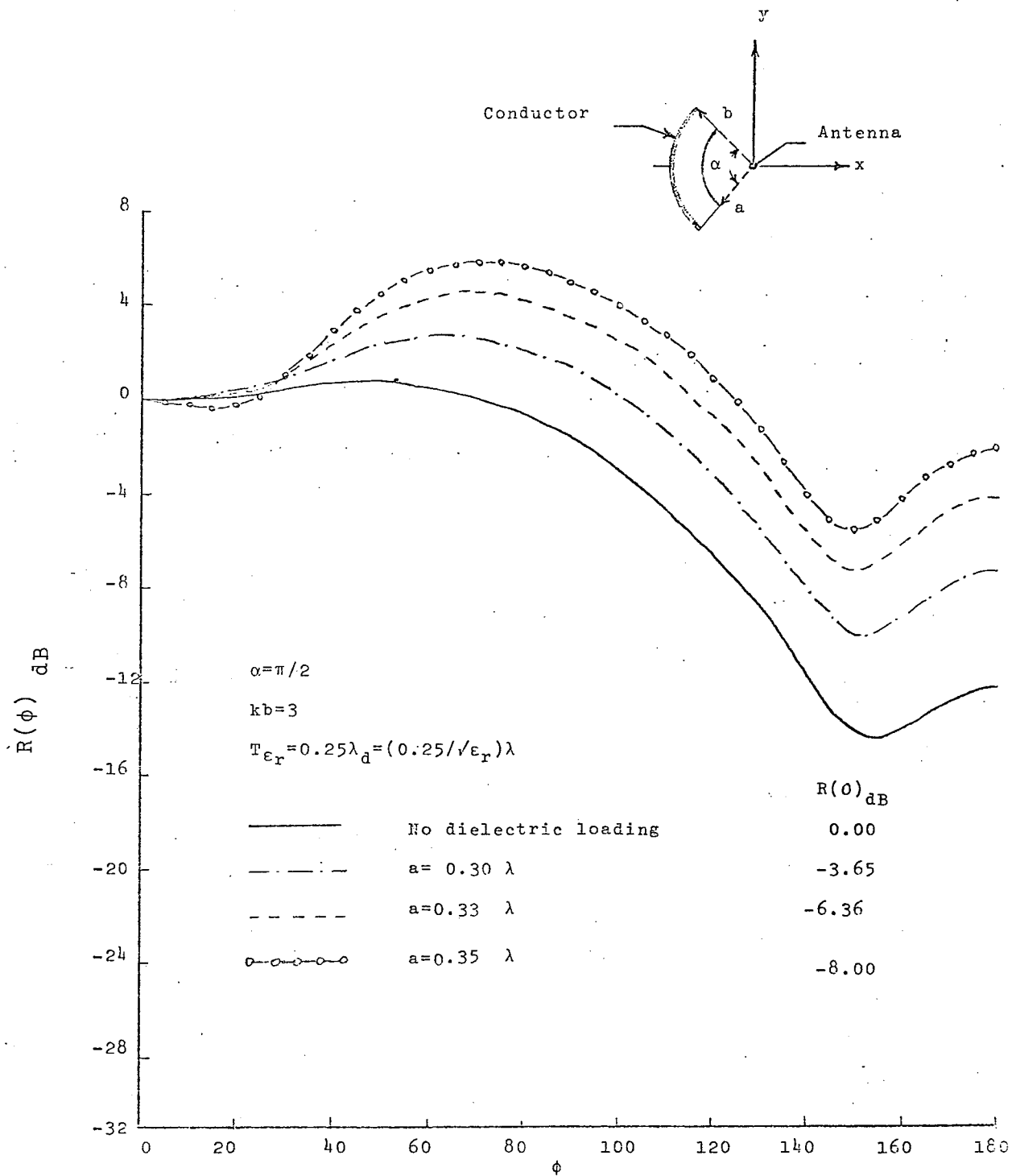


Figure 4.7 Radiation patterns for different  $b$

Figure 4.8 Radiation patterns for different  $b$

Figure 4.9 Radiation patterns for different  $a$

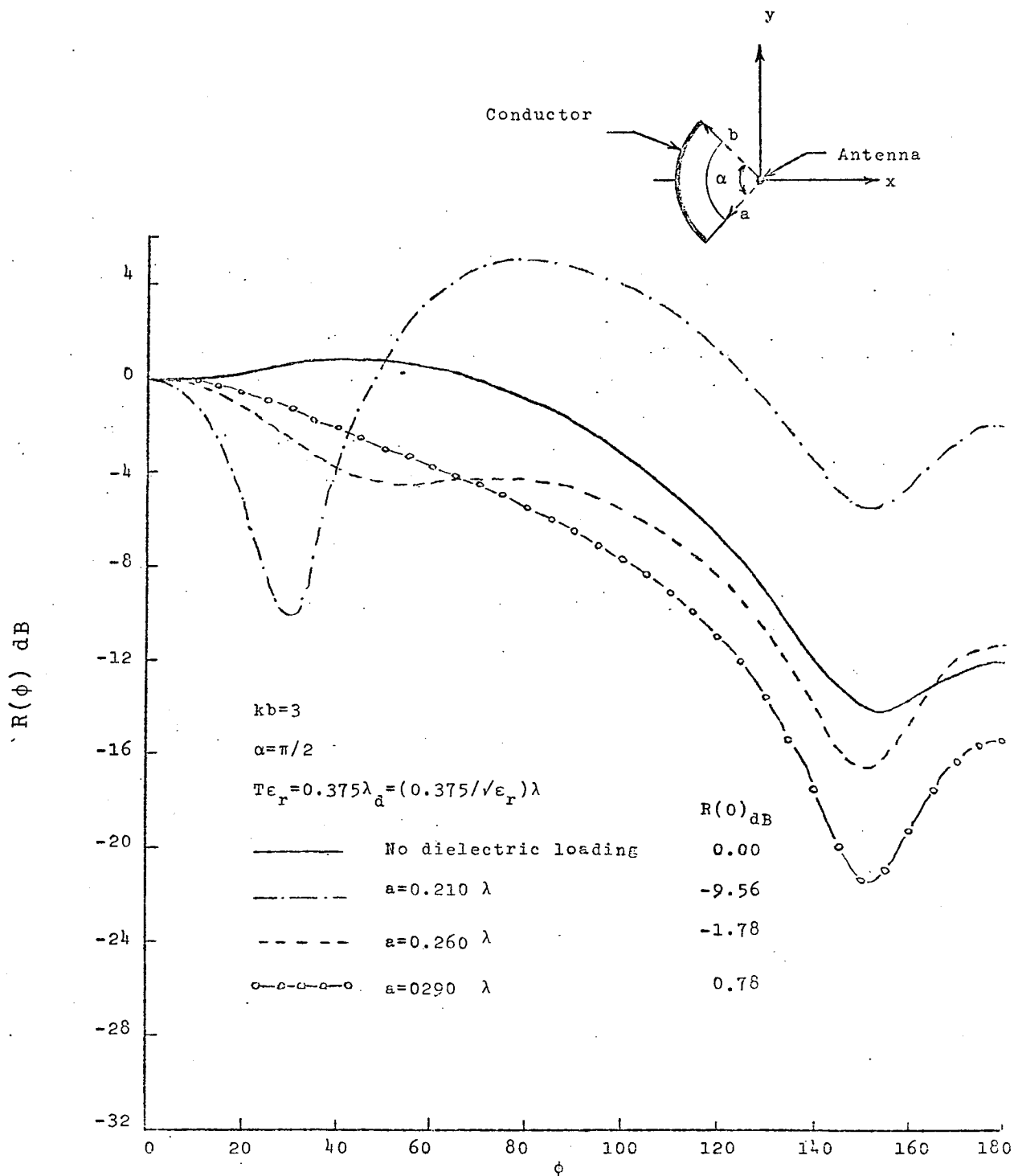


Figure 4.10 Radiation patterns for different a

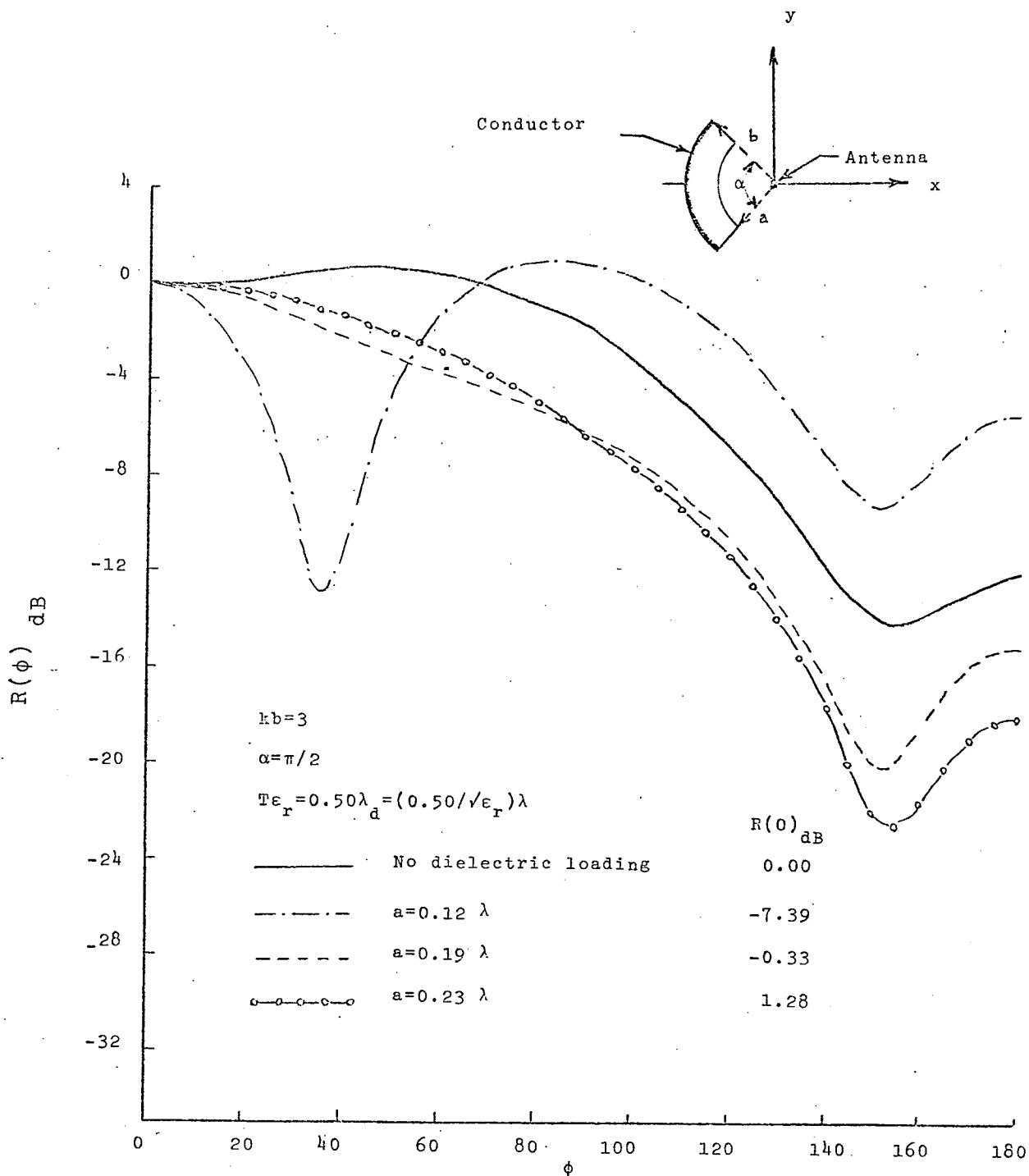


Figure 4.11 Radiation patterns for different a

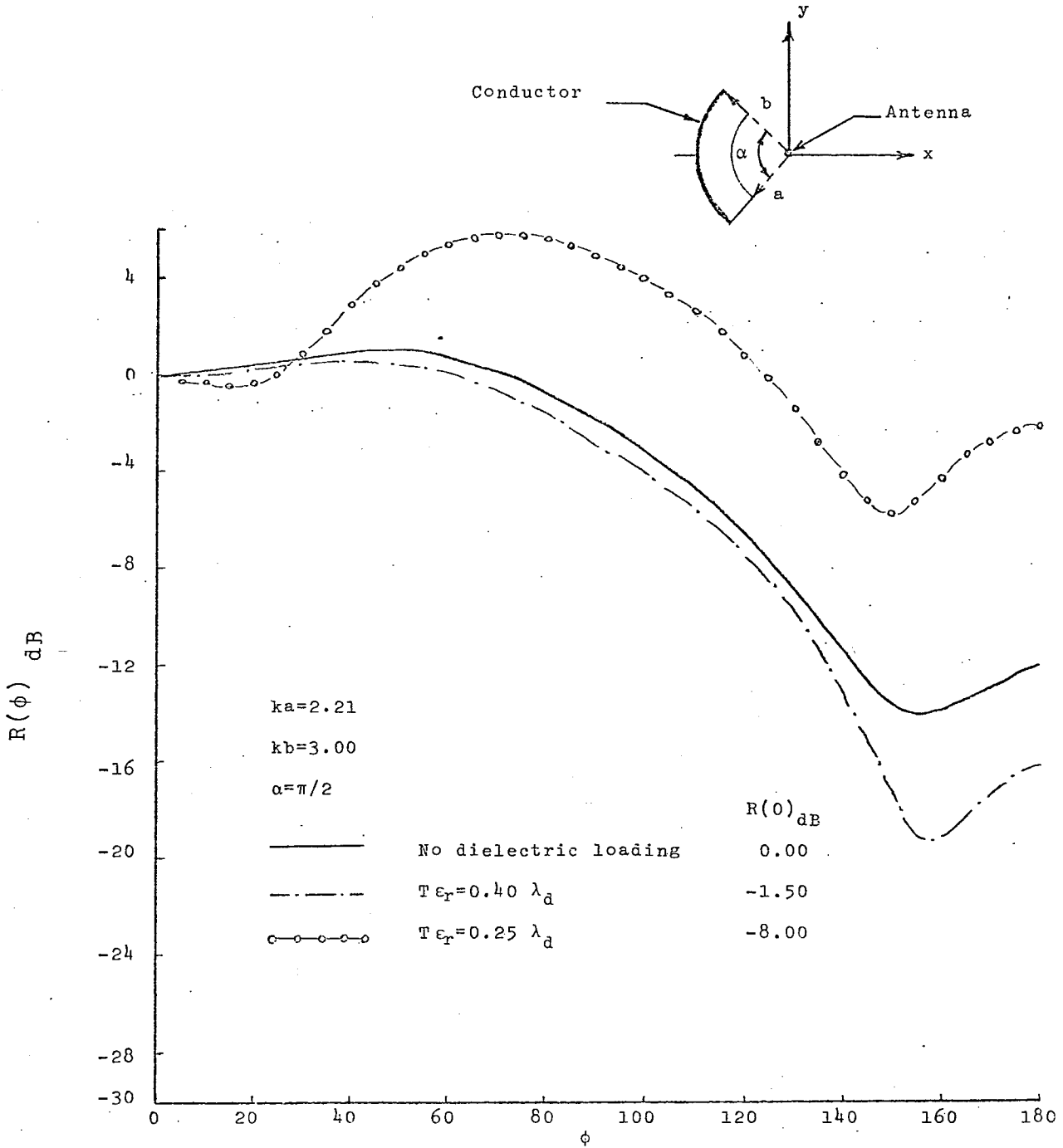


Figure 4.12 Radiation patterns for different electrical thickness

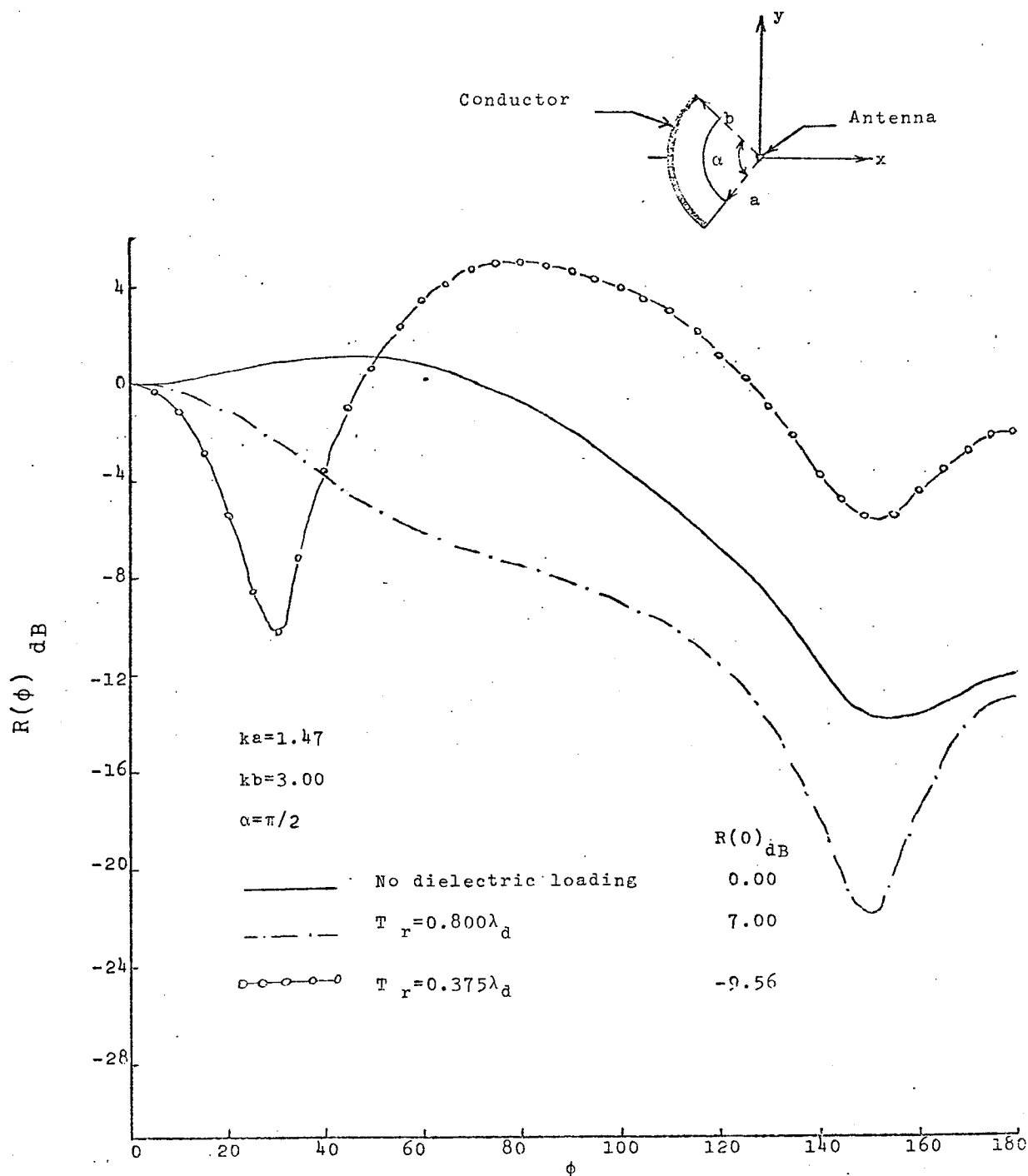


Figure 4.13 Radiation patterns for different electrical thickness

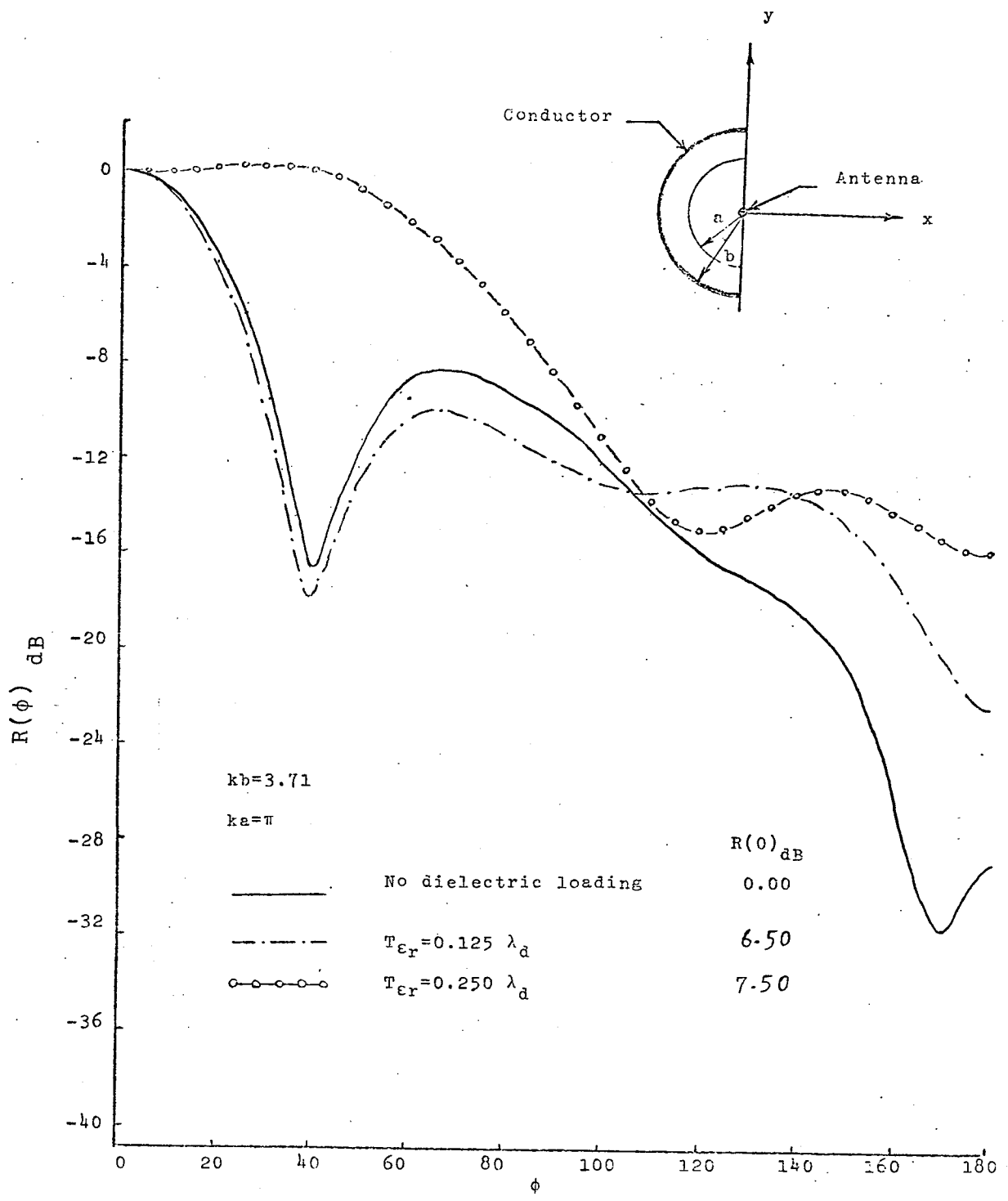


Figure 4.14 Radiation patterns for different electrical thickness

the effects of variations of the curvature of the illuminated surface. As expected, the general shape of the radiation pattern is more sensitive to this parameter than  $b$ , since part of the total energy is reflected from this surface. Otherwise there seems to be no logical way of interpreting the results obtained. Figures 4.12 to 4.14 illustrate the effects of variations of the electrical thickness of the dielectric layer. These figures show most clearly the strong effect of this parameter on the radiation pattern. A plausible physical explanation is that the wave penetrating the dielectric layer undergoes certain phase shift before emerging again from the illuminated side. This phase shift depends on the electrical thickness of the layer and the radii of the curvature of the illuminated surface. Therefore the wave could be phased in such a manner to cause the lobes of the radiation pattern (of an unloaded reflector) to be shifted and altered in magnitude or even generate new lobes. By comparing the radiation patterns of the loaded and unloaded reflector in figures 4.12 to 4.14, it is believed that by proper choice of the electrical thickness of the dielectric layer, it is possible to reduce the beam width of the main lobe and increase the front direction energy level of the reflector.

So far, in the results presented in this section, a uniform dielectric thickness was assumed. In order to study the effects of non-uniform distribution of dielectric

coating, and introducing a small air gap between the dielectric and the conducting surface, the radiation pattern for several test cases was computed. To restrict the figures to a reasonable number, a few cases are shown in figures 4.15 to 4.19. In general, it was observed that non-uniform distribution of coating broadened the beam width and increased the back radiation. This was probably due to introduction of new edges which caused diffraction of the wave incident upon them. However, in few cases, it was observed that introducing small air gap between the dielectric layer and the wall of the reflector (figures 4.16 to 4.19) would result in narrowing the main lobe at the expense of increasing the back radiation.

So far, it has been shown that the most effective parameters on the overall performance of a loaded cylindrical reflector are the electrical length and the curvature of the illuminated surface. Even though it seems that there is no systematic way to determine the optimum value for these parameters, nevertheless, it is possible to generate enough results to be able to decide on an optimum design with the aid of the available modern computing facilities.

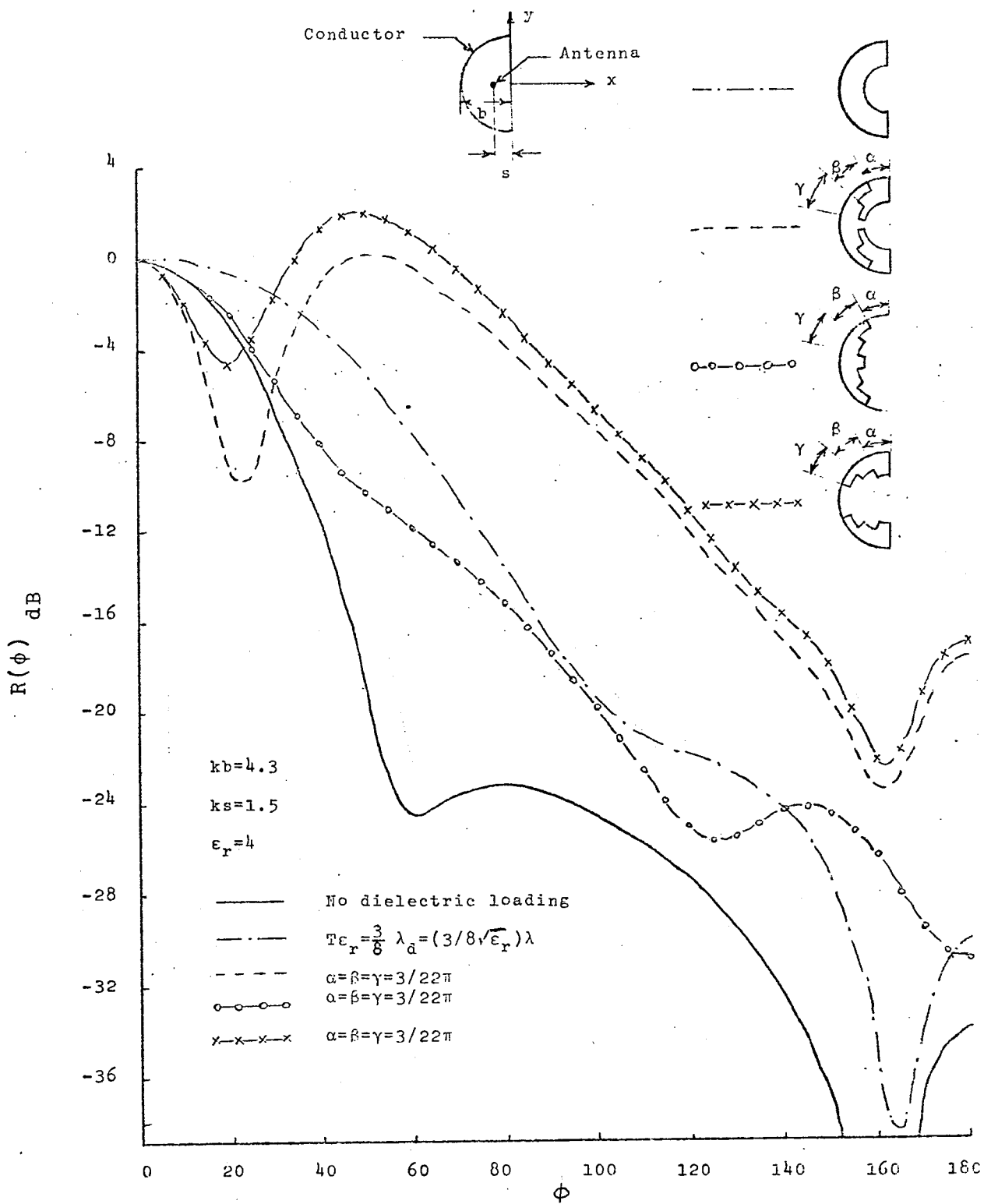


Figure 4.15 Radiation patterns for variously shaped dielectric loading

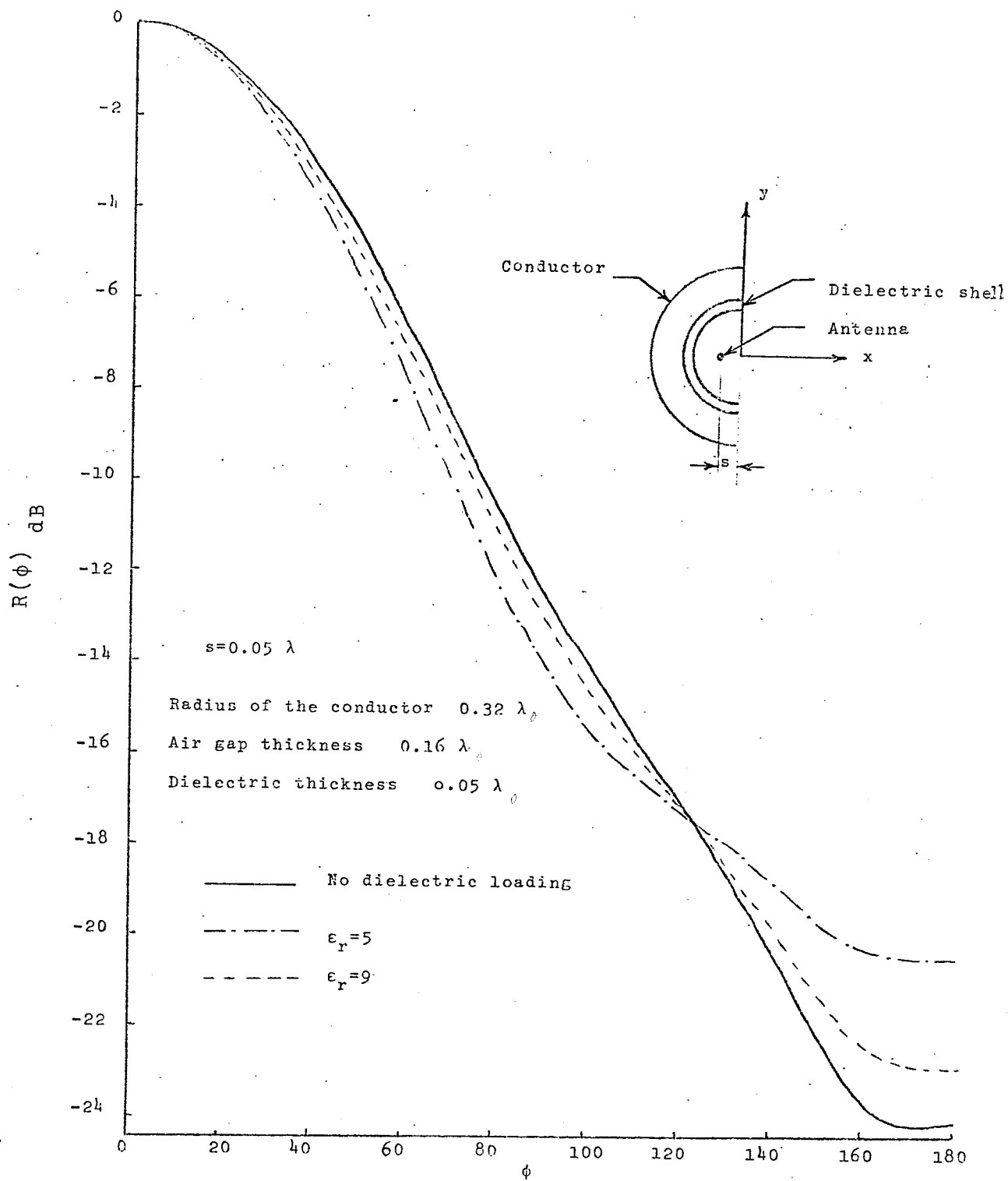


Figure 4.16 Effects of air gap on the radiation pattern for different dielectric constants

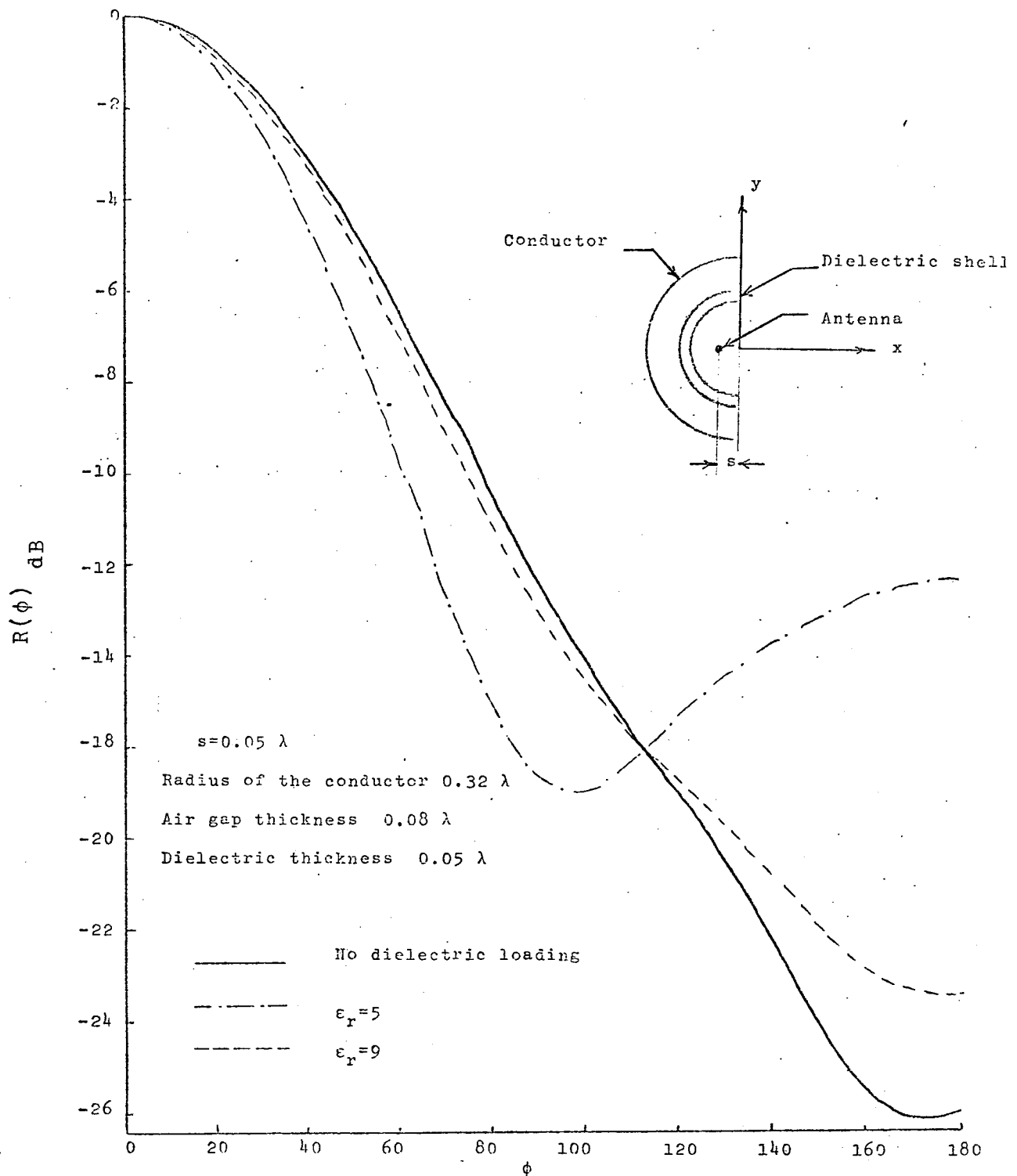


Figure 4.17 Effects of air gap on the radiation pattern for different dielectric constants

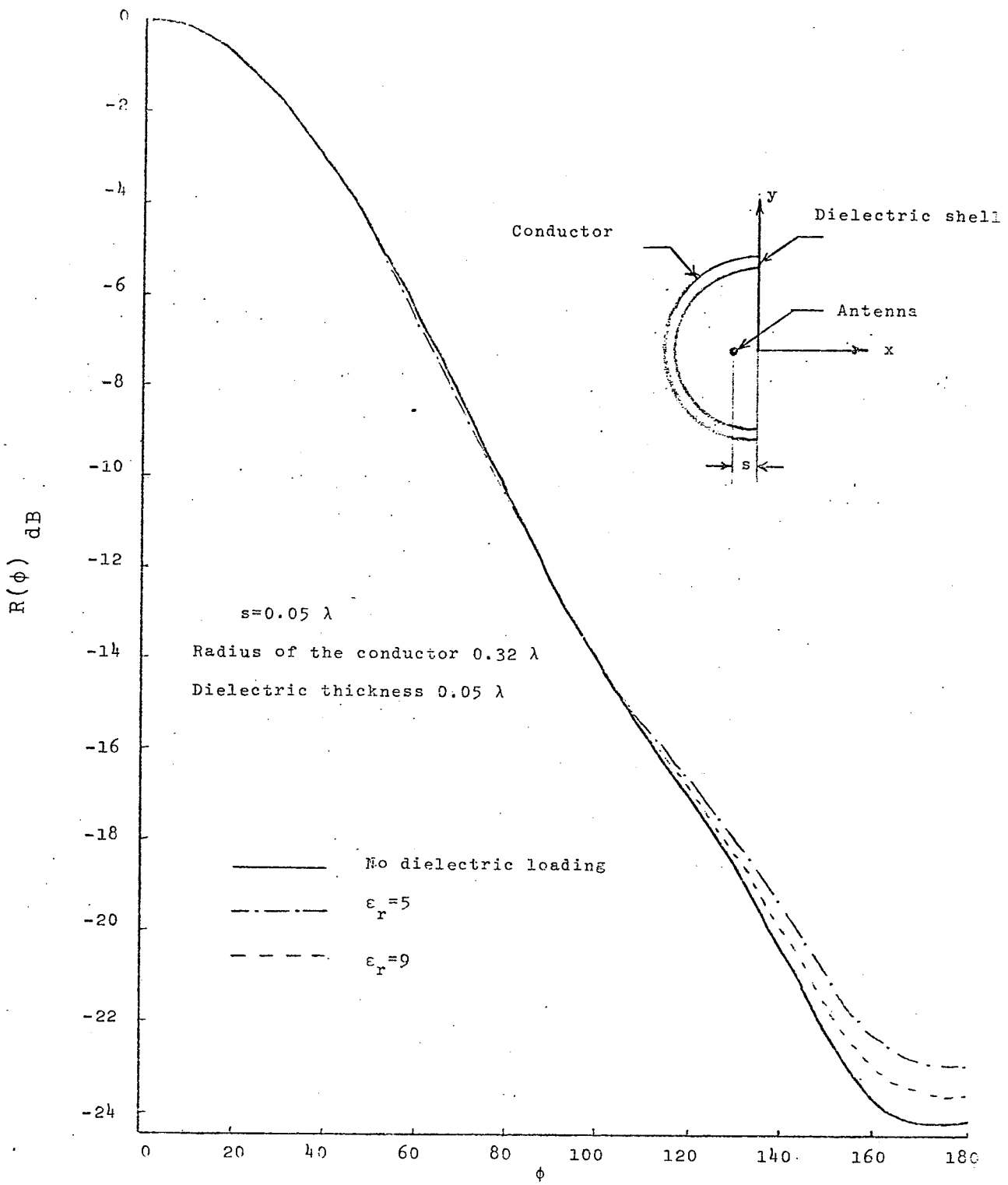


Figure 4.18 Radiation patterns for different dielectric constants

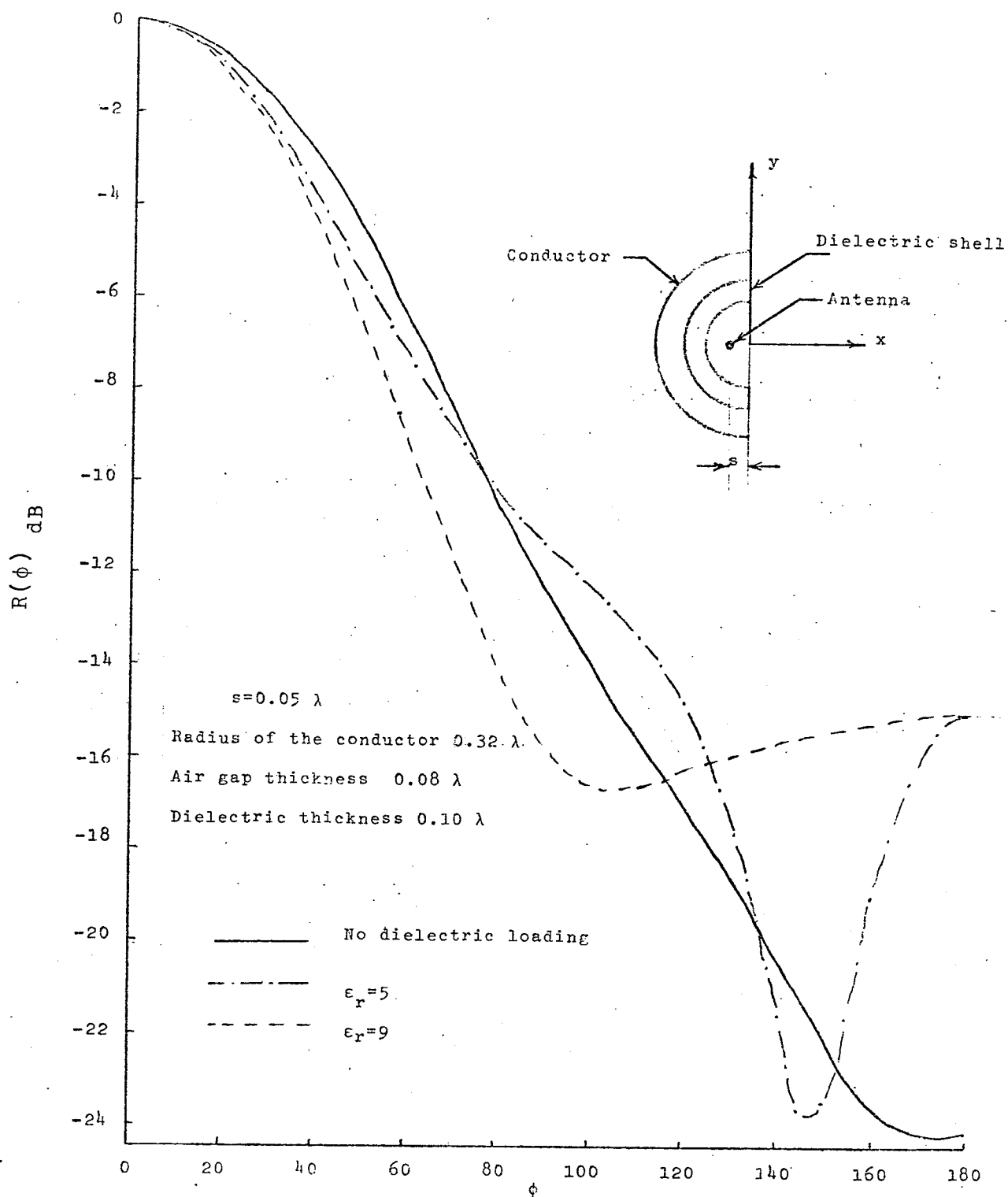


Figure 4.19 Effects of air gap on the radiation pattern for different dielectric constants

## CHAPTER FIVE

## EFFECTS OF SURFACE DEFORMATION OF CONVENTIONAL REFLECTORS

## 5.1- Introduction.

Reflectors are widely used to modify the radiation pattern of a radiating element in a suitable manner. There are several types of focusing reflector antennas commonly used in microwave frequency range for particular purposes. However, among the most economical and versatile type of reflectors, corner, cylindrical and parabolic reflectors are of special interest. Generally, a corner reflector is used as an active antenna and is most practical where apertures of one or two wavelengths are of convenient size. When it is convenient to build antennas with apertures of many wavelengths, parabolic reflectors can be used to provide highly directional antennas. Because of their large wavelength size, such antennas can be designed using the approximate solution borrowed from the ray theory to obtain highly directive beams, large gain, precision direction finding and high degree of resolution of complex targets in the case of radar application.

The exploration of a wide angular region with such sharp beams requires an involved scanning operation. This problem can be overcome by broadening the radiation pattern in one direction. The cylindrical reflectors are quite suitable for this purpose since they produce fan beams, that is, a field pattern which is wide in one plane and narrow in

the other.

In order to obtain a predetermined fan beam radiation, which has been used extensively in radar antenna design, the conventional cylindrical reflectors are shaped in such a way to produce the desired pattern in the broad beam plane .

So far, most of the information available for this type of reflectors has been obtained through the use of ray theory which is only applicable if the characteristic dimension of the reflector is much greater than the wavelength. However, for dimensions of the order of the wavelength, this approach most likely is not able to yield results with acceptable accuracy.

The purpose of this chapter is to investigate the radiation characteristics of a few commonly used types of reflectors of moderate cross sections by means of numerical techniques developed in the earlier chapter. It also studies the possibilities of beam shaping by surface deformations and improving the radiation characteristics of these types of reflectors in a desired fashion.

In the following section, first the radiation pattern of three types of commonly used reflectors ( corner, parabolic and circular cylindrical reflectors) will be compared, for a line source excitation. The second step would be the investigation of the effects of surface deformation on these focusing elements and finally the best results for each case (if any) will be compared against each other.

## 5.2- Numerical results.

Results of this series of computations are the radiation patterns presented in figures 5.1 to 5.7. It has been assumed that the reflectors are infinite along the z direction. This assumption will transform the problem into a two-dimensional one. Generally when the axial length of a reflector is more than a few wavelengths, this assumption leads to results of acceptable accuracy.

Figures 5.1 to 5.3 show the radiation patterns of three types of reflectors mentioned before. The geometry of the structures are shown in these figures. As a base for comparison, the apertures of the reflectors are kept constant and equal for all the reflectors. The area of the reflecting surfaces is also kept equal to each other as close as possible. Figure 5.1 shows the effects of the source separation distance from the reflecting surface on the radiation pattern of a circular cylindrical reflector. For this particular geometry it was found that setting (  $ks=1.5$  ) results in a less back radiation without a significant decrease in the front direction energy level. Figure 5.2 illustrates the dependence of the focal number (  $F_n$  ) of a parabolic reflector. Here the focal number is,

$$F_n = f/D \quad (5.1)$$

where f is the focal length of the parabolic reflector, as shown in the figure, and D is the diameter of the aperture.

For a line source located at the focus of the reflector, the amplitude distribution of field over the aperture becomes more tapered to the edges of the aperture as  $F_n$  <sup>33, 37</sup> decreases which means reduction in edge illumination. This may be desired in order to reduce the minor-lobe levels and back radiated energy, but at the expense of lower radiation level in the front direction as it is evident from figure 5.2. By decreasing  $f$ , since  $D$  is kept constant,  $F_n$  decreases. As a result of tapering aperture illumination, the back scattered energy becomes smaller but the level of the energy drops rapidly.

Figure 5.3 is intended to show the effects of the variation of the source separation on the radiation pattern of a corner reflector. This figure shows that by decreasing the antenna separation from the apex of the corner reflector beyond a certain limit, the back radiation increases. This is expected, since by decreasing the source separation, the effective aperture of a corner reflector decreases. Furthermore, if,

$$k_s > k\ell/2 \quad (5.2)$$

where  $\ell$  is the length of the reflector, the main lobe becomes broader. As <sup>37</sup>expected the optimum value for the antenna separation is,

$$k_s \approx k\ell/2 \quad (5.3)$$

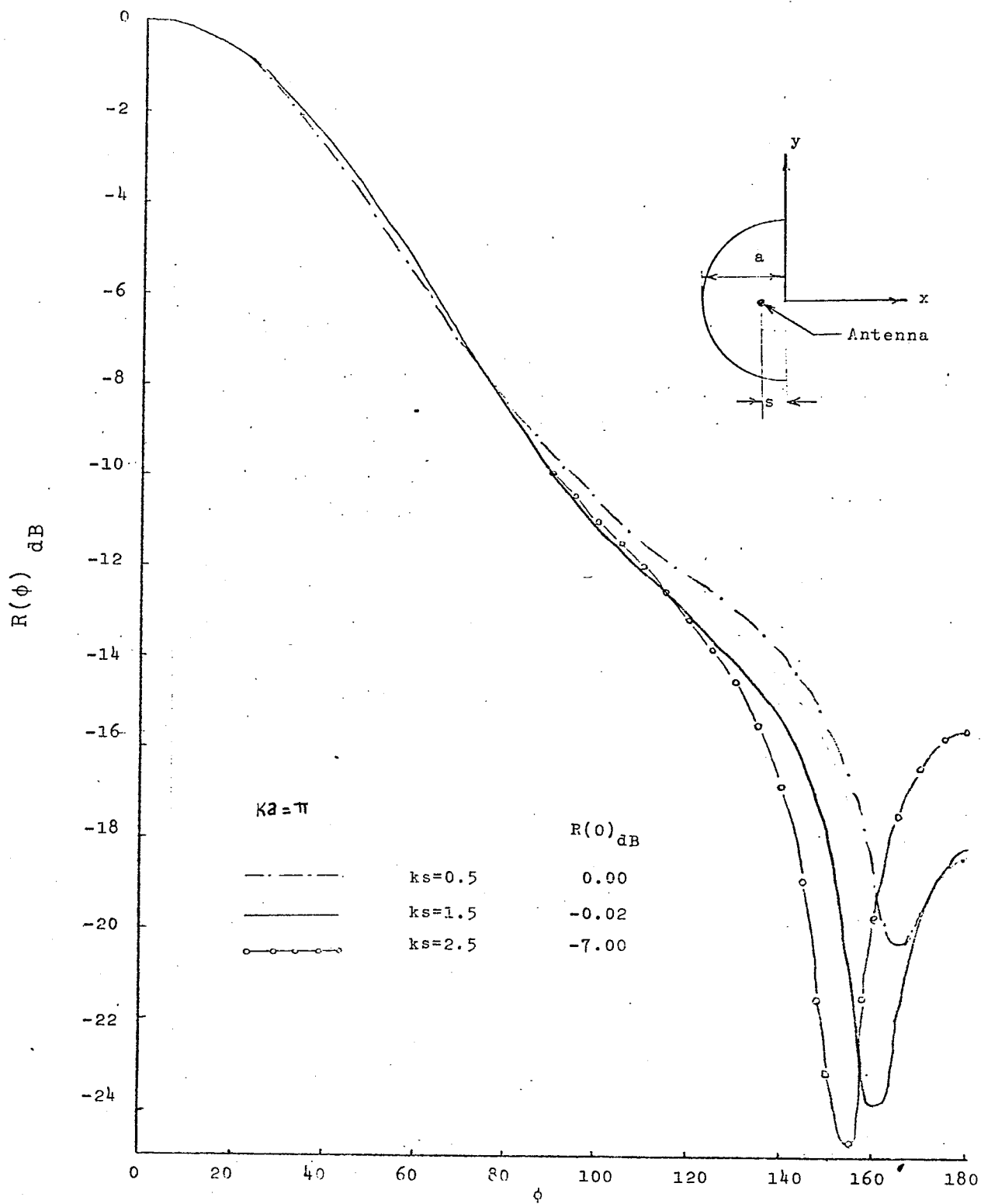


Figure 5.1 Radiation patterns of a circular cylindrical reflector for different source separations.

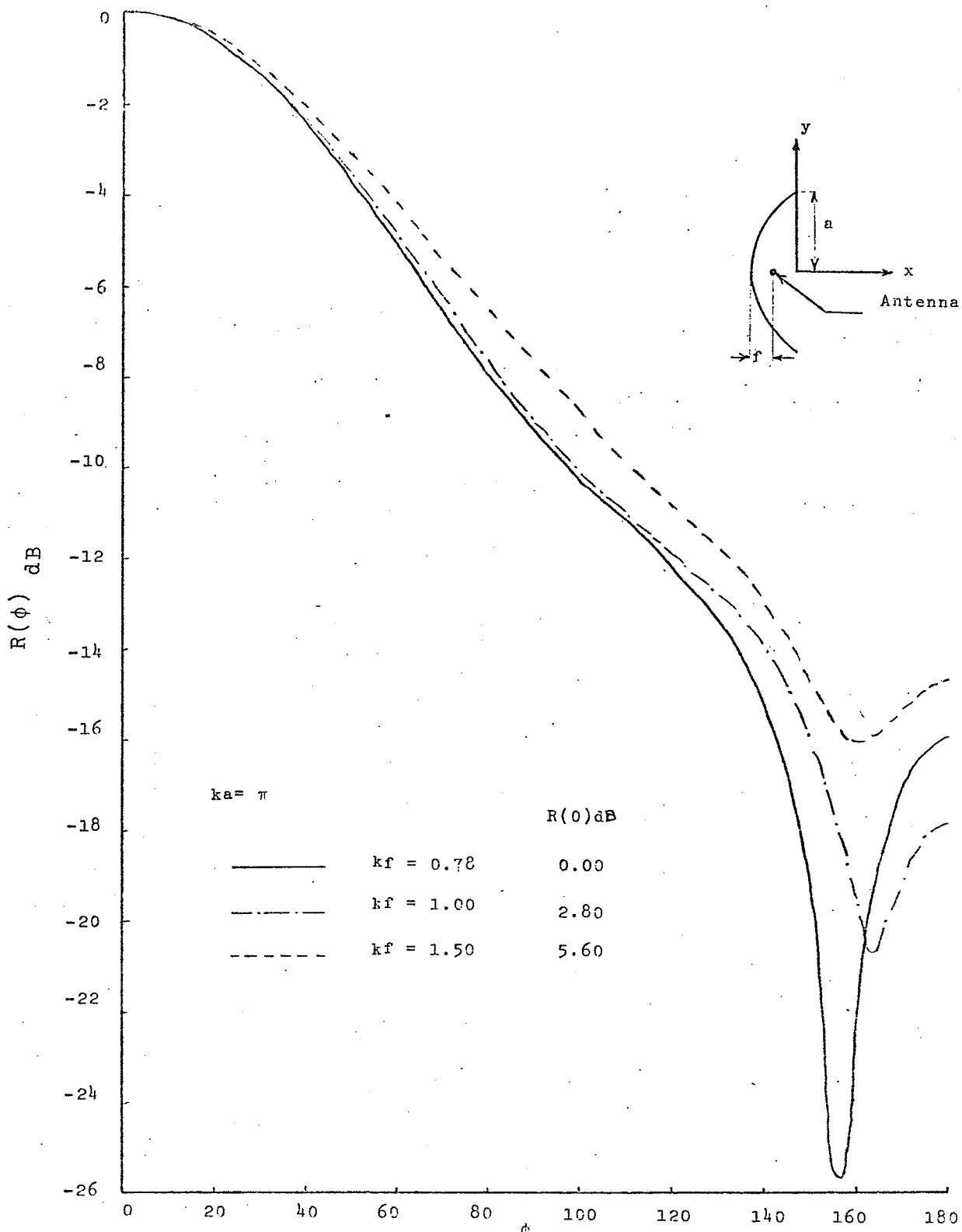


Figure 5.2 Radiation patterns of a parabolic reflector for different focal distances

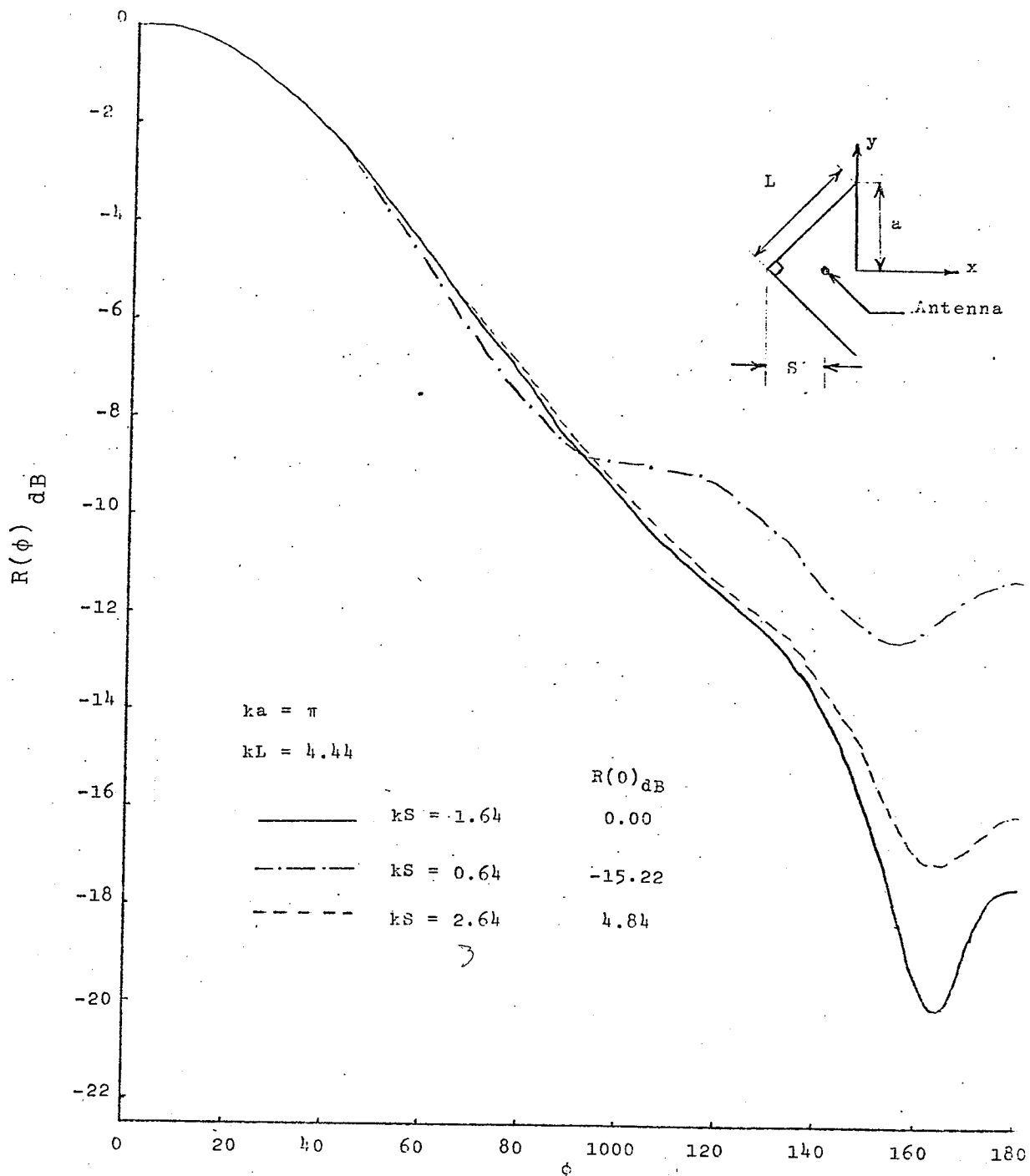


Figure 5.3 Radiation patterns of a corner reflector for different source separations

In order to compare the three types of reflectors studied in this section, the best case from each figure was chosen and is shown in figure 5.4. The basis of this selection was mainly a compromise between narrower beam width, less diffracted energy and more radiation level in the front direction. As it can be seen, from the above points of view, the circular cylindrical reflector shows the best result among the three types of reflectors with moderate cross sectional dimension.

In order to suppress the diffraction around the edges of the reflecting surfaces, it was decided to investigate the effects of introducing flares of plane metallic sheets at the edges. To study the probable effects of this body deformation on the radiation pattern of the reflector antennas, several cases were tested and results are presented in figures 5.5 to 5.7. The geometry of the antenna structure for each case is also given in the corresponding figure. The results are quite satisfactory, since in all cases, the introduction of the flares result in narrower beam width and less edge diffraction. A plausible physical interpretation is that the energy diffracted by the edges will be reflected back to the front direction by the conducting plates. The new edges introduced by these plates are too far from the source to diffract a significant amount of energy. The optimum value for the angle ( $\beta$ ) between the plates and the x-axis is found to be 45 degrees for both types of reflectors. Figure 5.7 compares the best result obtained

for each case. It shows that the back scattered energy is less for the modified circular cylindrical reflector and the energy level in the front direction is much greater than that of the parabolic type.

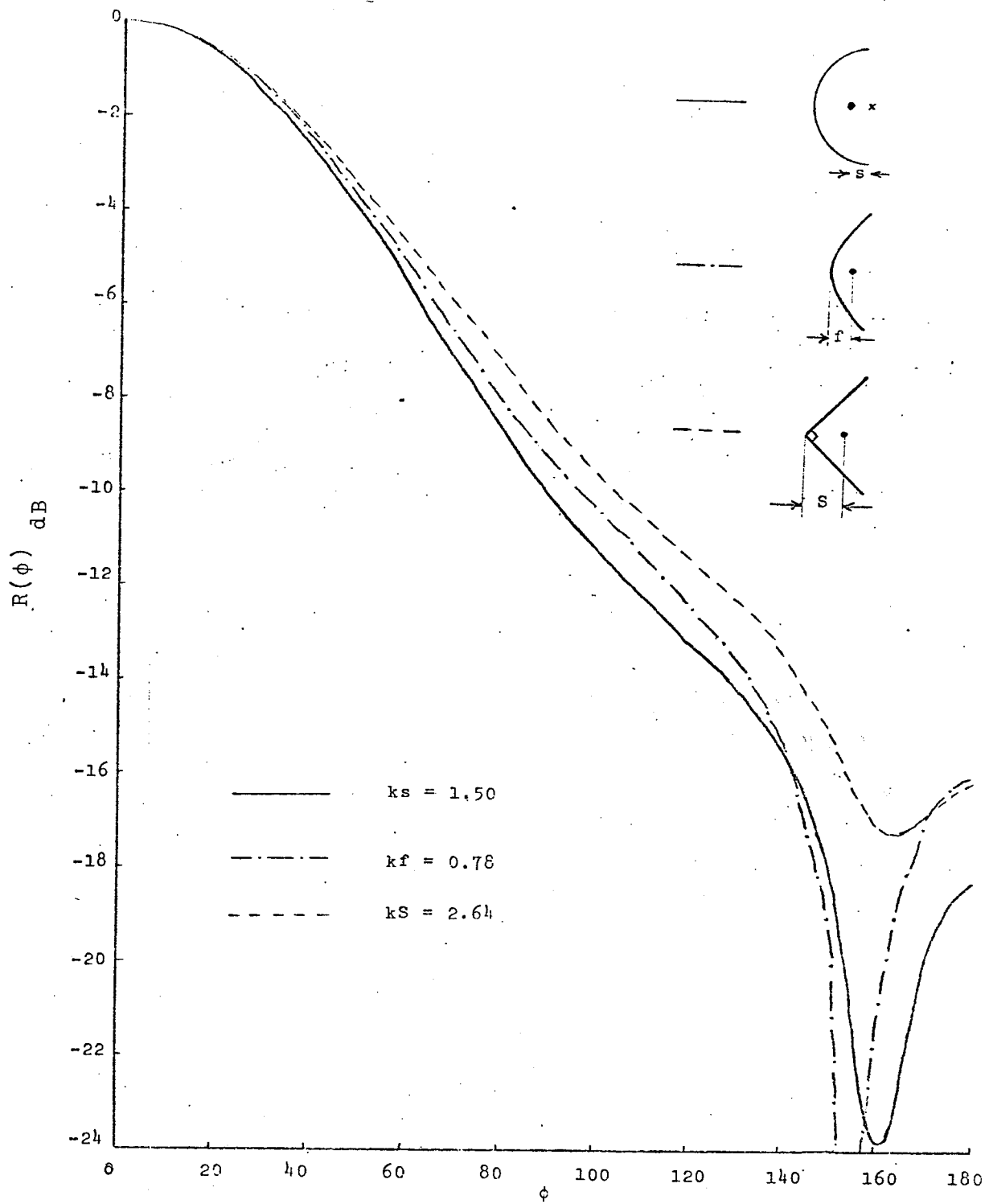


Figure 5.4 Comparison of the radiation patterns of the three types of the reflectors

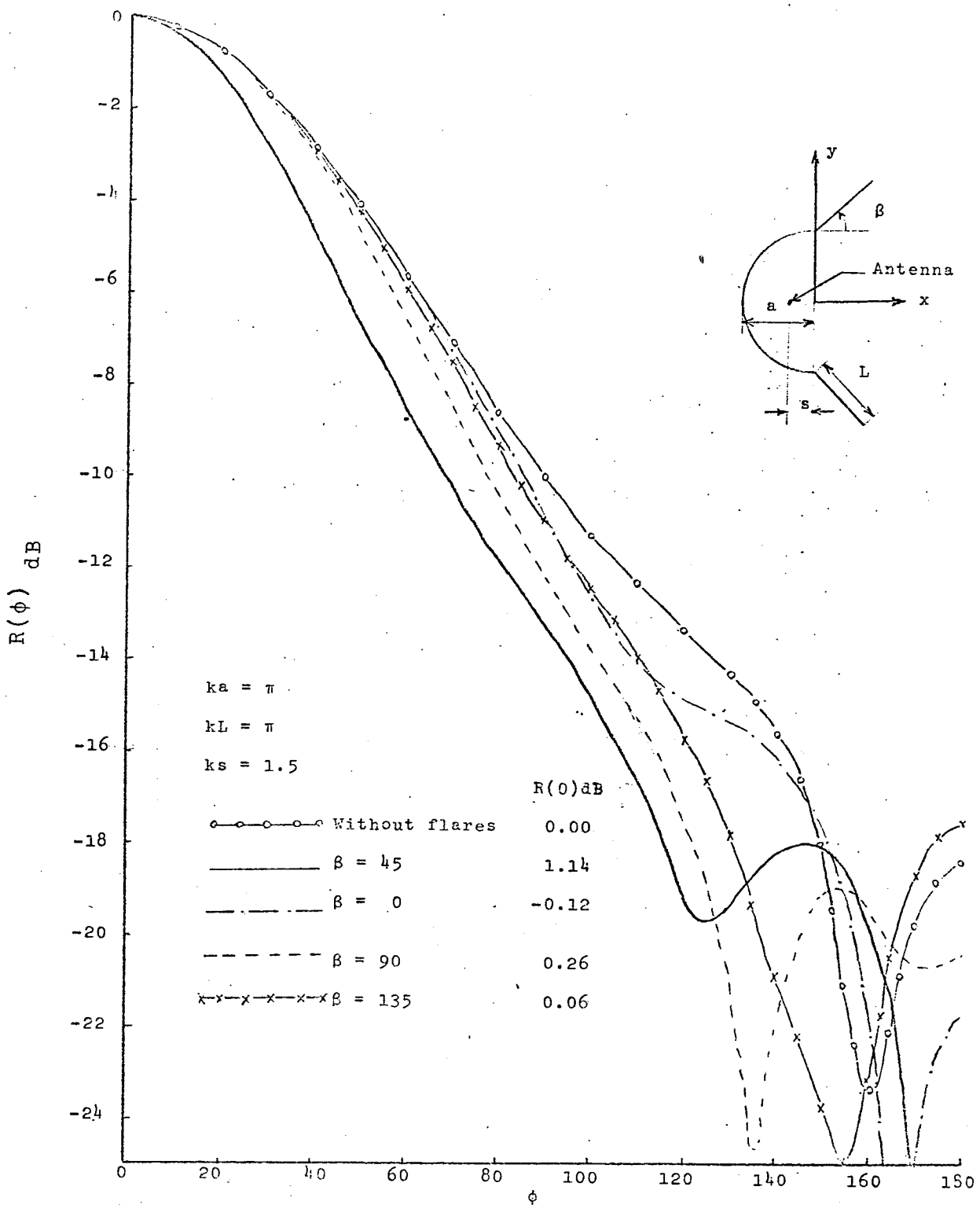


Figure 5.5 Effects of conducting plane sheets on the radiation pattern of a semicircular cylindrical reflector

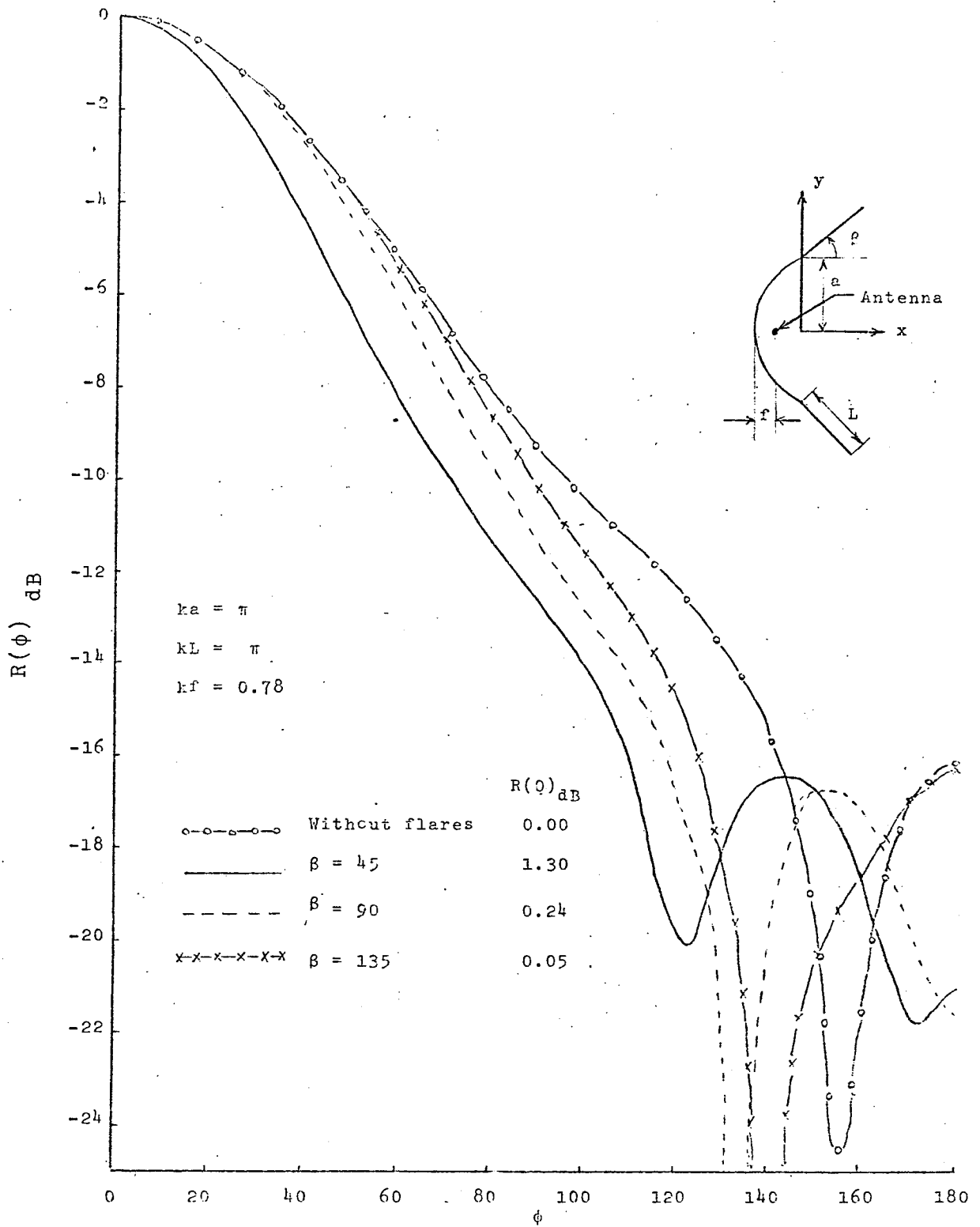


Figure 5.6 Effects of conducting plane sheets on the radiation pattern of a parabolic reflector

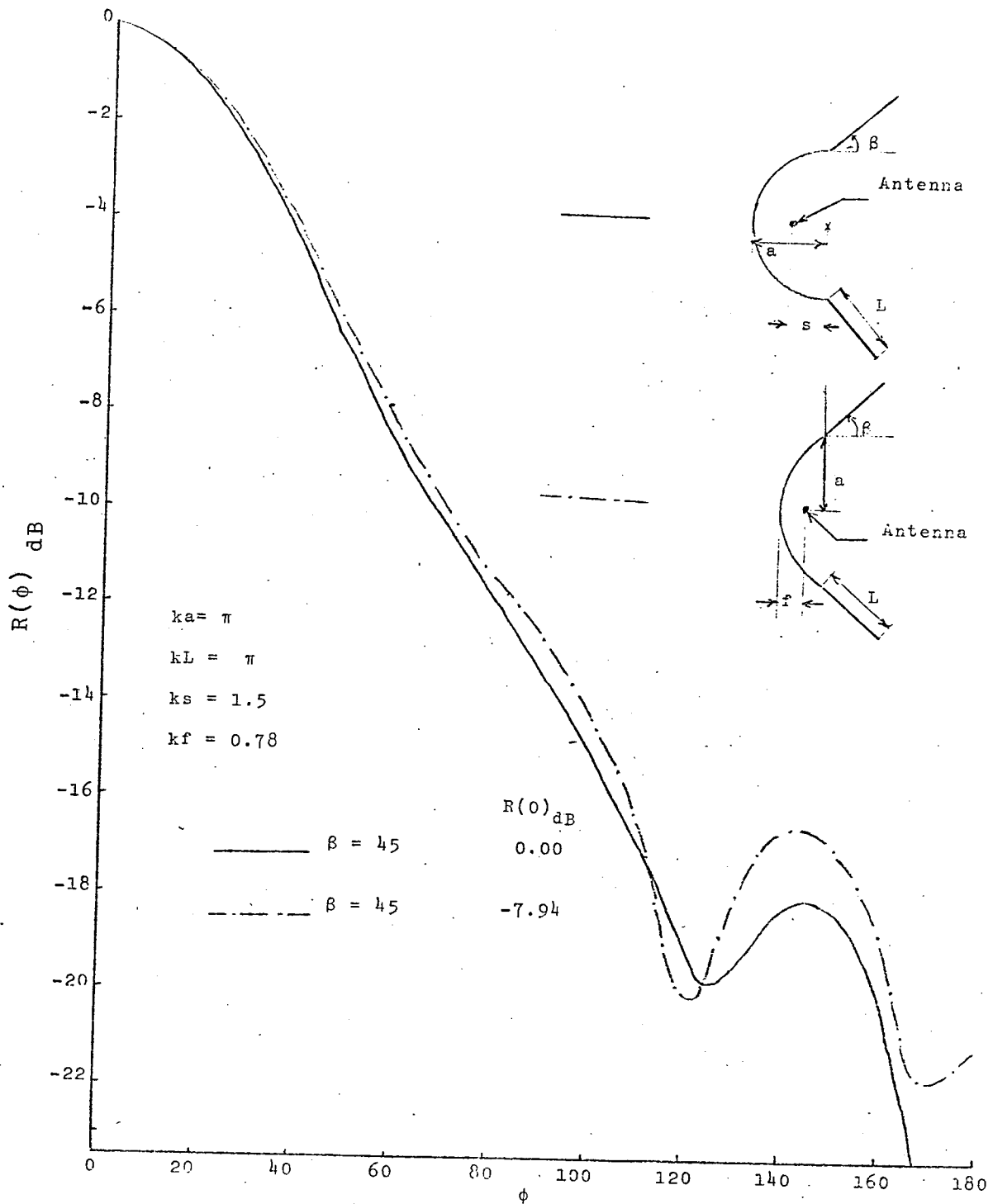


Figure 5.7 Comparison of the radiation patterns of the modified reflectors

## CHAPTER SIX

## CONCLUSIONS

In this thesis, the general scattering problem of a perfectly conducting or a dielectric loaded reflector was described by an integral equation of the induced surface and polarization currents. The problem is then solved by an application of the moment method. The principal limitations of moment method in application to large conducting objects were pointed out and were overcome by utilizing the physical optics approximation. The total current distribution was assumed to be the sum of the physical optics and a difference current, which accounted for the contribution of the discontinuities and the difference of the true and the physical optics currents. It was shown that using this method, reasonably accurate solution could be obtained with step sizes as large as  $0.17\lambda$ . This was a significant improvement over the conventional moment method, where a step size of  $0.05\lambda$  was required.

The method was then applied to study the radiation characteristics of large reflectors,  $ka=50$  and  $100$ . The difference current was shown to be localized to the edges of the reflectors and could be determined by sampling a fractional portion of the reflector contour near each edge. This in fact reduced the large reflector surface to small regions near each edge and, consequently, could provide a numerical solution for reflectors of any size.

The effects of variously shaped dielectric loadings on the radiation patterns of cylindrical reflector were also investigated. It was found that the electrical thickness and the dielectric surface curvature were the most important parameters for the overall behavior of these antenna systems. By a proper choice of these parameters, it was possible to reduce the beamwidth and, as a result, to increase the directivity of the reflectors.

Finally, the effects of surface deformations of conventional cylindrical and parabolic reflectors were investigated by introducing conducting sheets at their edges. These conducting sheets generally improved the directivity of the reflectors, and gave an optimum directivity for a 45 degree angle between the sheets and the symmetrical axis of the reflectors.

## APPENDIX A

## a- The Method of Moment

The basic idea of the method of moment is to reduce an operator equation to a matrix equation and then solve the matrix equation by known techniques.

Following Harrington<sup>12</sup>, let us consider an integral equation of the inhomogeneous type,

$$L(f) = g \quad (1 A)$$

where,  $L$  is an integral operator,  $f$  is the unknown function to be determined and  $g$  is the known function. Let  $f$  be expanded in a series of linearly independent functions,

$$f = \sum_n \alpha_n f_n \quad (2 A)$$

where,  $\alpha_n$ 's ( $n=1,2,\dots$ ) are in general complex constant coefficients and  $f_n$ 's are expansion functions (basis functions). Equation (2 A) holds if it is an infinite summation and  $f_n$ 's form a complete set of linearly independent functions. For an approximate solution, however, the summation is usually truncated at  $n=N$ , where the lower limit of  $N$  depends on the desired degree of accuracy of the solution. Furthermore, the set of  $f_n$  should be chosen in

such a way that to approximate  $f$  reasonably well in the prescribed region. Substituting (2 A) into (1 A) and using the linearity of  $L$  results in,

$$\sum_{n=1}^N \alpha_n L(f_n) = g \quad (3 A)$$

Now we define an inner product  $\langle f, g \rangle$  to satisfy,

$$\begin{aligned} \langle f, g \rangle &= \langle g, f \rangle \\ \langle af + bg, h \rangle &= a \langle f, h \rangle + b \langle g, h \rangle \\ \langle f^*, f \rangle &\begin{cases} > 0 & \text{if } f \neq 0 \\ = 0 & \text{if } f = 0 \end{cases} \end{aligned} \quad (4 A)$$

where,  $a$  and  $b$  are scalars and  $*$  denotes complex conjugate. For different problems, different suitable inner product definitions may be chosen, but subject to (4 A). Now, define a set of linearly independent testing functions,  $W_n$ 's ( $n=1, 2, \dots, N$ ). Taking the inner product of (3 A) with each  $W_m$  leads to,

$$\sum_n \alpha_n \langle W_m, L(f_n) \rangle = \langle W_m, g \rangle \quad m=1, 2, \dots, N \quad (5 A)$$

In matrix form, (5 A) may be cast in the form of,

$$\begin{pmatrix} l \\ mn \end{pmatrix} \begin{pmatrix} \alpha \\ n \end{pmatrix} = \begin{pmatrix} g \\ m \end{pmatrix} \quad (6 A)$$

If the matrix  $(l_{mn})$  is not singular, then,

$$\begin{pmatrix} \alpha \\ n \end{pmatrix} = \begin{pmatrix} l_{mn} \end{pmatrix}^{-1} \begin{pmatrix} g \\ m \end{pmatrix} \quad (7 A)$$

where,  $(l_{mn})^{-1}$  is the inverse of  $(l_{mn})$ . After solving (7 A) for  $\alpha_n$ 's, then the unknown quantity  $f$  may be approximated by,

$$f \approx \sum_{n=1}^N \alpha_n f_n \quad (8 A)$$

b- Approximation techniques for the expansion and weighting functions.

In order to solve the inhomogeneous integral equation (1 A), the first task is to choose an appropriate set for the expansion functions. In fact, there are an infinite number of sets that may be used for this purpose. However, determination of the proper set depends on the desired degree of accuracy of the solution and the ease of evaluation of the matrix elements and the computing cost factor. It should also be chosen in such a way that to give an accuracy consistent with the accuracy of the integration techniques used for evaluating sub integrals related to the coefficient matrix.

Several useful expansion functions, with their

degree of accuracy are given in , namely, pulse, triangle, first order Taylor series and piecewise parabolic functions. Pulse function is the least and parabolic function is the most accurate ones in these series of expansion functions.

For the case of weighting functions, again we may use an infinite number of sets. However, a complicated form of weighting function results in evaluating complex integrals for determining the elements of the coefficient matrix. The simplest way is to use a set of Dirac's delta functions. In terms of the point matching technique, this is equivalent to enforce the integral equation at  $N$  discrete points on the contour of the integration. Throughout this thesis, the computations are carried out by a first order approximation, that is, the pulse and delta functions are used for the expansion and the weighting functions, respectively.

### c- Pulse and Dirac's delta functions.

The simplest form of expansion functions is the pulse function illustrated in figure A.

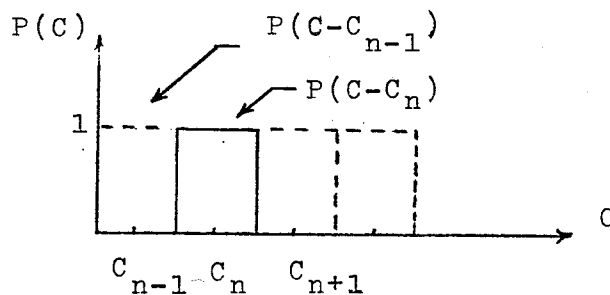


Figure A Pulse function

A linear combination of pulse functions results in a step approximation to  $f$ , which is depicted in figure B.

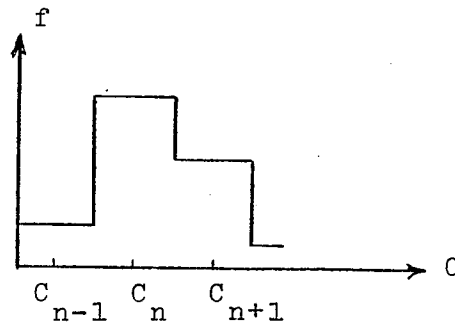


Figure B Step approximation

Therefore,

$$f_n = P(C - C_n) = \begin{cases} 1 & (C_n + C_{n-1})/2 < C < (C_{n+1} + C_n)/2 \\ 0 & \text{elsewhere} \end{cases} \quad (9 A)$$

For the case of weighting function, we choose a set of Dirac's delta functions located at the center of each interval on  $C$ , as it is illustrated in figure C.

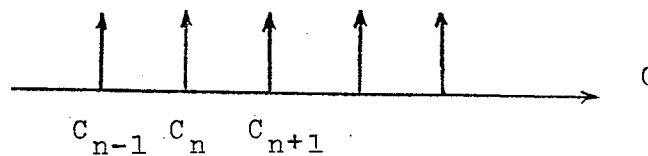


Figure C Delta functions

According to the definition of the Dirac's delta function, we have,

$$\begin{aligned} \delta_n(\tilde{\rho} - \tilde{\rho}_n) &= 0 && \text{when } \tilde{\rho} \neq \tilde{\rho}_n && (10 A) \\ \int_C \delta_n(\tilde{\rho} - \tilde{\rho}_n) dc &= 1 && \text{when } \tilde{\rho} = \tilde{\rho}_n \end{aligned}$$

For use in this work, a suitable inner product is defined as,

$$\langle W_m, P \rangle = \int_C W_m \cdot P dc \quad (11 A)$$

Taking the inner product of  $f$  and  $\delta_m$  results in,

$$\langle \delta_m(\tilde{\rho} - \tilde{\rho}_m), f(\tilde{\rho}) \rangle = \int_C f(\tilde{\rho}) \cdot \delta(\tilde{\rho} - \tilde{\rho}_m) dc = f(\tilde{\rho}_m) \quad (12 A)$$

Now, if the contour  $C$  of the integration is divided into a total of  $N$  intervals, the sampled density of the unknown in the center of the  $n$ th interval is,

$$J_n = \alpha_n P_n = \begin{cases} \alpha_n & \text{on } \Delta C_n \\ 0 & \text{elsewhere} \end{cases} \quad (13 A)$$

where,

$$\Delta C_n = (C_{n+1} - C_n) \quad (14 \text{ A})$$

c- Determination of the coefficient matrix.

In order to determine the elements of the coefficient matrix, we take the specific example of an integral equation in the form of,

$$E_i(\tilde{\rho}) = (k\eta/4) \int_C J(\tilde{\rho}') H_0^2(k|\tilde{\rho} - \tilde{\rho}'|) dc' \quad (15 \text{ A})$$

where,

$$g = E_i(\tilde{\rho})$$

$$f = J(\tilde{\rho}) \quad (16 \text{ A})$$

$$L = (k\eta/4) \int_C H_0^2(k|\tilde{\rho} - \tilde{\rho}'|) dc'$$

From the equations 5,9,10 and 11 we have,

$$l_{mn} = \langle W_m, L(f_n) \rangle = (k\eta/4) \int_C H_0^2(k|\tilde{\rho}_m - \tilde{\rho}_n'|) dc' \quad (17 \text{ A})$$

where  $\tilde{\rho}_m$  and  $\tilde{\rho}_n$  are the positional vectors of the mid-points of  $\Delta C_m$  and  $\Delta C_n$ , respectively. The crudest approximation for

evaluating the integral appearing in (17 A) is to assume that the interval  $\Delta C_n$  is sufficiently small to neglect the variation of the integrand over  $\Delta C_n$ , for the case when  $m \neq n$

Therefore,

$$l_{mn} \approx (k\eta/4) \Delta C_n H_0^2(k|\tilde{\rho}_m - \tilde{\rho}_n|) \quad m \neq n \quad (18 \text{ A})$$

For diagonal elements ( $m=n$ ), the Hankel function has a singularity on the  $n$ th interval. The Hankel function cannot be integrated directly. However, if the interval lengths are small enough, then the argument is small and the Hankel function can be approximated by ,

$$H_0^2(k|\tilde{\rho}_m - \tilde{\rho}_n|) = 1 - (j2/\pi)L_n(\gamma k \Delta C / 2)$$

where  $\gamma$  is given by,

$$\gamma = 1.7810724$$

An application of (19 A) to (17 A) results in,

$$l_{nn} \approx (k\eta/4) \Delta C_n \{1 - (j2/\pi)L_n(\gamma k \Delta C_n/4e)\}$$

Using the equations 2,7,18 and 20, the approximate current

distribution over the contour  $C$  can be obtained with the aid of a digital computer. Once the current distribution is found, other parameters of the engineering interest can be computed by simple integrations.

## BIBLIOGRAPHY

- (1) K. K. Mei and J. G. Van Bladel " Scattering by perfectly conducting rectangular cylinders " IEEE Trans. on Antennas and Propagation, Vol. AP-11, pp.185-192, March 1963.
- (2) M. G. Andreassen " Scattering from parallel metallic cylinders with arbitrary cross sections " IEEE Trans. on Antennas and Propagation, Vol. AP-12, pp.746-754, November 1964.
- (3) M. G. Andreassen " Scattering from bodies of revolution " IEEE Trans. on Antennas and Propagation, Vol. AP-13, pp. 303-310, March 1965.
- (4) M. G. Andreassen " Scattering from cylinders with arbitrary surface impedance " Proceeding of the IEEE, Vol.53, pp.812-817, August 1965.
- (5) J. H. Richmond " Scattering by a dielectric cylinder of arbitrary cross section shape " IEEE Trans. on Antennas and Propagation, Vol. AP-13, pp.334-341, May 1965.
- (6) J. H. Richmond " TE-Wave scattering by a dielectric cylinder of arbitrary cross-section shape " IEEE Trans. on Antenna and Propagation, Vol. AP-14, pp.460-464, July 1966.
- (7) R. F. Harrington and J. R. Mautz " Straight wires with arbitrary excitation and loading " IEEE Trans. on Antennas and Propagation, Vol. AP-15, pp.502-515, July 1967.

- (8) R.F. Harrington and J. R. Mautz " Electromagnetic behavior of circular wire loops with arbitrary excitation and loading " Proc. IEE(London), Vol. 115, January 1968.
- (9) A. B. Baghdasarian and D. J. Angelakos " Scattering from conducting loops and solution of circular loop antennas by numerical methods " Proc. of the IEEE, Vol. 53,pp. 818-822, August 1965.
- (10) Y. S. Yeh and K. K. Mei " Theory of conical equiangular-spiral antennas(Part I-Numerical Technique) " IEEE Trans. on Antennas and Propagation, Vol. Ap-15, pp.634-639, September 1967.
- (11) R. F. Harrington " Matrix methods for field problems " Proc. of the IEEE, Vol. 55, pp.136-149, February 1967.
- (12) R. F. Harrington " Field computation by moment methods " Macmillan Company, 1968.
- (13) R. Mittra " Computer techniques for electromagnetics " Pergamon Press, 1973. pp. 159-177.
- (14) R. Wallenberg " Two-dimensional scattering and radiation from perfectly conducting cylinders of arbitrary shape " PhD. dissertation, June 1968. Syracuse University.
- (15) L. Shafai " An improved integral for the numerical solution of two-dimensional diffraction problems " Canadian Journal of Physics, Vol. 48, No. 8, pp.954-963, 1969.
- (16) L. Shafai and P. Bhartia " Scattering properties of certain conducting cylindrical geometries " Canadian Journal of Physics, Vol.51, No. 8, pp. 861-864, 1973.

- (17) L. Shafai and Y. S. El-Moazzen " Radiation patterns of an antenna near a conducting strip " IEEE Trans. on Antennas and Propagation, Vol. AP-20, No. 5, pp. 642-644, September 1972.
- (18) S. T. M. Abdelmessih and G. Sinclair, Canadian Journal of Physics, Vol. 45, p. 1305, 1967.
- (19) J. Meixner, New York University Report EM-72, 1954.
- (20) A. F. Kay and J. F. Nihen " Scattering and currents induced on sharp and rounded corners " IEEE Trans. on Antennas and Propagation, Vol. AP-14, pp. 112-114 January 1966.
- (21) J. A. Kinzel " Large reflector antenna pattern computation using moment methods " IEEE Trans. on Antennas and Propagation, Vol. AP-22, pp. 116-118, January 1974.
- (22) M. D. Tew and L. L. Tsai " A method toward improved convergence of moment method solutions " Proc. of the IEEE, Vol. 20, pp. 1436-1437, November 1972.
- (23) C. M. Knop " External admittance of an axial slot on a coated metal cylinder " Radio Science 3 (New series), pp. 803-817, 1968.
- (24) Y. S. El-Moazzen and L. Shafai " Effect of dielectric loading on the radiation power of an axial slot antenna " AEU-Electronics and Communication, pp. 47-48, 1973.
- (25) M. A. K. Hamid, P. Bhartia, A. Mohsen, W. M. Boerner, R. J. Boulanger " Diffraction by dielectric-loaded conical horn antennas " URSI Symp., Stresa, Italy, pp. 363-366, 1968.

- (26) M. A. K. Hamid and A. Mohsen " Diffraction by dielectric loaded horns and corner reflectors " IEEE Trans. on Antennas and Propagation, Vol. AP-17, pp.660-662, Sep. 1969.
- (27) M. A. K. Hamid, R. J. Boulanger, N. J. Mostowj, A. Mohsen " Radiation characteristics of dielectric-loaded horn antennas " Electronics Letters, Vol. 6, No.1, pp.20-21, January 197 .
- (28) G. N. Tsandoulas and W. D. Fitzgerald " Aperture efficiency enhancement in dielectrically loaded horns " IEEE Trans. on Antennas and Propagation, Vol. AP-20, pp. 69-74, January 1972.
- (29) S. J. Towaij " Radiation by dielectric-loaded antennas with airgaps " A PhD. dissertation, University of Manitoba, Winnipeg, Manitoba, Canada, May 1974.
- (30) L. Shafai " Radiation from an axial slot antenna coated with a homogeneous material " Canadian Journal of Physics Vol. 50, No. 23, pp.3072-3077, 1972.
- (31) L. Shafai and R. K. Chugh "Resonance effects in slotted spherical antennas coated with homogeneous materials " Canadian Journal of Physics, Vol. 51, No. 22, pp. 2341-2346, 1973.
- (32) J. A. Stratton " Electromagnetic Theory " McGraw-Hill Book Company, 1941.
- (33) S. Silver " Microwave antenna theory and design " M.I.T. Radiation Laboratories Series, Vol. 12, McGraw-Hill Book Company, 1949.

- (34) R. F. Harrington " Time Harmonic Electromagnetic Fields " McGraw-Hill Book Company, 1961.
- (35) I.S. Gradshteyn and I.M. Ryzhik "Table of Integrals, Series and Products" Academic Press, p.671&738, 1965.
- (36) M. Abramowitz and I..A. Stegun " Handbook of Mathematical Functions " Dover Publications, Inc., p.364, 1968.